Spatio-temporal analysis of rainfall and its effect for landslide triggering in São Miguel Island (Azores Archipelago)

Tese de Doutoramento

Rui Filipe Fagundes Silva

Doutoramento em

Geologia

Ponta Delgada
2026

Spatio-temporal analysis of rainfall and its effect for landslide triggering in São Miguel Island (Azores Archipelago)

Tese de Doutoramento

Rui Filipe Fagundes Silva

Orientadores

Professor Doutor Rui Tiago Fernandes Marques

Professor Auxiliar da Faculdade de Ciências e Tecnologia da Universidade dos Açores

Professor Doutor José Luís Gonçalves Moreira da Silva Zêzere

Professor Catedrático do Instituto de Geografia e Ordenamento do Território da Universidade de Lisboa

Tese elaborada para obtenção do grau de Doutor em Geologia, especialidade de Riscos Geológicos

Thesis submitted to the University of the Azores in fulfilment of the requirements for the degree of Doctor in Geology with specialty in Geological Risks.

INSTITUTO DE INVESTIGAÇÃO EM VULCANOLOGIA E AVALIAÇÃO DE RISCOS

UAc
UNIVERSIDADE DOS AÇORES

This research was supported by FCT – Foundation for Science and Technology

Rui Filipe Fagundes Silva was supported by PhD Grant from Foundation for Science and Technology (UI/BD/152207/2021)

REPÚBLICA PORTUGUESA | EDUCAÇÃO, CIÊNCIA E INOVAÇÃO

fct Fundação para a Ciência e a Tecnologia

PREAMBLE

I affirm that this thesis was independently conceived and crafted for its intended purpose. It incorporates three original papers, which have been submitted to and published in reputable scientific journals.

The author fully contributed to the entire process of each scientific article from conceiving and designing the analysis, to collecting and preparing data, performing the analysis, writing the article and all the stages of article peer-review and revision.

The involvement of co-authors underscores the collaborative effort among researchers and acknowledges their contributions to team-based research, as evidenced by the papers listed below:

- Silva, R.F., Marques, R. & Zêzere, J.L. (2024). Spatial distribution, temporal trends and impact of landslides on São Miguel Island from 1900 to 2020 based on an analysis of the Azores historical natural hazards database. Nat Hazards 120, 2617–2638. https://doi.org/10.1007/s11069-023-06296-0
- Silva, R. F., Marques, R., Zêzere, J. L. & Fragoso, M. (2025). Rainfall Patterns and Trends on São Miguel Island (Azores, Portugal): A Hierarchical Clustering and Trend Analysis Approach. Climate, 13(11), 238. https://doi.org/10.3390/cli13110238
- Silva, R.F., Marques, R. & Zêzere, J.L. (2026). A New Approach for Developing Combined Empirical Rainfall-Triggered Landslide Thresholds: Application to São Miguel Island (Azores, Portugal) Water, 18(6), 673. https://doi.org/10.3390/w18060673

TABLE OF CONTENTS

LIST OF FIGURES

CHAPTER 3 | RAINFALL PATTERNS AND TRENDS ON SÃO MIGUEL ISLAND (AZORES, PORTUGAL): A HIERARCHICAL CLUSTERING AND TREND ANALYSIS APPROACH

CHAPTER 4 | A NEW APPROACH FOR DEVELOPING COMBINED EMPIRICAL RAINFALL-TRIGGERED LANDSLIDE THRESHOLDS: APPLICATION TO SÃO MIGUEL ISLAND (AZORES, PORTUGAL)

LIST OF TABLES

CHAPTER 2 | SPATIAL DISTRIBUTION, TEMPORAL TRENDS AND IMPACT OF LANDSLIDES ON SÃO MIGUEL ISLAND FROM 1900 TO 2020 BASED ON AN ANALYSIS OF THE AZORES HISTORICAL NATURAL HAZARDS DATABASE

CHAPTER 3 | RAINFALL PATTERNS AND TRENDS ON SÃO MIGUEL ISLAND (AZORES, PORTUGAL): A HIERARCHICAL CLUSTERING AND TREND ANALYSIS APPROACH

CHAPTER 4 | A NEW APPROACH FOR DEVELOPING COMBINED EMPIRICAL RAINFALL-TRIGGERED LANDSLIDE THRESHOLDS: APPLICATION TO SÃO MIGUEL ISLAND (AZORES, PORTUGAL)

ACKNOWLEDGEMENTS

With the completion of this doctoral thesis, I feel it is my duty to express my gratitude to all those who, through their contributions, have helped me achieve this goal. I would like to thank:

To the Director of the Instituto de Investigação em Vulcanologia e Avaliação de Riscos (IVAR), Professor Fátima Viveiros, and the former Director, Professor José Pacheco; and to the President of the Centro de Informação e Vigilância Sismovulcânica dos Açores (CIVISA), Professor Gabriela Queiroz, and the former President, Professor Rui Marques, I express my gratitude for providing the institutional conditions and support that facilitated the completion of this work.

To the Director of the PhD Program in Geology at the University of the Azores, Professor José Virgílio Cruz, I express my gratitude for the support provided in legal matters related to the doctoral project.

To Professor Rui Marques, my "scientific father" and supervisor of this doctoral project, I express my deepest gratitude for the knowledge he generously shared, for his constant availability to review and critically assess my work, and for his insightful comments and suggestions. His clarity in resolving doubts, together with his enthusiasm, friendship, and unwavering dedication, were fundamental to the development and completion of this thesis.

To Professor José Luís Zêzere, scientific supervisor of this doctoral project, I express my sincere gratitude for his continuous encouragement, collaboration, meticulous text revisions, unfailing availability, and outstanding commitment to my academic development. His guidance was fundamental to the completion of this thesis. It has been a great privilege to be supervised by one of the world's leading experts in this scientific area.

To Professor Marcelo Fragoso, I am grateful for his collaboration in the development of one of the scientific articles included in this thesis. His extensive knowledge and expertise were crucial to strengthening the scientific foundations of the article and contributed significantly to the progress of this work.

To my colleagues and friends Nuno Cabral and Maria João Poim for their professionalism and dedication in supporting the extensive, and at times exhausting, process of collecting, analysing, and selecting information for the documentation of landslide events.

To the Regional Delegation of the Instituto Português do Mar e da Atmosfera (IPMA) and to the Direção Regional do Ambiente e Ação Climática-Secretaria Regional do

Ambiente e Ação Climática do Governo Regional dos Açores for providing the rainfall data used in this study.

To my fellow PhD colleagues, for their friendship, for the good times, for sharing ideas, and for their companionship during moments of “mental block”.

To all staff and researchers at the Centro de Informação e Vigilância Sismovulcânica dos Açores (CIVISA) and the Instituto de Investigação em Vulcanologia e Avaliação de Riscos (IVAR), I am grateful for their friendship.

To my parents, siblings and grandparents for their unwavering support in my education, academic progress, and the confidence they place in me.

To my closest friends, for their friendship and companionship, for their support, and for always offering words of encouragement to keep me going in this PhD journey.

To my fellow members and friends from the Tuna Académica da Universidade dos Açores (TAUA), of which I was an active member until 2024, for being my second family; for the unforgettable moments, the memories of travels, performances, and gatherings that I cherish.

To my colleagues and friends from Casa do Triângulo – Associação Cívica and from Orfeão Cardeal Humberto Medeiros, for their interest in my academic progress. Being a member of these associations allowed me to grow personally and made this PhD process easier.

To my friends and family from São Jorge Island, for their support and interest in my academic journey and my work.

ABSTRACT

Landslides are the most frequent natural hazard in the Azores archipelago, due to its volcanic origin and geomorphology, geographical location, and climatic setting characterised by high levels of rainfall. In this context, understanding the factors that control the occurrence of these phenomena, and their temporal evolution is fundamental for the assessment and mitigation of the associated risk.

This study is based on the documentary database NATHA (Natural Hazards in Azores), compiled from a systematic analysis of historical sources and regional press archives, to identify and characterise landslide events on São Miguel Island between 1900 and 2020. A total of 236 events were catalogued, responsible for 82 fatalities, 41 injuries, 305 displaced people, and the total or partial destruction of 66 buildings. Spatial analysis revealed significant differences among municipalities, with Povoação being the most affected, accounting for about 59% of the total fatalities. Rainfall was identified as the main triggering factor in approximately 70% of the events, which occur mostly during the wettest months of the year, between November and March. Temporal analysis revealed a greater concentration of events after 1996, associated with a change in the rainfall regime, demonstrating, for the first time in the Azores, the influence of climate change on landslides occurrence.

Rainfall patterns and trends on São Miguel Island were further analysed using hierarchical clustering and non-parametric trend tests, identifying four homogeneous rainfall clusters and a strong orographic effect, with altitude as the main regulator of rainfall. A strong positive correlation between altitude and Mean Annual Precipitation (MAP) was observed, with an increase of approximately 180 mm per 100 m of elevation. Despite an increased frequency of intense rainfall days, total annual and seasonal rainfall display a marked decreasing trend, particularly during autumn and winter, with reductions between 41% and 55%. The study suggests that the predominantly positive phase of the North Atlantic Oscillation (NAO) observed in the most recent period has contributed, at least in part, to this decreasing trend in rainfall.

The study proposes a new approach for the development of combined empirical rainfall thresholds. An innovative combined empirical rainfall threshold approach was proposed, integrating a preparatory threshold related to prior soil saturation with a triggering threshold associated with rainfall on the day of the event. Validation demonstrated that the use of this combined threshold provides better performance than the preparatory threshold alone, particularly in reducing false positives and improving predictive accuracy. The study shows that areas with more friable and "younger" volcanic materials, such as Sete Cidades and Furnas volcanoes, are the most susceptible to landslides, exhibiting lower normalised rainfall thresholds. The highest values of the monthly probabilities of threshold exceedance are associated with

December and January. It is also observed that both short-duration intense rainfall events and long-duration rainfall events are associated with return periods of less than five years.

Overall, this work provides a comprehensive, integrated, detailed, and innovative characterisation of the landslide hazard and its relationship with rainfall on the São Miguel Island, establishing a robust knowledge base for optimising risk prevention and management strategies under current and future geoclimatic threats.

RESUMO

Os movimentos de vertente representam o perigo natural mais frequente no arquipélago dos Açores, devido à sua origem e geomorfologia vulcânicas, à localização geográfica e ao enquadramento climático, caracterizado por elevados níveis de precipitação. Neste contexto, a compreensão dos fatores que controlam a ocorrência destes fenómenos e a sua evolução temporal constitui um elemento fundamental para a avaliação e mitigação do risco associado.

Este estudo baseia-se na base de dados documental NATHA (*Natural Hazards in Azores*), construída a partir da análise sistemática de fontes históricas e de arquivos de imprensa regional. Através desta base de dados, foi possível identificar e caracterizar os eventos de instabilidade geomorfológica ocorridos na ilha de São Miguel entre 1900 e 2020. Foram catalogados 236 eventos, responsáveis por 82 vítimas mortais, 41 feridos, 305 desalojados e pela destruição total ou parcial de 66 edifícios. A análise da distribuição espacial revelou diferenças significativas entre os municípios da ilha, sendo o município da Povoação mais afetado, registando cerca de 59% do total de vítimas mortais. A precipitação foi responsável por cerca de 70% dos eventos catalogados, que ocorrem na sua maioria durante os meses mais húmidos do ano, entre novembro e março. A análise temporal revelou uma maior concentração de eventos após 1996, associada a alterações no regime de precipitação, demonstrando, pela primeira vez nos Açores, a influência das alterações climáticas na ocorrência de movimentos de vertente.

O estudo dos padrões e tendências da precipitação na ilha de São Miguel recorreu à análise de *clustering* hierárquico e a testes não-paramétricos de tendência. Foram identificados quatro *clusters* de precipitação homogéneos, que confirmam a existência de um forte efeito orográfico, em que a altitude desempenha o papel de principal regulador da precipitação. Foi observada uma forte correlação positiva entre a altitude e a precipitação, com um aumento de aproximadamente 180 mm de Precipitação Média Anual (PMA) por cada 100 m de altitude. A análise temporal mostrou reduções significativas na precipitação anual e sazonal, embora a frequência de dias com precipitação mais intensa tenha aumentado. Esta redução é particularmente crítica durante o outono e o inverno, com quebras máximas na precipitação entre 41% e 55%. O estudo sugere que a fase predominantemente positiva da Oscilação do Atlântico Norte (NAO) no período mais recente contribuiu, pelo menos em parte, para esta tendência de decréscimo da precipitação.

O estudo propõe uma abordagem inovadora para o desenvolvimento de limiares empíricos combinados de precipitação, integrando um limiar preparatório, relacionado com a saturação prévia do solo, e um limiar de desencadeamento, associado à precipitação no dia do evento. A validação demonstrou que a utilização deste limiar combinado apresenta um desempenho superior ao limiar preparatório isolado, nomeadamente na redução de falsos positivos e na melhoria da precisão preditiva. As áreas com materiais vulcânicos mais friáveis e "jovens", como os vulcões das Sete Cidades e das Furnas, são mais suscetíveis, evidenciando limiares de precipitação normalizados mais baixos. Os valores mais elevados das probabilidades mensais de excedência dos limiares, estão associados aos meses de dezembro e janeiro. Verifica-se, igualmente, que tanto os eventos de precipitação intensa de curta duração como os de longa duração estão associados a períodos de retorno inferiores a cinco anos.

Os resultados fornecem uma caraterização integrada, detalhada e inovadora do perigo de movimentos de vertente e da sua relação com a precipitação na ilha de São Miguel, estabelecendo uma base de conhecimento robusta para a otimização de estratégias de prevenção e gestão do risco no contexto das ameaças geoclimáticas atuais e futuras.

CHAPTER 1

1 | GENERAL INTRODUCTION

1.1 | Problem definition

Globally, about 56.9% of the world's population lives in urban areas and is expected to rise to 68% by 2050 (UNCTAD 2023). In the coming decades, the level of urbanisation is expected to increase in all regions, but with considerable variation. North America, Latin America and the Caribbean may reach 90% of urbanization by 2050, Europe 85%, Oceania just over 70% and Africa and Asia 59% and 66%, respectively. This demographic shift implies that more people and assets will be concentrated in hazard-prone areas, amplifying the risks and increasing the need for risk mitigation strategies and resilient urban planning.

Economic growth and technological development during the 20th century have paradoxically coincided with an increase in natural disasters. In recent decades, the frequency and severity of such events have risen sharply, and their devastating impacts, both economic and human, have shown almost exponential growth (Guha-Sapir et al. 2017). According to the International Disaster Database (EM-DAT), more than 17,297 natural disasters occurred worldwide between 1900 and 2024, with approximately 87% of the events recorded after 1980 (EM-DAT 2024). These disasters claimed more than 32 million lives, affected 8.8 billion people, and caused estimated economic losses of US$ 7.2 trillion (EM-DAT 2024). Despite the known limitations of EM-DAT (Jones et al. 2023), these figures underscore the global relevance of understanding and managing natural hazards.

The increase in natural disasters may be related to inadequate land-use planning, which has heightened human exposure to risks, particularly in large cities and along coastal regions (Hallegatte 2014). Even though natural disasters originate from Earth processes, their frequency and impacts are often intensified by climate change (Montanya and Valera 2016). The increase of intense droughts, storms, floods, and landslides are recognised as direct or indirect consequences of climate change (Parry et al. 2007; Knutson et al. 2010; Gariano and Guzzetti, 2016; Otto et al. 2018; Cook et al. 2018; Kimuli et al. 2021), whereas other hazards, such as earthquakes, tsunamis, and volcanic eruptions, show no clear increase in frequency (Cooper et al. 2018; Wang 2025).

Among these hazards, landslides show a clear increasing trend worldwide. Since 1900, landslides have affected approximately 14 million people, caused approximately 64,000 fatalities (EM-DAT 2024), and resulted in economic losses exceeding US$ 20.6 million (EM-DAT 2024). It is important to note that most landslide events are small-scale, causing limited material damage and few casualties; as such, they are often underrepresented in global disaster databases, such as EM-DAT, because the criteria for inclusion are generally restricted to large magnitude or high impact events. The true impact of landslides is also difficult to assess because the damages and fatalities associated with an event are sometimes attributed to its trigger or to other simultaneous events (e.g. storms, floods), leading to an underestimation of their true economic and social impacts (Nadim et al. 2006).

In Portugal mainland, landslides and floods claimed 1,251 human lives between 1865 and 2010 (an average of 8.6 per year), displaced 14,191 people and left 41,844 homeless. Flash floods and floods alone accounted for the majority of these impacts: 81 % of total deaths, 94.2 % of total displaced people and 96.3 % of total homeless people (Zêzere et al. 2014).

São Miguel Island (Azores, Portugal) has been affected by landslides since its settlement in the mid-fifteenth century. Several landslide events with significant socio-economic impact have been reported in historical accounts. The most catastrophic and deadliest event on record occurred on 22 October 1522, when an earthquake with a maximum intensity X (EMS-98) (Silveira et al. 2003) triggered several landslides across the island. The earthquake and an associated debris flow killed 5,000 people and destroyed the entire village of Vila Franca do Campo, the island's capital at that time (Frutuoso 1981). Since 1900, hundreds of damaging landslide events have been recorded (Marques 2013). More recently, on 31 October 1997, nearly 1,000 shallow landslides were triggered by intense rainfall (Gaspar et al. 1997; Marques et al. 2008), causing 29 fatalities in the village of Ribeira Quente, seven injuries, 69 people left homeless, and total economic losses estimated at €21.3 million (Cunha 2003). This event, the deadliest since the beginning of the 20th century, underscores the persistent threat posed by rainfall-triggered landslides on the island.

1.2 | Objectives and structure

The principal aim of this thesis is to investigate rainfall-triggered landslides on São Miguel Island. To achieve this aim, the thesis is structured around the following specific objectives, directly linked to the three scientific articles that compose this work:

1. Analyse the temporal and spatial distribution of landslide events and their impacts based on a historical database compiled from documentary sources, identifying the main triggering factors and seasonal patterns of occurrence;

2. Characterise the spatial and temporal variability of rainfall on São Miguel Island, identifying homogeneous rainfall regions and assessing annual and seasonal trends, as well as their relationships with altitude and large-scale atmospheric circulation patterns;

3. Define and evaluate rainfall thresholds for landslide initiation, integrating antecedent rainfall and event-day rainfall, and to assess their spatial variability in relation to local climatic conditions.

The thesis is organised into four chapters, each addressing a specific component of these objectives and collectively contributing to a comprehensive understanding of rainfall-induced landslide processes.

- **Chapter 1** sets the context for the study by discussing the growing exposure to natural disaster risks driven by global urbanisation. It highlights the near-exponential increase in both the frequency and impacts of natural disasters, particularly landslides, further intensified by factors such as inadequate land-use planning and climate change. This chapter also presents the thesis objectives and the conceptual background related to landslide databases, rainfall variability, and rainfall thresholds, introducing key methodologies underpinning this research, namely spatial clustering, trend analysis, and empirical rainfall threshold models derived from historical data;
- **Chapter 2** characterises landslide occurrence on São Miguel Island for the period 1900–2020 based on NATHA database. This chapter presents the analysis of: (i) temporal trends; (ii) geographic distribution; (iii) triggering factors; and (iv) impacts and spatiotemporal distribution of fatalities;
- **Chapter 3** presents a comprehensive analysis of the spatial and temporal rainfall patterns on São Miguel Island, identifying homogeneous rainfall regions using Ward's hierarchical clustering method, evaluating trends with the Mann–Kendall test and Sen's Slope Estimator, and investigating rainfall distribution in relation to altitude and the influence of the atmospheric circulation;
- **Chapter 4** proposes two combined rainfall thresholds to maximise landslide detection and reduce false alarms compared to a single-threshold approach. The methodology includes identifying landslide events in four rainfall stations (1977–2020), defining preparatory and trigger thresholds (R_{cum}– D and I_{D1} –D functions), performing back-analysis evaluation, normalising by Mean Annual Precipitation (MAP), and estimating of exceedance probability and return periods of landslide events.

1.3 | Conceptual framework

1.3.1 | Landslide databases

Interest in quantifying landslide risk began in 1971, when the International Association of Engineering Geology (IAEG) Commission on Landslides compiled a list of worldwide landslide events for UNESCO's annual summary of information on natural disasters. The data collected between 1971 and 1975 highlighted that landslides presented a significant global risk, accounting for about 14% of the total disaster related casualties (Varnes 1984).

In recent decades, the number of scientific publications on landslide risk assessment has grown substantially (Wu et al. 2015). The availability of well-organised, high-quality landslide databases and inventories is essential for reliable landslide risk assessment (van Westen et al. 2008; Taylor et al. 2015). Global landslide databases, such as the NASA Global Landslide Catalog and the Global Fatal Landslide Database (GFLD), provide valuable insights, while other databases (e.g. EM-DAT, NatCatSERVICE, GLIDE, DESINVENTAR) include landslide information, although these events are often aggregated under broader categories such as geophysical or climate-related hazards. Spatio-temporal analysis of global landslide records has highlighted the societal impacts of landslide occurrence and enabled the identification of geographic regions and countries most exposed to landslide hazard (Petley 2012).

Landslide databases play a crucial role in facilitating understanding and managing the risks associated with these phenomena. The systematic collection and analysis of landslide data improves understanding of the factors contributing to their occurrence, thereby supporting more effective prevention and mitigation strategies (Komac and Hribernik 2015). These databases compile historical records including location, frequency, magnitude, and conditioning and triggering factors (Gómez et al. 2023). Accurate inventories enable identification of high-risk areas, particularly in geomorphologically complex or urbanized regions, where the risk is higher. The analysis of landslide data provides the foundation for safe land-use planning, avoiding the occupation of susceptible areas and promoting the protection of lives and property (Ahmed 2015).

Despite the absence of an official natural disaster database in Portugal, several initiatives have emerged over the last two decades, often linked to MSc and PhD thesis conducted at universities, with scientific research as their main objective. In 2010, the Portuguese Foundation for Science and Technology funded the project *''DISASTER-GIS database on hydro-geomorphologic disasters in Portugal: a tool for environmental management and emergency planning*". The project aimed to create, exploit and disseminate a GIS database on disastrous floods and landslides occurred in the Portugal mainland from 1865 to 2010. Zêzere et al. (2014) present the database structure, as well as the spatial and temporal distribution of events, F-N curves and comparison with the EM-DAT database. The database includes a total of 1,621 floods and 281 landslides, compiled from 16 newspapers, involving the analysis of 145,344 individual issues.

In the Azores, many historical documents report the occurrence of natural events such as earthquakes, volcanic eruptions, degassing phenomena, storms, landslides, floods and tsunamis, which caused human fatalities and significant material losses. Marques (2004) and Marques et al. (2009) compiled and analyzed the historical documents describing the debris flow in Vila Franca do Campo triggered by the 22 October 1522 earthquake. This information was used to characterize the event and to define the starting points of the debris flow, subsequently used in probabilistic modeling of the debris flow propagation. Marques et al. (2008) compiled the flood and landslides events that occurred in the Povoação County (São Miguel Island) between 1976 and 2002 to define rainfall thresholds for landslide triggering and to analyse the temporal relationship between these events and the North Atlantic Oscillation (NAO). In a later work, Marques et al. (2010) updated this catalogue and redefined the rainfall thresholds, proposing the development of a Landslide Early-Warning System for Povoação County. Silva (2018) presents a historical synthesis of the landslides events that have affected the parish of Lajedo (Flores Island).

Marques (2013) describes the NATHA database (Natural Hazards in Azores), presenting the structure, the data collection methodology, the characterization of landslide events and the analysis of their temporal and spatial distribution. The present PhD thesis updated and modified the database structure. The NATHA database compiles information for cataloguing and characterizing natural events in the Azores archipelago, including earthquakes, volcanic eruptions, degassing phenomena, storms, landslides, floods and tsunamis. All relevant information from the analysed documents was collected and integrated into the database.

1.3.2 | The rainfall as a triggering factor for landslides

The triggering of a landslide results from the interaction of multiple factors, which can be classified according to their function and timescale. The categories of factors that promote slope instability are widely recognised, including the intrinsic characteristics of the terrain (geology, geomorphology, soil/rock properties), physical processes, and anthropogenic processes (Popescu 1994; Wieczorek 1996).

Crozier and Glade (2005) proposed three stages of slope stability: preparatory, predisposing, and triggering factors. Ground characteristics (e.g. geology, slope) always act as predisposing factors for slope instability. The remaining factors can act as preparatory or triggering, depending on their intensity, duration, and the previous stability stage of the slope.

Predisposing factors are static terrain properties that condition the potential degree of slope instability, acting as catalysts that allow other destabilising factors to operate more effectively (Crozier and Glade 2005). Preparatory factors are dynamic and can promote a decrease in slope stability without directly triggering the movement; these processes can occur over varying time periods (Crozier and Glade 2005). Triggering factors directly initiate landslides, arising from geomorphological, physical, or anthropogenic processes, and act as the immediate stimulus for the event (Crozier and Glade 2005).

Rainfall is globally recognised as the most important landslide triggering factor (McColl 2022). Water infiltrates increasing the pore water pressure, reducing effective stress and, consequently, soil or rock mass shear strength (Schuster and Wieczorek 2002). In rock masses, water may also generate hydrostatic pressures within fractures. However, the role of rainfall in slope rupture is indirect, since landslides occur due to a temporary loss of shear strength caused by an increase in pore water pressure (Campbell 1975). Furthermore, groundwater conditions that cause slope instability are linked to rainfall via infiltration, soil characteristics and antecedent moisture conditions resulting from previous rainfall (Sidle et al. 2019). Effective antecedent rainfall is considered one of the most influential factors in landslides occurrence, as it captures the cumulative effect of rainfall on the initial soil moisture content (Cheng et al. 2025).

Different hydrological mechanisms are related to different landslides typologies. Shallow translational soil slips form on steep slopes at a critical depth of less than 1-2 m. (Van Asch et al. 1999), typically triggered by heavy rainfall of 1–15 days duration (Zêzere et al. 2005). The critical reduction in soil shear resistance and resulting slope failure is caused by a rapid rise in pore water pressure and a loss of soil apparent cohesion due to saturation (Iverson 2000). Deep-seated landslides (5-20 m depth) usually result from a steady rise in groundwater level, reducing shear strength of the involved rocks and soils (Van Asch et al. 1999). This type of landslide activity is typically associated with weeks of near-constant rainfall over periods ranging from 30 to 90 days (Zêzere et al. 2005). Debris flow is typically associated with intense short duration rainfall and their triggering factor is often associated with the formation of concentrated runoff (Zêzere et al. 2015). Surface runoff, whether in saturated or unsaturated soil conditions, provides water to debris materials accumulated in channels, raising pore pressure within the debris mass and potentially initiating debris flow (Van Asch et al. 1999).

1.3.3 | Rainfall spatial and temporal variability analysis

Rainfall distribution is determined by multiple factors that interact in complex ways. The spatial and temporal variability of rainfall represents one of the main challenges in climatological and hydrological analyses, as its understanding is hindered by the combined influence of multiple factors that extend beyond local physiographic elements, including processes associated with atmospheric circulation and ocean–atmosphere interactions (Glawion et al. 2024).

Regional atmospheric circulation represents one of the main mechanisms controlling rainfall in specific territories. Dominant pressure systems exert a particular influence on rainfall variability, determining the trajectory of storm systems and the duration of wet and dry periods (Hakam et al. 2025). Changes in large-scale atmospheric pressure configurations, particularly those associated with modes of variability such as the Arctic Oscillation and the North Atlantic Oscillation, significantly modulate regional rainfall (Busuioc et al. 2001; Unal et al. 2012).

Orographic effects significantly shape rainfall patterns through the uplift of moist air masses, adiabatic cooling, and the formation of rain shadow zones (Zhang et al. 2025). Maximum rainfall occurs on windward slopes, while leeward areas receive reduced amounts (Pamungkas et al. 2025). Rainfall efficiency depends on wind speed, atmospheric stability, and the height of the topographic barrier (Cornejo et al. 2024), with orographic mechanisms contributing more than 50% of total rainfall during extreme events (Xu et al. 2025). Altitude is a critical factor, with rainfall increasing up to a peak that depends on local atmospheric circulation (Xu et al. 2021). Slope orientation and topographic complexity modulate rainfall through their effects on moisture convergence (Yang et al. 2025). Thus, an integrated understanding of these factors is essential for characterising the rainfall regimes and supporting water resource management and climate change adaptation decisions.

Temporal rainfall trends are fundamental for understanding climate change impacts and for the effective management of water resources. Statistical methods for rainfall trend analysis include non-parametric tests and complementary graphical approaches (Ayala and Palance 2025). The Mann–Kendall test detects statistically significant monotonic trends in time series, while Sen's slope estimator quantifies the magnitude of change per unit of time (Gül 2025). Innovative Trend Analysis (ITA) provides a graphical approach that visualises changes across different data levels and is more efficient because it does not require assumptions such as those associated with parametric tests (Yetik et al. 2023). Complementarily, the Spearman correlation test validates trend results, while tests such as Pettitt and Worsley identify abrupt change points in the series (Kaushal et al. 2025).

The identification of spatial clusters of rainfall stations, based on the characterisation of the rainfall regime, represents a fundamental step in the sectorisation of a territory. This approach allows the region to be divided into homogeneous parcels, accounting for the spatial variability of rainfall and other climatic factors (Santos et al. 2014).

Various approaches have been employed in scientific literature to examine spatial rainfall patterns, including L-moments (Guttman 1993; Modarres and Sarhadi 2011), k-means clustering (Isik and Singh 2008; Machiwal et al. 2017), regional frequency analysis (Medina-Cobo et al. 2017), harmonic analysis (Suhaila and Jemain 2009), spatial correlation functions (Şen and Habib 2001), multivariate regression (Sabziparvar et al. 2015), empirical orthogonal functions (Jebari et al. 2009; Santos et al. 2017), Pearson's correlation (Haines and Olley 2017), support vector machines (Lin et al. 2017), and spatial interpolation (Gupta et al. 2017).

Cluster analysis has been widely applied in classification studies (Jackson and Weinand 1995). Unlike statistical techniques that rely on predefined distributions, it groups data based on observed similarities. Clustering methods can be hierarchical or non-hierarchical, with the latter more commonly used. Hierarchical clustering organizes clusters in a structured way, reflecting similarities or differences through either a top-down or bottom-up approach. This involves progressively merging the closest data points based on the shortest distance until all are grouped. Ward's hierarchical method (Ward 1963) is often employed for climate and hydrology classification, as it consistently outperforms other techniques (e.g. Masoodian 1998; Domroes et al. 1998; Unal et al. 2003; Martin et al. 2007; Lyra et al. 2014).

Sectorisation of study areas can be very useful for a more refined definition of rainfall thresholds associated with landslide triggering (Valenzuela et al. 2019). This approach improves model calibration, ensuring that rainfall thresholds are adjusted to the specifics of each sector, reducing false alarms and detection failures (Calvello et al. 2014). It also allows for the optimisation of early warning systems, enabling more effective interventions, as well as improving the allocation of resources for disaster prevention and response (Segoni et al. 2015). Furthermore, it supports urban and land-use planning, reducing exposure to geotechnical risks.

1.3.4 | Rainfall thresholds for landslide occurrence

Rainfall thresholds link rainfall patterns to landslide events, defining critical values of intensity or duration indicating high likelihood of slope failure (Caracciolo et al. 2017; Martinović et al. 2018). They vary according to local characteristics, such as topography, soil type, and vegetation cover, and are essential for predicting landslide occurrences and for developing early warning systems.

Early warning systems use these rainfall thresholds to monitor weather conditions in real time and issue alerts and alarms when landslides risk increases (Wei et al. 2018). This preventive approach significantly contributes to reducing damage by allowing measures such as preventive evacuations (Abraham et al. 2020). However, the effectiveness of these systems depends on the quality and comprehensiveness of the available databases.

Although previous studies relate rainfall amount required for landslide triggering, Caine (1980) proposes for the first time a global minimum thresholds for shallow landslides through a potential equation based on rainfall intensity-duration conditions. Rainfall thresholds have since become widely used and are the subject of many scientific studies (e.g. De Vita et al. 1998; Guzzetti et al. 2007, 2008; Marques et al. 2008; Zêzere et al. 2015; Segoni et al. 2018; Sun et al. 2023).

Empirically based models rely on statistical analysis of rainfall records in combination with historical records of landslide occurrence, allowing the identification of rainfall thresholds above which the probability of slope instability increases significantly. The spatial scale of application of these thresholds can vary. Initially, Guzzetti et al. (2007) distinguished three levels: global, regional, and local. Global thresholds are derived from international datasets and provide general values, independent of local climatic and geological conditions (Caine 1980; Hong and Adler, 2008). Regional thresholds are defined for areas with similar meteorological, geological, and morphological characteristics (Leonarduzzi and Molnar 2020), while local thresholds correspond to single landslide events or limited areas ranging from a few metres to several hundred square kilometres (Giannecchini 2005). Segoni et al. (2018) proposed a more detailed classification based on geographical and administrative boundaries, distinguishing global, national, regional, basin-scale, local, and slope-scale thresholds. The scale of analysis directly influences data resolution and, consequently, the accuracy and reliability of the thresholds obtained.

Various types of empirical rainfall thresholds can be defined according to the rainfall variables considered. Event-based thresholds include intensity–duration (ID) relationships, the most common, linking maximum intensity to rainfall duration and exhibiting asymptotic behaviour for short durations (Brunetti et al. 2010; Staley et al. 2013; Ma et al. 2015). Other formats include event-duration (ED) thresholds, relating event duration to cumulative rainfall (Peruccacci et al. 2017; He et al. 2020), and event-intensity (EI) thresholds, linking total rainfall to average intensity (Onodera et al. 1974). Antecedent rainfall is also critical, particularly for deep-seated landslides triggered by prolonged rainfall, and is expressed as accumulated rainfall over different temporal windows (Martelloni et al. 2012; Nafarzadegan et al. 2013). There are also studies that combine event rainfall with antecedent rainfall to improve predictive capability (Pereira and Zêzere 2012; Lee et al. 2015).

In some cases, thresholds are normalised using Mean Annual Precipitation (MAP) or mean monthly rainfall (MDP), facilitating comparisons across climatically and geologically diverse areas (Glade et al. 2000; Mathew et al. 2014; He et al. 2020). Other approaches integrate simplified hydroclimatic or hydrological models, particularly where detailed geotechnical or meteorological data are lacking (Jakob and Weatherly 2003). Notably, the trigger–cause framework proposed by Bogaard and Greco (2018) integrates antecedent hydrological conditions and rainfall triggers through soil water balance calculations, providing an effective conceptual tool for understanding landslide initiation.

Recent advances have emphasised probabilistic approaches, which assign confidence levels to rainfall thresholds and reduce false alarms (Peres et al. 2018; Gariano et al. 2023), as well as the incorporation of high-resolution spatial rainfall datasets derived from radar and gridded products (Millán-Arancibia et al. 2023). Furthermore, machine learning techniques are increasingly applied to explore non-linear relationships between rainfall and landslide occurrence, enabling the development of more adaptive and dynamic thresholds suitable for varying environmental conditions and future climate scenarios (Han and Semnani 2025).

Rainfall thresholds used to predict landslides are often evaluated for their effectiveness using the ROC (Receiver Operating Characteristic) metric, which is widely applied in the validation of landslide susceptibility models (e.g. Beguería 2006; Mathew et al. 2014; Zêzere et al. 2015). The ROC metric is based on the analysis of a confusion matrix, which organises the results into four main categories: true positives (correctly predicted events), false positives (incorrectly predicted events), true negatives (correctly predicted non-events), and false negatives (unpredicted events) (Chicco and Jurman 2023).

The most commonly used ROC metrics are described by Staley et al. (2013). The true positive rate (TP_{rate}) measures the proportion of landslide occurrences correctly identified based on the threshold. The false positive rate (FP_{rate}) indicates the percentage of rainfall events above the threshold that have no corresponding landslide data. The false alarm rate (FA_{rate}) reflects the proportion of incorrect predictions relative to the total number of rainfall events exceeding the threshold. Lastly, the threat score (TS) is used to evaluate the threshold that optimises correct predictions while minimising false positive (FP) and false negative (FN) rates.

This approach enables the measurement of sensitivity (the proportion of correctly predicted events) and specificity (the proportion of correctly predicted non-events), generating an ROC curve that relates these two metrics (e.g. Gariano et al. 2015; Rosi 2023). This technique helps to identify the ideal balance between minimising false alarms and maximising the detection of actual events, which is essential for early warning systems and risk management strategies.

In recent years, research in this field has evolved significantly with the incorporation of machine learning (ML) and artificial intelligence (AI) to enhance the predictive capability of thresholds (Chiang et al. 2022; Zhu et al. 2025). Models such as random forests, neural networks, and gradient boosting are being employed to analyse large volumes of rainfall data, soil sensor records, and topographic information (Distefano et al. 2022; Villaça et al. 2024; Shao et al. 2025).

Moreover, the integration of high-resolution remote sensing data, such as from Synthetic Aperture Radar (SAR) satellites and drones, has provided more detailed monitoring of slope conditions, allowing the refinement of thresholds (Filho 2021; Chen et al. 2025; Cheng et. 2025). This combination of new technologies and advanced methodologies aims to develop increasingly accurate and adaptable warning systems tailored to the specific characteristics of different regions.

References

Abraham, M. T., Satyam, N., Pham, B. T., Pradhan, B., Segoni, S. & Bulzinetti, M. A. (2020). Using Field-Based Monitoring to Enhance the Performance of Rainfall Thresholds for Landslide Warning. *Water*, *12*(12), 3453. https://doi.org/10.3390/w12123453

Ahmed, B. (2015). Landslide susceptibility modelling applying user-defined weighting and data-driven statistical techniques in Cox's Bazar Municipality, Bangladesh. *Natural Hazards*, *79*(3), 1707–1737. https://doi.org/10.1007/s11069-015-1922-4

Ayala, J. J. H., & Palance, M. (2025). Exploring trends in Earth's precipitation using satellite-gauge estimates from NASA's GPM-IMERG. *Earth*, 6(4). https://doi.org/10.3390/earth6040130

Beguería, S. (2006). Validation and evaluation of predictive models in hazard assessment and risk management. *Natural Hazards*, *37*(3), 315-329. https://doi.org/10.1007/s11069-005-5182-6

Bogaard, T. & Greco, R. (2018). Invited perspectives: Hydrological perspectives on precipitation intensity-duration thresholds for landslide initiation: proposing hydro-meteorological thresholds. *Natural Hazards and Earth System Sciences*, *18*(1), 31-39. https://doi.org/10.5194/nhess-18-31-2018

Brunetti, M. T., Peruccacci, S., Rossi, M., Luciani, S., Valigi, D. & Guzzetti, F. (2010). Rainfall thresholds for the possible occurrence of landslides in Italy. *Natural Hazards and Earth System Sciences*, *10*(3), 447–458. https://doi.org/10.5194/nhess-10-447-2010

Busuioc, A., Chen, D., & Hellström, C. (2001). Temporal and spatial variability of precipitation in Sweden and its link with the large-scale atmospheric circulation. *Tellus A: Dynamic Meteorology and Oceanography*, 53(3), 348–367. https://doi.org/10.3402/tellusa.v53i3.12193

Caine, N. (1980). The rainfall intensity–duration control of shallow landslides and debris flows. Geografiska Annaler: Series A, Physical Geography, 62(1–2), 23–27. https://doi.org/10.2307/520449

Calvello, M., D'Orsi, R. N., Piciullo, L., Paes, N., Magalhaes, M. & Lacerda, W. A. (2014). The Rio de Janeiro early warning system for rainfall-induced landslides: Analysis of performance for the years 2010–2013. *International Journal of Disaster Risk Reduction*, *12*, 3–15. https://doi.org/10.1016/j.ijdrr.2014.10.005

Campbell, R.H. (1975). Soil slips, debris flows and rainstorms in the Santa Monica Mountains and vicinity, Southern California. *U.S. Geological Survey Professional Paper 851*, Denver, Colorado, 51 p. https://doi.org/10.3133/pp851

Caracciolo, D., Arnone, E., Conti, F. L. & Noto, L. V. (2017). Exploiting historical rainfall and landslide data in a spatial database for the derivation of critical rainfall thresholds. *Environmental Earth Sciences*, *76*(5). https://doi.org/10.1007/s12665-017-6545-5

Chen, B., Maurer, J. & Gong, W. (2025). Applications of UAV in landslide research: a review. Landslides 22, 3029–3048. https://doi.org/10.1007/s10346-025-02547-2

Cheng, C., Li, Y., Zhu, D., Liu, Y., Wu, Y., Lin, D. & Guo, H. (2025). Rain-Induced Shallow Landslide Susceptibility Under Multiple Scenarios Based on Effective Antecedent Precipitation. *Applied Sciences*, *15*(11), 6241. https://doi.org/10.3390/app15116241

Cheng, Y., Pang, H., Li, Y., Fan, L., Wei, S., Yuan, Z. & Fang, Y. (2025). Applications and advancements of spaceborne InSAR in landslide monitoring and susceptibility mapping: a systematic review. *Remote Sensing*, *17*(6), 999. https://doi.org/10.3390/rs17060999

Chiang, J. L., Kuo, C. M. & Fazeldehkordi, L. (2022). Using deep learning to formulate the landslide rainfall threshold of the potential large-scale landslide. *Water*, *14*(20), 3320. https://doi.org/10.3390/w14203320

Chicco, D. & Jurman, G. (2023). The Matthews correlation coefficient (MCC) should replace the ROC AUC as the standard metric for assessing binary classification. *BioData Mining*, *16*(1), 4. https://doi.org/10.1186/s13040-023-00322-4

Cook, B. I., Mankin, J. S. & Anchukaitis, K. J. (2018). Climate change and drought: From past to future. *Current Climate Change Reports*, *4*(2), 164-179. https://doi.org/10.1007/s40641-018-0093-2

Cooper, C., Swindles, G., Savov, I., Schmidt, A., & Bacon, K. (2018). Evaluating the relationship between climate change and volcanism. https://doi.org/10.1016/j.earscirev.2017.11.009

Cornejo, I. C., Rowe, A. K., Rasmussen, K. L., & DeHart, J. C. (2024). Orographic controls on extreme precipitation associated with a Mei-yu front. *Monthly Weather Review*. https://doi.org/10.1175/MWR-D-23-0170.1

Crozier, M.J. & Glade, T. (2005). Landslide hazard and risk: issues, concepts and approach. *In*: Glade, T., Anderson, M.G. and Crozier, M.J. (Eds.), *Landslide risk assessment*. John Wiley, 1-40. https://doi.org/10.1002/9780470012659.ch1

Cunha, A. (2003). The October 1997 landslides in São Miguel Island, Azores, Portugal. In: Hervás, J. (ed.) Lessons Learnt from Landslide Disasters in Europe. European Commission Joint Research Center, Ispra, Italy, 27–32.

De Vita, P., Reichenbach, P., Bathurst, J. C., Borga, M., Crosta, G., Crozier, M. J., Glade, T., Guzzetti, F., Hansen, A. & Wasowski, J. (1998). Rainfall-triggered landslides: a reference list. *Environmental Geology*, *35*(2), 219–233. https://doi.org/10.1007/s002540050308

Distefano, P., Peres, D. J., Scandura, P. & Cancelliere, A. (2022). Brief communication: Introducing rainfall thresholds for landslide triggering based on artificial neural networks. *Natural Hazards and Earth System Sciences*, *22*(4), 1151-1157. https://doi.org/10.5194/nhess-22-1151-2022

Domroes, M., Kaviani, M. & Schaefer, D. (1998) An Analysis of Regional and Intra-annual Rainfall Variability over Iran using Multivariate Statistical Methods. Theor Appl Climatol 61, 151–159. https://doi.org/10.1007/s007040050060

EM-DAT (2024). The OFDA/CRED International Disaster Database, www.emdat.be.

Filho, G. M. R. (2021). Performance of rainfall threshold for flood identification from ground-and satellite-based (sub) daily data. PhD thesis in Civil and Environmental Engineering with emphasis on Water Resources. Federal University of Paraíba.

Frutuoso, G. [1522–91] (1981). Livro Quarto das Saudades da Terra. In: Frutuoso, G. (ed.) Saudades da Terra, 2ª edn. Instituto Cultural de Ponta Delgada, Ponta Delgada, II, 285–327.

Gariano, S. L. & Guzzetti, F. (2016). Landslides in a changing climate. *Earth-science reviews*, *162*, 227-252. https://doi.org/10.1016/j.earscirev.2016.08.011

Gariano, S. L., Brunetti, M. T., Iovine, G., Melillo, M., Peruccacci, S., Terranova, O., ... & Guzzetti, F. (2015). Calibration and validation of rainfall thresholds for shallow landslide forecasting in Sicily, southern Italy. *Geomorphology*, *228*, 653-665. https://doi.org/10.1016/j.geomorph.2014.10.019

Gariano, S. L., Melillo, M., Brunetti, M. T., Kumar, S., Mathiyalagan, R. & Peruccacci, S. (2023). Challenges in defining frequentist rainfall thresholds to be implemented in a landslide early warning system in India. In *Progress in Landslide Research and Technology, Volume 1 Issue 1, 2022* (pp. 409-416). Cham: Springer International Publishing. https://doi.org/10.1007/978-3-031-16898-7_27

Gaspar, J. L., Wallenstein, N., Coutinho, R., Ferreira, T., Queiroz, G., Pacheco, J., ... & Malheiro, A. (1997). Considerações sobre a ocorrência dos movimentos de massa registados na madrugada de 31 de Outubro de 1997 na ilha de S. *Miguel, Açores, Relatório Técnico-científico*, *17*.

Giannecchini, R. (2005). Rainfall triggering soil slips in the southern Apuan Alps (Tuscany, Italy). *Advances in Geosciences*, *2*, 21–24. https://doi.org/10.5194/adgeo-2-21-2005

Glade, T., Crozier, M. J. & Smith, P. (2000). Applying Probability Determination to Refine Landslide-triggering Rainfall Thresholds Using an Empirical "Antecedent Daily Rainfall Model''. *Pure and Applied Geophysics*, *157*(6), 1059-1079. https://doi.org/10.1007/s000240050017

Glawion, L., Polz, J., Kunstmann, H., Fersch, B., & Chwala, C. (2024). Global spatio-temporal ERA5 precipitation downscaling to km and sub-hourly scale using generative AI. *npj Climate and Atmospheric Science*. https://doi.org/10.1038/s41612-025-01103-y

Gómez, D., García, E. F. & Aristizábal, E. (2023). Spatial and temporal landslide distributions using global and open landslide databases. Natural Hazards, 117(1), 25–55. https://doi.org/10.1007/s11069-023-05848-8

Guha-Sapir, D., Hoyois, P., Wallemacq, P. & Below, R. (2017). Annual disaster statistical review 2016. Technical report, Centre for Research on the Epidemology of Disasters (CRED). http://emdat.be/sites/default/files/adsr 2016.pdf.

Gül, B. (2025). Investigation of precipitation data of Diyarbakır province with different trend analysis methods. *Kahramanmaraş Sütçü İmam Üniversitesi Mühendislik Bilimleri Dergisi*. https://doi.org/10.17780/ksujes.1567174

Gupta, A., Kamble, T. & Machiwal, D. (2017) Comparison of ordinary and Bayesian kriging techniques in depicting rainfall variability in arid and semi-arid regions of north-west India. Environmental Earth Sciences, 76, 512. https://doi.org/10.1007/s12665-017-6814-3

Guttman, N. B. (1993) The use of L-moments in the determination of regional rainfall climates. Journal of Climate, 6, 2309–2325. https://doi.org/10.1175/1520-442(1993)006%3C2309:TUOLMI%3E2.0.CO;2

Guzzetti, F., Peruccacci, S., Rossi, M. & Stark, C. P. (2007). Rainfall thresholds for the initiation of landslides in central and southern Europe. Meteorology and Atmospheric Physics, 98(3–4), 239–267. https://doi.org/10.1007/s00703-007-0262-7

Guzzetti, F., Peruccacci, S., Rossi, M. & Stark, C. P. (2008). The rainfall intensity–duration control of shallow landslides and debris flows: an update. *Landslides*, *5*(1), 3-17. https://doi.org/10.1007/s10346-007-0112-1

Haines, H.A. & Olley, J.M. (2017) The implications of regional variations in rainfall for reconstructing rainfall patterns using tree rings. Hydrological Processes, 31, 2951–2960. https://doi.org/10.1002/hyp.11238

Hakam, O., Bouras, E. H., Amazirh, A., Ongoma, V., Eddamiri, S., Saidi, L., Zerouali, A., & Chehbouni, A. (2025). Influence of atmospheric and oceanic circulation patterns on precipitation variability in North Africa with a focus on Morocco. *Scientific Reports*, 15. https://doi.org/10.1038/s41598-025-02718-0

Hallegatte, S. (2014). Natural disasters and climate change. *Cham: Springer International Publishing*. https://doi.org/10.1007/978-3-319-08933-1

Han, Y. & Semnani, S. J. (2025). Important considerations in machine learning-based landslide susceptibility assessment under future climate conditions. *Acta Geotechnica*, *20*(1), 475-500. https://doi.org/10.1007/s11440-024-02363-3

He, S., Wang, J. & Liu, S. (2020). Rainfall event–duration thresholds for landslide occurrences in China. *Water*, *12*(2), 494. https://doi.org/10.3390/w12020494

Hong, Y. & Adler, R. F. (2008). Predicting global landslide spatiotemporal distribution: Integrating landslide susceptibility zoning techniques and real-time satellite rainfall estimates. *International Journal of Sediment Research*, *23*(3), 249–257. https://doi.org/10.1016/S1001-6279(08)60022-0

Isik, S. & Singh, V.P. (2008) Hydrologic regionalization of watersheds in Turkey. Journal of Hydrologic Engineering 13(9), 824-834. https://doi.org/10.1061/(ASCE)1084-0699(2008)13:9(824)

Iverson, R. M. (2000). Landslide triggering by rain infiltration. *Water Resources Research*, *36*(7), 1897–1910. https://doi.org/10.1029/2000WR900090

Jackson, I. J. & Weinand, H. (1995). Classification of tropical rainfall stations: a comparison of clustering techniques. *International Journal of Climatology*, *15*(9), 985-994. https://doi.org/10.1002/joc.3370150905

Jakob, M. & Weatherly, H. (2003). A hydroclimatic threshold for landslide initiation on the North Shore Mountains of Vancouver, British Columbia. *Geomorphology*, *54*(3-4), 137-156. https://doi.org/10.1016/S0169-555X(02)00339-2

Jebari, S., Berndtsson, R., Uvo, C. & Bahri, A. (2009) Regionalizing fine time-scale rainfall affected by topography in semi-arid Tunisia. Hydrological Sciences Journal, 52(6), 1199–1215. https://doi.org/10.1623/hysj.52.6.1199

Jones, R. L., Kharb, A. & Tubeuf, S. (2023). The untold story of missing data in disaster research: a systematic review of the empirical literature utilising the Emergency Events Database (EM-DAT). *Environmental Research Letters*, *18*(10), https://doi.org/10.1088/1748-9326/acfd42

Kaushal, A., Pyasi, S., Galkate, R. V., Shrivastava, R., Yadav, V. S., Patel, A., & Patel, L. (2025). Assessment of climatic trends and change points in the Western agro-climatic zone of Madhya Pradesh, India. *International Journal of Environment and Climate Change*, 15(11). https://doi.org/10.9734/ijecc/2025/v15i115135

Kimuli, J. B., Di, B., Zhang, R., Wu, S., Li, J. & Yin, W. (2021). A multisource trend analysis of floods in Asia-Pacific 1990–2018: implications for climate change in sustainable development goals. *International Journal of Disaster Risk Reduction*, *59*, 102237. https://doi.org/10.1016/j.ijdrr.2021.102237

Knutson, T. R., McBride, J. L., Chan, J., Emanuel, K., Holland, G., Landsea, C., ... & Sugi, M. (2010). Tropical cyclones and climate change. *Nature geoscience*, *3*(3), 157-163. https://doi.org/10.1038/ngeo779

Komac, M. & Hribernik, K. (2015). Slovenian national landslide database as a basis for statistical assessment of landslide phenomena in Slovenia. *Geomorphology*, *249*, 94–102. https://doi.org/10.1016/j.geomorph.2015.02.005

Lee, S., Won, J.-S., Jeon, S. W., Park, I., Lee, M. J. (2015). Spatial Landslide Hazard Prediction Using Rainfall Probability and a Logistic Regression Model. *Mathematical Geosciences*, *47*(5), 565–589. https://doi.org/10.1007/s11004-014-9560-z

Leonarduzzi, E. & Molnar, P. (2020). Deriving rainfall thresholds for landsliding at the regional scale: daily and hourly resolutions, normalisation, and antecedent rainfall.

Natural Hazards and Earth System Sciences, *20*(11), 2905–2919. https://doi.org/10.5194/nhess-20-2905-2020

Lin, G.F., Chang, M.J. & Wu, J.T (2017) A hybrid statistical downscaling method based on the classification of rainfall patterns. Water Resources Management, 31(1), 377–401. https://doi.org/10.1007/s11269-016-1532-2

Lyra, G.B., Oliveira-Júnior, J.F. & Zeri, M. (2014) Cluster analysis applied to the spatial and temporal variability of monthly rainfall in Alagoas state, Northeast of Brazil. Int J Climatol 34, 3546–3558. https://doi.org/10.1002/joc.3926

Ma, T., Li, C., Lu, Z. & Bao, Q. (2015). Rainfall intensity–duration thresholds for the initiation of landslides in Zhejiang Province, China. *Geomorphology*, *245*, 193-206. Peruccacci, S., Brunetti, M. T., Gariano, S. L., Melillo, M., Rossi, M. & Guzzetti, F. (2017). Rainfall thresholds for possible landslide occurrence in Italy. *Geomorphology*, *290*, 39-57. https://doi.org/10.1016/j.geomorph.2015.05.016

Machiwal, D., Dayal, D. & Kumar, S. (2017) Long-term rainfall trends and change points in hot and cold arid regions of India. Hydrological Sciences Journal, 62(7), 1050–1066. https://doi.org/10.1080/02626667.2017.1303705

Marques, R. (2004). *Contribuição para o conhecimento da instabilidade geomorfológica nos Açores: estudo de movimentos de vertente associados a diferentes mecanismos desencadeantes*. Tese de Mestrado no ramo de Geologia, especialidade de Vulcanologia e Riscos Geológicos. Departamento de Geociências. Universidade dos Açores. 147 p.

Marques, R. (2013). Estudo de movimentos de vertente no concelho da Povoação (ilha de São Miguel, Açores): inventariação, caracterização e análise da susceptibilidade. PhD Thesis in Geology, Geosciences Department, University of the Azores.

Marques, R., Zêzere, J. L., Trigo, R., Gaspar, J. L. & Trigo, I. (2008). Rainfall patterns and critical values associated with landslides in Povoação County (São Miguel Island, Azores): relationships with the North Atlantic Oscillation. Hydrological Processes, 22, 478–494. https://doi.org/10.1002/hyp.6879

Marques, R., Zêzere, J.L., Amaral, P., Gaspar, J.L. & Queiroz, G. (2010). Empirical Landslides Early-Warning System (ELEWS-Pov) development for the Povoação county (S. Miguel island, Azores) based on the application of the Generalized Extreme Values distribution (GEVd) for rainfalltriggering thresholds assessment. *In*: Bateira C., Soares, L., Gomes, A. E Chaminé, H.I. (Eds), *Proceedings of V Congresso Nacional de Geomorfologia*. Oporto, 8 - 11 december 2010. Associação Portuguesa de Geomorfólogos. 327-332.

Marques, R., Zêzere, J.L., Gaspar, J.L. & Amaral, P. (2009). Reconstituição e modelação probabilística da escoada detrítica de Vila Franca do Campo desencadeada pelo sismo de 22 de Outubro de 1522 (S. Miguel, Açores). *Publicações da Associação Portuguesa de Geomorfólogos*. VI: 175-182.

Martelloni, G., Segoni, S., Fanti, R. & Catani, F. (2012). Rainfall thresholds for the forecasting of landslide occurrence at regional scale. *Landslides*, *9*(4), 485–495. https://doi.org/10.1007/s10346-011-0308-2

Martin, T.N., Storck, L. & Dourado Neto, D. (2007) Simulação estocástica da radiacão fotossinteticamente ativa e da temperatura do ar por diferentes métodos. Pesquisa Agropecuária Brasileira 42(9), 1211–1219. https://doi.org/10.1590/S0100-204X2007000900001

Martinović, K., Gavin, K., Reale, C. & Mangan, C. (2018). Rainfall thresholds as a landslide indicator for engineered slopes on the Irish Rail network. *Geomorphology*, *306*, 40–50. https://doi.org/10.1016/j.geomorph.2018.01.006

Masoodian, S.A. (1998) An analysis of Tempo-Spatial variation or rainfall in Iran (Doctoral dissertation, University of Isfahan).

Mathew, J., Babu, D. G., Kundu, S., Kumar, K. V. & Pant, C. C. (2014). Integrating intensity–duration-based rainfall threshold and antecedent rainfall-based probability estimate towards generating early warning for rainfall-induced landslides in parts of the Garhwal Himalaya, India. *Landslides*, *11*(4), 575-588. https://doi.org/10.1007/s10346-013-0408-2

McColl, S. T. (2022). Landslide causes and triggers. In *Landslide hazards, risks, and disasters* (pp. 13-41). Elsevier. https://doi.org/10.1016/B978-0-12-818464-6.00011-1

Medina-Cobo, M.T., García-Marín, A.P., Estévez, J., Jiménez-Hornero, F.J. & Ayuso-Muñoz, J.L. (2017) Obtaining homogeneous regions by determining the generalized fractal dimensions of validated daily rainfall data sets. Water Resources Management, 31(7), 2333–2348. https://doi.org/10.1007/s11269-017-1653-2

Millán-Arancibia, C. & Lavado-Casimiro, W. (2023). Rainfall thresholds estimation for shallow landslides in Peru from gridded daily data. *Natural Hazards and Earth System Sciences*, *23*(3), 1191-1206. https://doi.org/10.5194/nhess-23-1191-2023

Modarres, R & Sarhadi, A. (2011) Statistically-based regionalization of rainfall climates of Iran. Global and Planetary Change, 75(1-2), 67-75. https://doi.org/10.1016/j.gloplacha.2010.10.009

Montanya, C. N. & Valera, P. (2016). Climate change and its impact on the incarcerated population: A descriptive review. *Social Work in Public Health, 31,* 348–357. https://doi.org/10.1080/19371918.2015.1137513

Nadim, F., Kjekstad, O., Peduzzi, P., Herold, C. & Jaedicke, C. (2006). Global landslide and avalanche hotspots. *Landslides*, *3*(2), 159-173. https://doi.org/10.1007/s10346-006-0036-1

Nafarzadegan, A. R., Talebi, A., Malekinezhad, H. & Emami, N. (2013). Antecedent rainfall thresholds for the triggering of deep-seated landslides (Case study: Chaharmahal & Bakhtiari province, Iran). *Ecopersia*, *1*(1), 23-39.

Onodera, T., Yoshinaka, R., Kazama, H. (1974). Slope failures caused by heavy rainfall in Japan. *Journal of the Japan Society of Engineering Geology*, *15*(4), 191–200. https://doi.org/10.5110/jjseg.15.191

Otto, F. E. L. , K. van der Wiel , G. J. van Oldenborgh , S. Philip , S. F. Kew , P. Uhe , & Cullen, H. (2018). Climate change increases the probability of heavy rains in Northern England/Southern Scotland like those of storm Desmond—A real-time event attribution revisited. *Environ. Res. Lett.*, *13*, 024006, https://doi.org/10.1088/1748-9326/aa9663.

Pamungkas, C. M. A., Maulidita, U., Maurits, Y., & Putrantijo, N. (2025). Transect analysis of orographic precipitation in the Mount Rinjani region: Case study of the Sembalun Valley. *International Journal of Geosciences and Environmental Studies*. https://doi.org/10.53697/ijgaes.v2i3.4976

Parry, M. L. (Ed.). (2007). Climate change 2007-impacts, adaptation and vulnerability: Working group II contribution to the fourth assessment report of the IPCC (Vol. 4). Cambridge University Press.

Pereira, S. & Zêzere, J. L. (2012). Empirically-based rainfall thresholds for debris flow occurrence in the North of Portugal. *XII Reunión Nacional de Geomorfología*, 109-112.

Peres, D. J., Cancelliere, A., Greco, R. & Bogaard, T. A. (2018). Influence of uncertain identification of triggering rainfall on the assessment of landslide early warning thresholds. *Natural Hazards and Earth System Sciences*, *18*(2), 633-646. https://doi.org/10.5194/nhess-18-633-2018

Peruccacci, S., Brunetti, M. T., Gariano, S. L., Melillo, M., Rossi, M., & Guzzetti, F. (2017). Rainfall thresholds for possible landslide occurrence in Italy. *Geomorphology, 290*, 39–57. https://doi.org/10.1016/j.geomorph.2017.03.031

Petley, D. (2012). Global patterns of loss of life from landslides. *Geology*, *40*(10), 927-930. https://doi.org/10.1130/G33217.1

Popescu, M. E. (1994). A suggested method for reporting landslide causes. *Bulletin de l'Association Internationale de Géologie de L'ingénieur*. 50: 71 – 74. https://doi.org/10.1007/BF02594958

Rosi, A. (2023). Exploring the Use of Pattern Classification Approaches for the Recognition of Landslide-Triggering Rainfalls. *Sustainability*, *15*(20), 15145. https://doi.org/10.3390/su152015145

Sabziparvar, A.A., Movahedi, S., Asakereh, H., Maryanaji, Z. & Masoodian, S.A. (2015) Geographical factors affecting variability of rainfall regime in Iran. Theoretical and Applied Climatology 120(1–2), 367–376. https://doi.org/10.1007/s00704-014-1174-3

Santos, E. B., Silva, C. M. S. E. & Lucio, P. S. (2014). Precipitation regionalization of the Brazilian Amazon. *Atmospheric Science Letters*, *16*(3), 185–192. https://doi.org/10.1002/asl2.535

Santos, M., Fragoso, M. & Santos, J. A. (2017) Regionalization and susceptibility assessment to daily rainfall extremes in mainland Portugal, Applied Geography. 86, 128-138. https://doi.org/10.1016/j.apgeog.2017.06.020

Schuster, R. L., & Wieczorek, G. F. (2002). Landslide triggers and types. In J. Rybar, J. Stemberk, & P. Wagner (Eds.), *Proceedings of the 1st European Conference on Landslides* (pp. 59–78). A. A. Balkema.

Segoni, S., Piciullo, L. & Gariano, S. L. (2018). A review of the recent literature on rainfall thresholds for landslide occurrence. Landslides, 15(8), 1483–1501. https://doi.org/10.1007/s10346-018-0966-4

Segoni, S., Rosi, A., Battistini, A., Moretti, S., Casagli, N., Catani, F., Lagomarsino, D. & Rossi, G. (2015). Technical Note: An operational landslide early warning system at regional scale based on space–time-variable rainfall thresholds. *Natural Hazards and Earth System Sciences*, *15*(4), 853–861. https://doi.org/10.5194/nhess-15-853-2015

Şen, Z. & Habib, Z. (2001) Monthly spatial rainfall correlation functions and interpretations for Turkey. Hydrological Sciences Journal, 46(4), 525–535. https://doi.org/10.1080/02626660109492848

Shao, X., Yan, W., Yan, C., Zhao, W., Wang, Y., Shi, X., ... & Jin, J. (2025). Explainable Machine Learning for Mapping Rainfall-Induced Landslide Thresholds in Italy. *Applied Sciences*, *15*(14), 7937. https://doi.org/10.3390/app15147937

Sidle, R. C., Greco, R. & Bogaard, T. (2019). Overview of Landslide Hydrology. *Water*, *11*(1), 148. https://doi.org/10.3390/w11010148

Silva, R. F. (2018) Desenvolvimento de um protótipo computacional para análise e cartografia automática da suscetibilidade a movimentos de vertente. Dissertação de Mestrado em Vulcanologia e Riscos Geológicos. Universidade dos Açores, Ponta Delgada. 142 p.

Silveira, D., Gaspar, J. L., Ferreira, T. & Queiroz, G. (2003). Reassessment of the historical seismic activity with major impact on S. Miguel Island (Azores). Natural Hazards and Earth System Sciences, 3, 1–8. https://doi.org/10.5194/nhess-3-615-2003

Staley, D. M., Kean, J. W., Cannon, S. H., Schmidt, K. M. & Laber, J. L. (2013). Objective definition of rainfall intensity-duration thresholds for the initiation of post-fire debris flows in southern California. *Landslides*, *10*(5), 547–562. https://doi.org/10.1007/s10346-012-0341-9

Suhaila, J. & Jemain, A.A. (2009) A comparison of the rainfall patterns between stations on the East and the West coasts of Peninsular Malaysia using the smoothing model of rainfall amounts. Meteorological Applications 16(3), 391–401. https://doi.org/10.1002/met.137

Sun, Y., Zhang, J., Wang, H. & Lu, D. (2023). Probabilistic thresholds for regional rainfall induced landslides. *Computers and Geotechnics*, *166*, 106040. https://doi.org/10.1016/j.compgeo.2023.106040

Taylor, F. E., Malamud, B. D., Freeborough, K. & Demeritt, D. (2015). Enriching Great Britain's national landslide database by searching newspaper archives. *Geomorphology*, *249*, 52-68. https://doi.org/10.1016/j.geomorph.2015.05.019

Unal, Y. S., Deniz, A., Toros, H., & Incecik, S. (2012). Temporal and spatial patterns of precipitation variability for annual, wet, and dry seasons in Turkey. *International Journal of Climatology*, 32(3), 392–405. https://doi.org/10.1002/joc.2274

Unal, Y., Kindap, T. & Karaca, M. (2003) Redefining the climate zones of Turkey using cluster analysis. Int J Climatol 23(9), 1045–1055. https://doi.org/10.1002/joc.910

UNCTAD (2023). UNCTAD Handbook of Statistics 2023. UN.

Valenzuela, P., Zêzere, J. L., Domínguez-Cuesta, M. J. & Mora García, M. A. (2019). Empirical rainfall thresholds for the triggering of landslides in Asturias (NW Spain). *Landslides*, *16*(7), 1285–1300. https://doi.org/10.1007/s10346-019-01170-2

Van Asch, T. W. J., Buma, J., & Van Beek, L. P. H. (1999). A view on some hydrological triggering systems in landslides. *Geomorphology, 30*(1–2), 25–32. https://doi.org/10.1016/S0169-555X(99)00042-2

Van Westen, C. J., Castellanos, E. & Kuriakose, S. L. (2008). Spatial data for landslide susceptibility, hazard, and vulnerability assessment: An overview. *Engineering geology*, *102*(3-4), 112-131. https://doi.org/10.1016/j.enggeo.2008.03.010

Varnes, D. J. (1984). Commission on the Landslides of the IAEG, UNESCO. *Landslide Hazard Zonation: A Review of Principles and Practice*, *3*, 61.

Villaça, C., Santos, P. P. & Zêzere, J. L. (2024). Modelling the rainfall threshold for shallow landslides considering the landslide predisposing factors in Portugal. *Landslides*, *21*(9), 2119-2133. https://doi.org/10.1007/s10346-024-02284-y

Wang, R. (2025). The interactions between earthquakes and climate. Applied and Computational Engineering. https://doi.org/10.54254/2755-2721/2025.20066

Ward, J.H.Jr. (1963) Hierarchical grouping to optimize an objective function. Journal of the American Statistical Association, 58, 236–244. https://doi.org/10.2307/2282967

Wei, L.-W., Huang, C.-M., Chi, C.-C., Chen, H., Chiu, C.-L. & Lee, C.-T. (2018). Adopting the rainfall index and landslide susceptibility for the establishment of an early warning model for rainfall-induced shallow landslides. *Natural Hazards and Earth System Sciences*, *18*(6), 1717–1733. https://doi.org/10.5194/nhess-18-1717-2018

Wieczorek, G. F. (1996). Landslide triggering mechanisms. *Transportation Research Board Special Report*, 247, 76-90.

Wu, X., Chen, X., Zhan, F. B. & Hong, S. (2015). Global research trends in landslides during 1991–2014: a bibliometric analysis. *Landslides*, *12*(6), 1215-1226. https://doi.org/10.1007/s10346-015-0624-z

Xu, L., Zheng, C., & Ma, Y. (2021). Variations in precipitation extremes in the arid and semi-arid regions of China. *International Journal of Climatology*, 41(3), 1542–1554. https://doi.org/10.1002/joc.6884

Xu, X., Huang, A., Zhang, Y., Yang, X., & Zhao, W. (2025). Impact of large-scale topography surrounding the Sichuan Basin on its regional hourly extreme precipitation in summer under specific weather patterns: A multi-case study. *Journal of Geophysical Research: Atmospheres*. https://doi.org/10.1029/2024JD042239

Yetik, A. K., Arslan, B., & Şen, B. (2024). Trends and variability in precipitation across Turkey: A multimethod statistical analysis. *Theoretical and Applied Climatology*, 155(1), 473–488. https://doi.org/10.1007/s00704-023-04645-4

Zêzere, J. L., Pereira, S., Tavares, A. O., Bateira, C., Trigo, R. M., Quaresma, I., ... & Verde, J. (2014). DISASTER: a GIS database on hydro-geomorphologic disasters in Portugal. *Natural hazards*, *72*(2), 503-532. https://doi.org/10.1007/s11069-013-1018-y

Zêzere, J. L., Trigo, R. M. & Trigo, I. F. (2005). Shallow and deep landslides induced by rainfall in the Lisbon region (Portugal): assessment of relationships with the North Atlantic Oscillation. *Natural Hazards and Earth System Sciences*, *5*(3), 331-344. https://doi.org/10.5194/nhess-5-331-2005

Zêzere, J. L., Vaz, T., Pereira, S., Oliveira, S. C., Marques, R., & Garcia, R. A. (2015). Rainfall thresholds for landslide activity in Portugal: A state of the art. *Environmental Earth Sciences, 73*(6), 2917–2936. https://doi.org/10.1007/s12665-014-3672-0

Zhang, M., Li, J., & Li, N. (2025). Steep orographic effects on local precipitation in the Hengduan Mountain region: Insights from an idealized modeling perspective. *Quarterly Journal of the Royal Meteorological Society*. https://doi.org/10.1002/qj.4931

Zhu, Y., Yin, K., Li, Y., Yang, H., Chen, H., Zhou, C. & Segoni, S. (2025). Leveraging artificial intelligence to quantify slope rainfall sensitivity for refining regional landslide rainfall thresholds. *Engineering Geology*, 108260. https://doi.org/10.1016/j.enggeo.2025.108260

CHAPTER 2

2 | SPATIAL DISTRIBUTION, TEMPORAL TRENDS AND IMPACT OF LANDSLIDES ON SÃO MIGUEL ISLAND FROM 1900 TO 2020 BASED ON AN ANALYSIS OF THE AZORES HISTORICAL NATURAL HAZARDS DATABASE

Abstract

Landslides are the most frequent type of natural hazard in the Azores archipelago, primarily due to the volcanic nature and geomorphological features of the islands. The NATHA (Natural Hazards in Azores) database is a repository of documents reporting those natural disaster events that have occurred on the Azores since their settlement in the mid–fifteenth century. This work presents and explores the landslide events that have occurred on São Miguel Island in the period 1900–2020. A total of 236 landslide events were catalogued. The temporal distribution of the landslide events reveals a higher concentration of events after 1996, which is related to a change in the rainfall regime but also to the increasing dissemination of information. The influence of climate change on landslide occurrence is demonstrated for the first time in the Azores. The landslide events catalogued in the NATHA database were responsible for 82 fatalities, 41 injuries and 305 people made homeless, while 66 buildings were partially or completely destroyed. The spatial distribution of landslide events shows that Povoação is the municipality most prone to landslide occurrence as well as to landslide impact. Rainfall was the triggering factor of most landslide events (70%) on São Miguel Island, and landslide events have been most frequent during the wettest months of the year from November to March. The obtained results demonstrate the need of landslides prevention and preparedness programs in specific areas of São Miguel Island.

Keywords: Landslides, Rainfall, NATHA database, São Miguel Island, Azores

Manuscript published in *Natural Hazards*

Journal Impact Factor: 3.7; 5-year Journal Impact Factor: 4.0

Silva, R.F., Marques, R. & Zêzere, J.L. (2024). Spatial distribution, temporal trends and impact of landslides on São Miguel Island from 1900 to 2020 based on an analysis of the Azores historical natural hazards database. Nat Hazards 120, 2617–2638. https://doi.org/10.1007/s11069-023-06296-0

2.1 | Introduction

According to EM–DAT (The International Disaster Database), since 1900 there have been more than 16,000 natural disasters worldwide that have resulted in 32 million deaths and nearly 5.9 trillion dollars in economic, social and environmental losses (EM–DAT 2022). The trend of increasing frequency and damage caused by natural disasters, particularly the occurrence of storms, floods, droughts and landslides, has been linked to climate change (Knutson et al. 2010, Cook et al. 2018, Froude and Petley 2018, Kimuli et al. 2021). The continuous growth of the world population, together with patterns of economic development, which have given rise to uncontrolled urbanization, leading many people to inhabit areas highly exposed to risk (Holcombe et al. 2016).

The compilation of data about any type of natural hazard (e.g. earthquakes, volcanic eruptions, storms, landslides, floods, tsunamis), including location, date of occurrence, triggering factors, economic and/or social impact, constitutes a primary approach to assess risk (Glade et al. 2001, Devoli et al. 2007, Van Den Eeckhaut and Hervás 2012). Moreover, reliable disaster databases are crucial for assessing the geographic distribution, temporal trends, the impact of a particular natural hazard type (Glade et al. 2001), and for evaluating the effectiveness of implemented measures to mitigate risk over time.

Natural hazards databases have different characteristics depending on their purpose and can be prepared based on various criteria and spatial and temporal scales. At the international, regional and national levels, there are several examples of natural and technological disasters databases. The EM–DAT is the most widely referenced database on disasters occurred worldwide (Panwar and Sen 2020). This database is compiled from diverse sources and includes data on natural and technological disasters occurred since 1900. However, EM–DAT employs stringent criteria for an event to be considered as a disaster and to be included in the database. An event must accomplish one of the following conditions: 1) occurrence of 10 or more fatalities; 2) existence of 100 or more affected people; 3) declaration of a state of emergency; and 4) request for international assistance. Since the criteria considered by EM–DAT are rather restrictive, many events that have occurred on the Azores, which caused significant economic and social losses, are not included in this database. The EM–DAT reports six natural disasters for Azores, including only one landslide event. Furthermore, there are errors in the information about natural disasters that occurred in the Azores, including inaccuracies in event dates and the number of fatalities.

Due to the geographic and geodynamic setting of the Azores archipelago, there is much geomorphologic evidence and numerous documental references that mention the occurrence of landslides over time, triggered by different factors (e.g. earthquakes, volcanic eruptions and rainfall). Landslides have been affecting São Miguel Island since its settlement in the mid-fifteenth century. Historical accounts have documented several landslide events with significant socio-economic impacts. On 22 October 1522, an earthquake with a maximum intensity X (EMS–98) (Silveira et al. 2003) triggered several landslides over the island, one of which was a debris flow of about 6.75x10^6 m^3 that covered an area of 4.5 km^2 (Marques et al. 2009). These landslides killed 5,000 people and destroyed the entire village of Vila Franca do Campo, the island's capital at that time (Frutuoso 1981). Through time, smaller landslides have been responsible for many deaths and generated major socio–economic impact in São Miguel. On 31 October 1997, about 1,000 landslides were triggered by a heavy rainfall episode (Gaspar et al. 1997), causing the death of 29 people in the parish of Ribeira Quente (Povoação municipality) together with 7 injuries and 69 people made homeless. An economic loss of 21.3 million euros was estimated for this event (Cunha 2003).

Landslide databases are fundamental tools used to assess landslide susceptibility, hazard and risk. They are important for supporting investigations regarding the spatial and temporal distribution of landslides and for predicting their occurrence in the future (Kirschbaum et al. 2015). Historical landslide databases have been developed for various countries and regions, mostly in Europe: such as Spain (Cuesta et al. 1999), Italy (Guzzetti et al. 2001; Niculiță et al. 2017; Piacentini et al. 2018), Ireland (Creighton 2006), United Kingdom (Foster et al. 2008), Norway (Jaedicke et al. 2009), Switzerland (Hilker et al. 2009), Greece (Kalantzi et al. 2010), Portugal (Zêzere et al. 2014; Pereira et al. 2014), Germany (Damm and Klose 2015), Albania (Jaupaj et al. 2017) and Czech Republic (Bíl et al. 2021). In other countries, such as Nicaragua (Devoli 2005), the United States of America (Elliott and Kirschbaum 2007), Canada (Septer 2007; Blais–Stevens et al. 2015), Nepal (Petley et al. 2007) and China (Li et al. 2016), there are also some studies on historical landslide databases. On a global scale, some authors have focused on compiling and comparing databases, analysing the data, and engaging in discussions regarding the rules for database construction and harmonization (e.g. Van Den Eeckhaut et al. 2013, Herrera et al. 2018, Gómez et al. 2023).

This paper aims to characterise the occurrence of landslides on São Miguel Island in the period 1900–2020 based on NATHA database (*Natural Hazards in Azores*; Marques 2013). The specific objectives of this work are: (1) to analyse the temporal trends of landslide events; (2) to analyse the geographic distribution of landslide events; (3) to analyse the triggering factors of landslide events; and (4) to analyse the impact and the spatiotemporal distribution of fatalities caused by landslide events.

2.2 | Study Area

The Azores archipelago is located in the North Atlantic Ocean and is composed of nine volcanic islands (Fig. 2.1). From a tectonic perspective, the archipelago is located at the triple junction between the Eurasian, African, and North American Plates. As a result of this context, seismic and volcanic events are common. However, landslides are the most prevalent type of geological hazard, primarily due to the volcanic composition and geomorphology F the islands (Marques 2013; Silva et al. 2018).

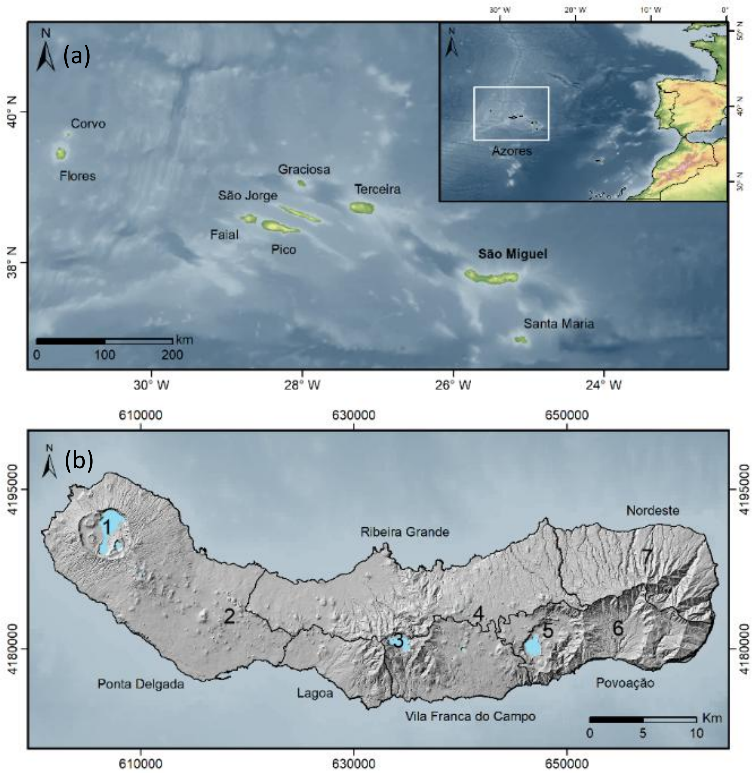

Figure 2.1 | (a) Geographic location and (b) municipalities (black lines) and morphostructural units of São Miguel Island: 1 – Sete Cidades Volcano; 2 – Picos Fissural Volcanic System; 3 – Fogo Volcano; 4 – Congro Fissural Volcanic System; 5 – Furnas Volcano; 6 – Povoacão Volcano and 7 – Nordeste Volcanic Complex.

São Miguel Island has an area of 744.6 km^2, with a maximum length of 64 km and width ranging between 8 and 15 km. The elevation ranges from 0 to1,143 m a.s.l. The island has a total of 133,390 inhabitants (INE 2021), divided into six municipalities: Lagoa, Nordeste, Ponta Delgada, Povoação, Ribeira Grande and Vila Franca do Campo (Fig. 2.1b). There are 3 active central volcanoes on the island, all with summit calderas: Furnas Volcano (Guest et al. 1999, 2015), Fogo Volcano (Wallenstein 1999; Wallenstein et al. 2015) and Sete Cidades Volcano (Queiroz 1997; Queiroz et al. 2015). Landslides commonly occur in distinct morphological structures characterised by steep slopes, such as the inner walls of calderas volcanoes, fault scarps, sea cliffs, and stream valleys, mostly composed of non–cohesive materials (pumice deposits) (Fig. 2.2a).

The central volcanoes are connected by the two fissural volcanic systems: Picos (Ferreira 2000; Ferreira et al. 2015) and Congro (Booth et al. 1978; Guest et al. 1999). The presence of extensive outcrops of basaltic lava flows and scoria strongly influences the morphology of the Picos Fissural Volcanic System. This region is characterised by gentle slopes and a poorly developed drainage network. Landslides in this area are mostly concentrated along the sea cliffs. Congro Fissural Volcanic System is dominated by scoria cones and associated lava flows. Additionally, there are some pumice cones, domes and maars. The entire area is covered by thick pumice fallout deposits from explosive eruptions of Fogo and Furnas volcanos. This area corresponds to an elevated region in the axial zone with elevations exceeding 500 m a.s.l. and gentle slopes that rise as it approaches the north and south coastlines. Landslides are common in this region, particularly along coastal cliffs and in deep narrow valleys.

The Nordeste Volcanic System and the Povoação Volcano are the oldest geologic formations of the island (Duncan et al. 2015). The Nordeste Volcanic System corresponds to a shield volcano composed mainly of basaltic lavas, which was subjected to extensive erosion that occurred both during and after the volcano activity. Povoação Volcano has an early lava shield followed by explosive trachytic activity and caldera collapse. Landslides affecting the Nordeste Volcanic System occur in areas where weathered basaltic lava flows (s.l.) are combined with steep slopes and very deep narrow valleys where intense fluvial erosion occurs. In Povoação Volcano, landslides are associated with the non–cohesive materials, predominantly pumice, which underwent significant erosion both during and after its volcanic activity (Fig. 2.2b).

Figure 2.2 | Examples of damaging landslide occurrences in (a) Furnas Volcano and (b) Povoação Volcano.

According to the Köppen–Geiger climate classification (Köppen 1936), the Azores has a temperate climate (C). Due to the spatial distribution of the islands, the climate can be classified, from east to west, as a transition between the Cs and Cf subtypes. São Miguel Island exhibits a climate with distinctly Atlantic characteristics, where two well–defined seasons can be identified based on the precipitation patterns: a wet season from October to March and a dryer season from April to September. The Mean Annual Precipitation on São Miguel Island ranges from 1,200 to 2,000 mm near the coast, and reaches up to 4,800 mm in the higher inland areas of the island (Fernandes 2004).

2.3 | Design of the NATHA database

2.3.1 | Data collection

The NATHA database (Marques 2013) is a repository of documents relating to natural disaster events that have occurred on the Azores. The database contains information regarding earthquakes, volcanic eruptions, degassing phenomena, landslides, storms, floods and tsunamis that have occurred since the settlement of the Azores in the mid–fifteenth century. The data collection process was based on historical accounts, scientific articles, theses, technical and scientific reports and newspapers.

In this study, the data was obtained exclusively from newspapers. Like in similar studies using newspapers as the primary source of data (e.g. Zêzere et al. 2014), the registered landslide events caused impact, such as fatalities, people made homeless, damage to buildings or road blockages. More than 55,500 newspaper specimens were consulted. Two newspapers were selected as the primary press archive: *Açoriano Oriental* and *Correio dos Açores* (Fig. 2.3). Both newspapers have a regional coverage and are published on São Miguel Island. *Açoriano Oriental* is the oldest newspaper in the Azores and Portugal and is still published today. It has been published weekly since April 18, 1835, and daily since January 1, 1979. *Correio dos Açores* has been published daily since May 1, 1920. In addition, six local weekly newspapers were surveyed to complement or validate certain events (Table 2.1).

Figure 2.3 | Examples of newspaper specimens reporting landslide disaster events: (a) article from *Açoriano Oriental* describing a landslide that killed 7 people in 1942; (b) newspaper cover of *Açoriano Oriental* describing a landslide that caused 29 fatalities in 1997 and (c) newspaper cover of *Correio dos Açores* describing a landslide that caused 3 fatalities in 2013.

Table 2.1 | Newspaper consulted to build the NATHA database.

Newspaper	**Period of publication**	**Category**	**Distribution**	**Local of publication**
Açoriano Oriental	1835–present	Weekly, daily after 1979	Regional	Ponta Delgada
O Povoacense	1879–1915	Weekly	Local	Povoação
Aurora Povoacence	1883–1919	Weekly	Local	Povoação
Gazeta Povoacense	1902–1904	Weekly	Local	Povoação
Correio Povoacense	1909–1911	Weekly	Local	Povoação
Ecos do Levante	1917–1919	Weekly	Local	Povoação
Correio dos Açores	1920–present	Daily	Regional	Ponta Delgada
A República	1923–1924	Weekly	Local	Povoação

2.3.2 | Database structure

The bibliographic data in the NATHA database is organised according to the type of consulted documents (Fig. 2.4). Whenever possible, extracts from the catalogued documents were included as images, obtained through photography or by scanning the original documents.

Each natural event included in the NATHA database consists of three groups of data: (1) information, (2) characterisation and (3) impact. The information field contains the date, time, and the type of event (earthquake (EA), volcanic eruption (ER), degassing phenomena (DG), storm (ST), landslide (LD), flash flood (FF) and tsunami (TS)). In the case of landslides, an event refers to a specific date that was characterised by slope instability occurrence, which may involve multiple landslides. The characterisation field contains specific details about each natural event, such as the type of landslide and the triggering factor. The impact field includes spatial information about the event, including the island, municipality, parish, and locality. It also includes data on fatalities, injuries, destroyed buildings, people made homeless and costs associated with the event, when available.

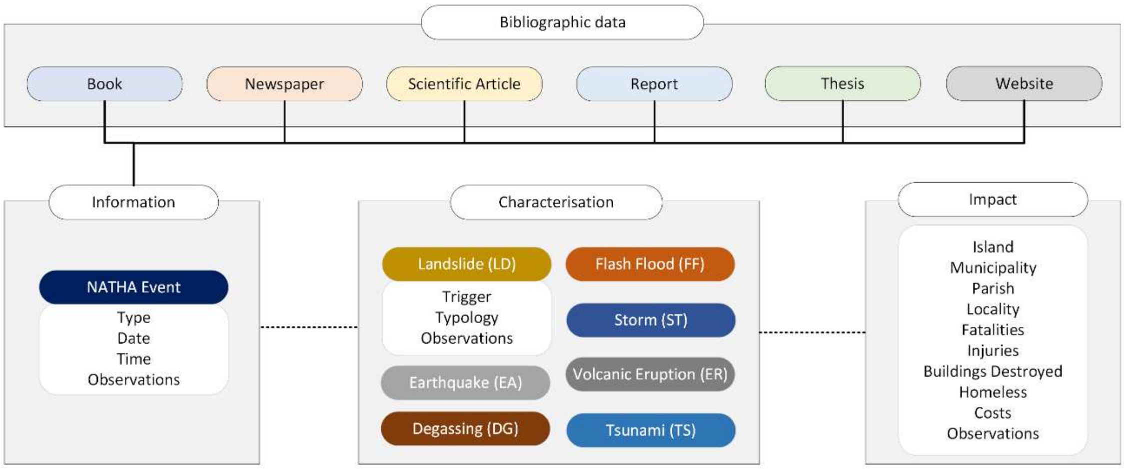

Figure 2.4 | NATHA database structure.

2.4 | Results

2.4.1 | Temporal trends of landslide events

The annual distribution of landslide events that caused impact on São Miguel Island during the time period 1900–2020 is presented in Figure 2.5. A total of 236 landslide events occurred on São Miguel Island were catalogued. When examining the temporal trends of these events, it is evident that there is no consistent increment and/or pattern in their distribution over time. However, two time periods can be distinguished: 1900–1995 and 1996–2020.

In the first period (1900–1995), the landslide events were less frequent than in the second period (1996–2020). The first time period represents 79% of the entire time series but includes only 42% of the registered events. The linear regression for the period 1900–1995 indicates an annual increase rate of 1.07 in landslide events (Fig. 2.5b). However, it is noteworthy that the periods of 1930–1949 and 1980–1989 exhibit a higher concentration of events.

The second time period covers 21% of the total tome series and contains 58% of the total landslide events. The rate of landslide events shows a significant increase of 5.74 events per year, which is five times higher than in the period 1900–1995 (Fig. 2.5b). During the period 1996–2020, landslide events were recorded every year. Moreover, more than 10 events were identified in the years 1996, 2007, 2010 and 2013, which were very wet years.

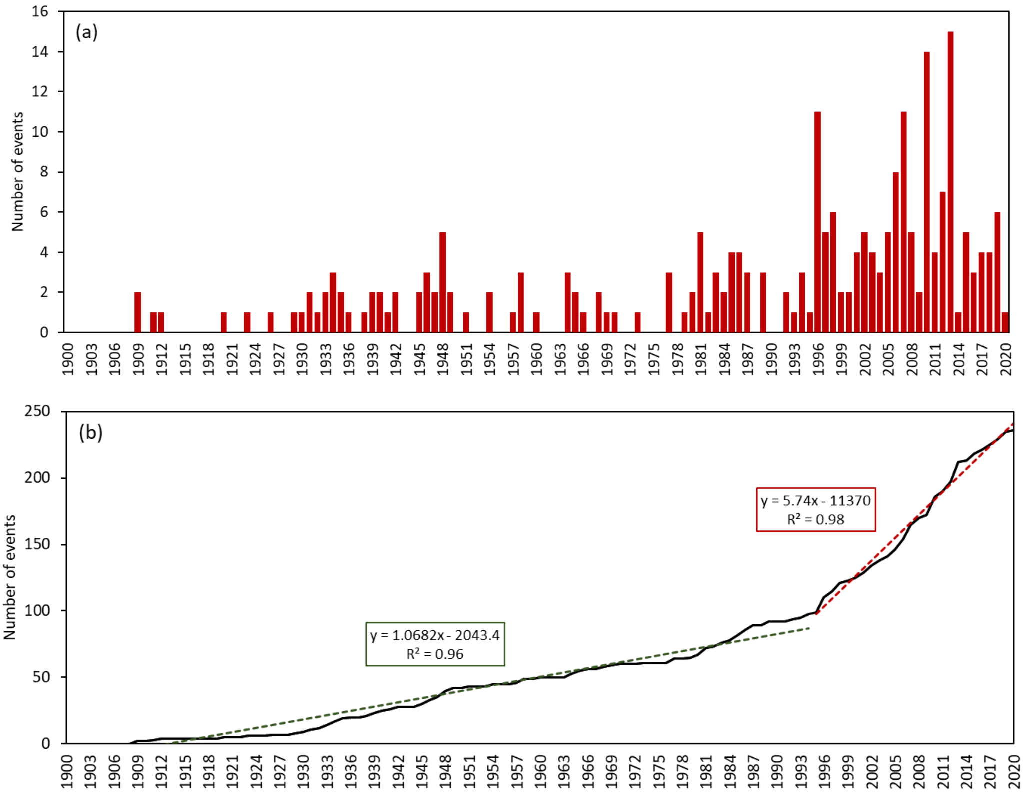

Figure 2.5 | (a) Temporal and (b) cumulative distribution of landslide events occurred on São Miguel Island in the period 1900–2020.

The cumulative distribution of landslide events that occurred in each municipality of São Miguel Island highlights some differences between municipalities (Fig. 2.6). During the period 1900–1995, Povoação registered the highest number of landslide events. Povoação and Ribeira Grande exhibit a similar increase in the number of events per year (0.35 and 0.32, respectively). In comparison, Ponta Delgada, Vila Franca do Campo, Lagoa and Nordeste registered a lower number of events, with increase of 0.27, 0.17, 0.07 and 0.09 events per year, respectively.

The 1996–2020 period was characterised by a significant increase in the number of events registered in all municipalities of the island. Ponta Delgada exhibits the highest increase (1.81 events per year), which is the approximately seven times higher than the first period. Similarly, Ribeira Grande and Povoação show substantial increase (1.76 and 1.59 events per year, respectively), which are about five times higher than the 1900–1995 period. Vila Franca do Campo, Lagoa and Nordeste also experienced an increase in the number of events during the 1996–2020 period, although lower when compared to the other municipalities.

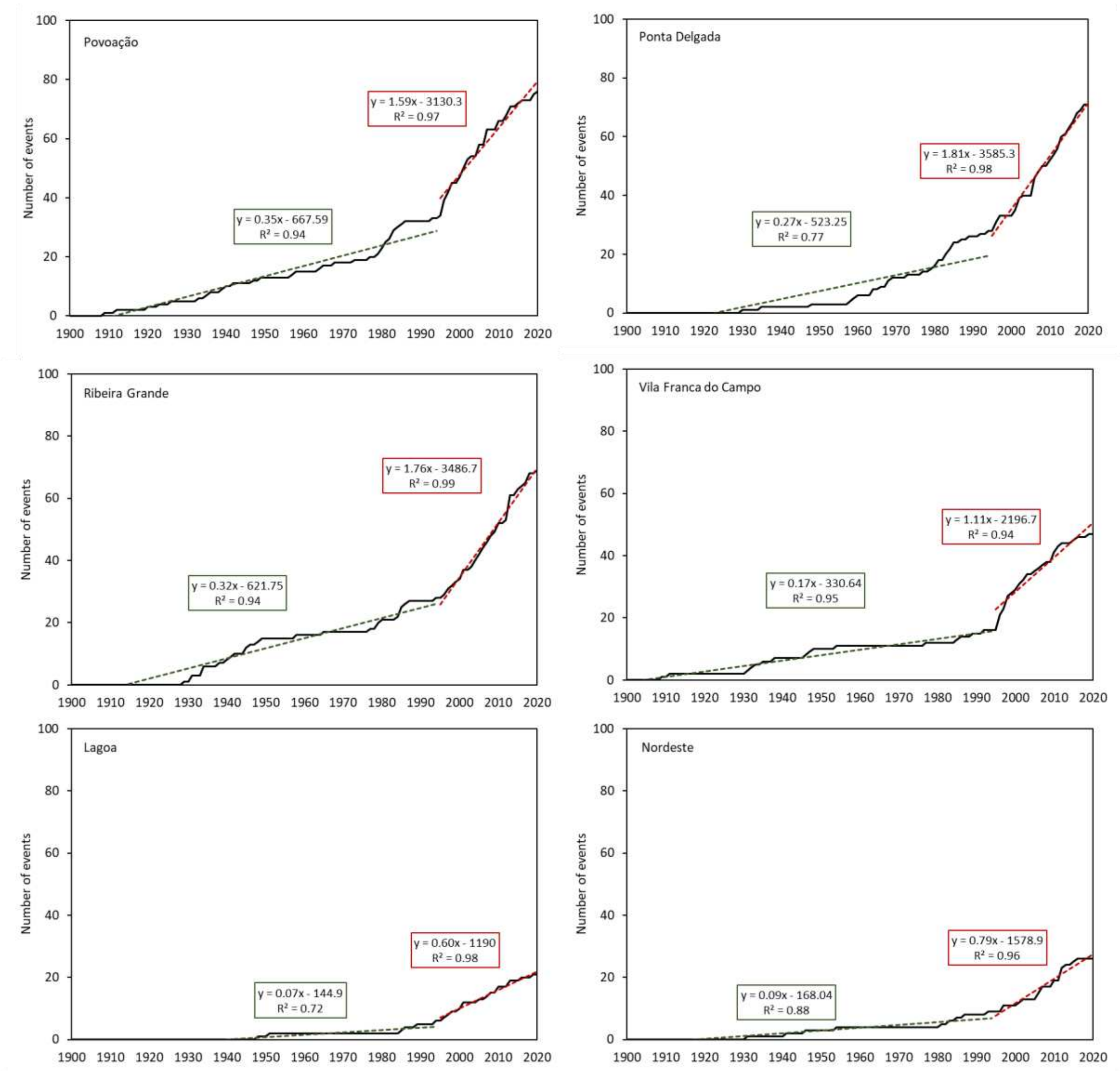

Figure 2.6 | Cumulative distribution of landslide events that occurred in each municipality of São Miguel Island in the period 1900–2020.

2.4.2 | Spatial distribution of landslide events

All municipalities of São Miguel Island have been affected by landslide events during the period 1900–2020. Povoação is the municipality with the highest number of landslide events, accounting 76 events (25% of the total). It is followed by Ponta Delgada (71 events, 23%), Ribeira Grande (69 events, 22%) and Vila Franca do Campo (47 events, 15%). In comparison, the municipalities of Nordeste and Lagoa registered a lower number of landslide events (26 and 21, respectively), corresponding to 8% and 7% of total landslide events, respectively.

The spatial distribution of these events across the municipalities normalised by 10 km^2 is shown in Figure 2.7. Povoacão is the municipality where most landslide events occurred (more than 6 per 10 km^2). Ponta Delgada, Ribeira Grande Vila Franca do Campo and Lagoa registered from 3 to 6 events per 10km^2 and Nordeste is the municipality with less landslide events (less than 3 per 10 km^2). It is worth noting that the distribution of landslide events summarised in Figure 2.7 represents neither the susceptibility nor the density of landslides of each municipality, but rather the recurrence of events that had some kind of impact and, as such, were referred to in the newspapers.

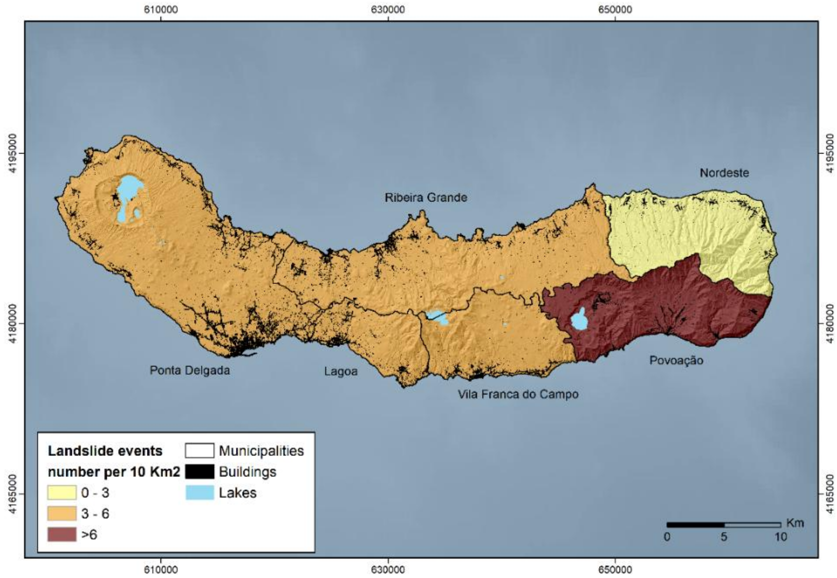

Figure 2.7 | Spatial distribution of landslide events (number per 10 km^2) in each municipality of São Miguel Islandin the period 1900–2020.

2.4.3 | Triggering factors of landslide events

The landslide events were classified based on their triggering factors, which include rainfall, earthquake, sea erosion and anthropic. Those cases where it was not possible to discriminate the triggering factor were classified as unknown. Rainfall was the triggering factor responsible for 70% of the registered landslide events on São Miguel Island. Sea erosion was the trigger of 8% of the events, followed by anthropic factors (4%) and earthquakes (2%). The relative frequency of these triggering factors in each municipality of São Miguel Island is depicted in Figure 2.8, with rainfall unsurprisingly dominating as the primary factor across all municipalities.

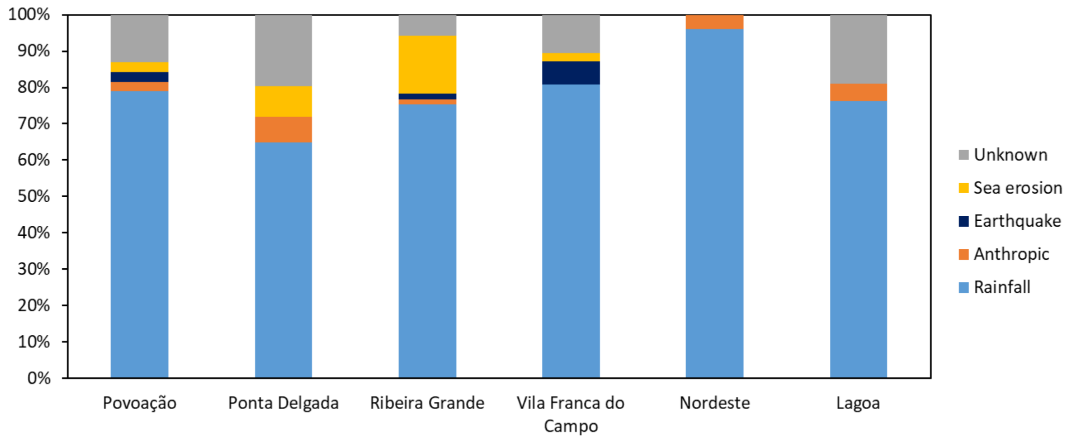

Figure 2.8 | Relative frequency of the triggering factors in each municipality of São Miguel Island.

2.4.4 | Analysis of the rainfall effect on landslide events

To gain better understanding of its impact on the occurrence of rainfall triggered landslide events, a detailed analysis of rainfall was made. For each municipality of the island, a specific meteorological station (MS) was selected for the rainfall analysis: Sete Cidades MS (Ponta Delgada), Chã da Macela MS (Lagoa), Fogo III MS (Ribeira Grande), Praia MS (Vila Franca do Campo), Monte Simplício MS (Povoacão) and Algarvia MS (Nordeste). Figure 2.9 illustrates the monthly average rainfall distribution registered in these meteorological stations for the period 2010-2020. The monthly rainfall distribution reveals a seasonal pattern, in which the 'rainiest season' lasts from October to March, while the summer period is the 'driest season', with minimal rainfall levels occurring in July. This depiction of the monthly rainfall distribution provides valuable insights into the temporal variations in precipitation on the island, which are vital for comprehending the underlying conditions contributing to landslide events.

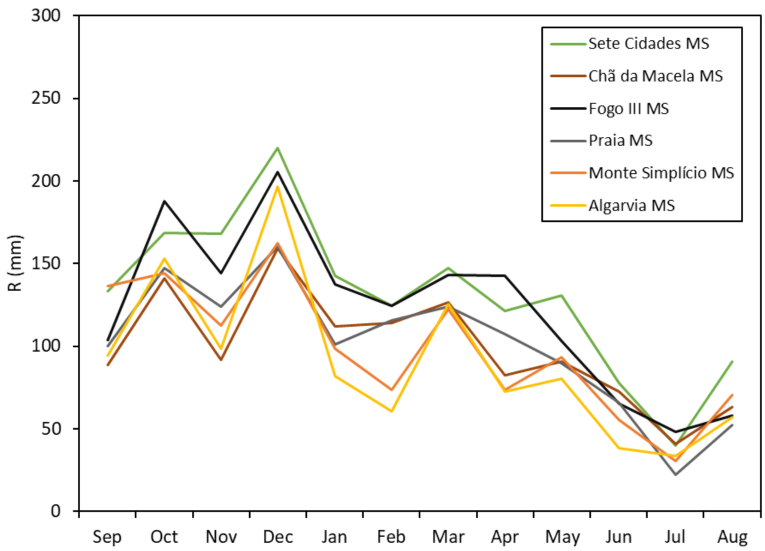

Figure 2.9 | Monthly rainfall average for different meteorological stations in São Miguel Island.

Figure 2.10 shows the monthly distribution of landslide events triggered by rainfall on São Miguel Island in the period 1900–2020. These events primarily take place during the rainiest months of the year, particularly between November and March, constituting 78% of the recorded events. The highest number of events occurred in December, followed by January and February with roughly the same number. The number of events registered from May to August is much lower, as this is the less rainy period along the year.

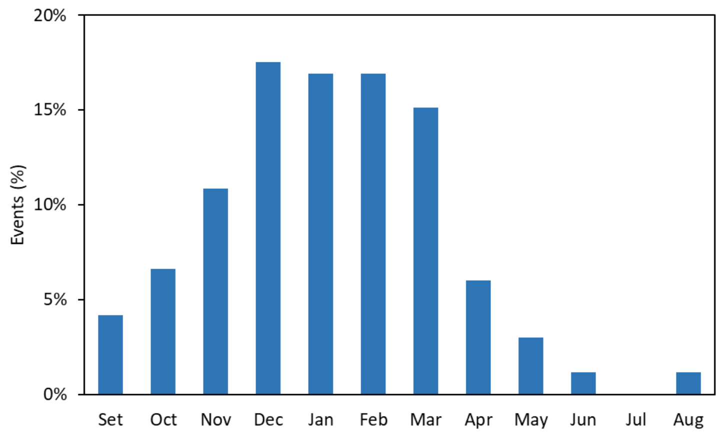

Figure 2.10 | Monthly distribution of landslide events on São Miguel Island in the period 1900–2020.

Figure 2.11 illustrates the monthly distribution of landslide events triggered by rainfall and their associated fatalities on São Miguel Island from 1900 to 2020. The data reveals that the maximum number of fatalities occurred in October and March. This is primarily attributed to two extreme events that took place in 1942 and 1997. Notably, the number of fatalities is not directly proportional to the number of landslide events. While December, January, February, and March account for approximately 60% of the total events, they only represent around 30% of the fatalities. This indicates that the severity of the events during these months, in terms of loss of life, may be relatively lower compared to other periods, but additional data is needed to confirm this hypothesis.

While there is a relationship between the monthly rainfall average and the occurrence of landslide events triggered by rainfall, the same does not hold for the number of fatalities resulting from landslide activity. In fact, fatal events are typically the consequence of landslides triggered by extreme rainfall episodes characterised by high intensity and short duration, which can occur during months with low monthly rainfall average. Therefore, it is crucial to consider not only the total rainfall amount but also the intensity and duration of rainfall events when assessing the potential impact of landslides on fatalities.

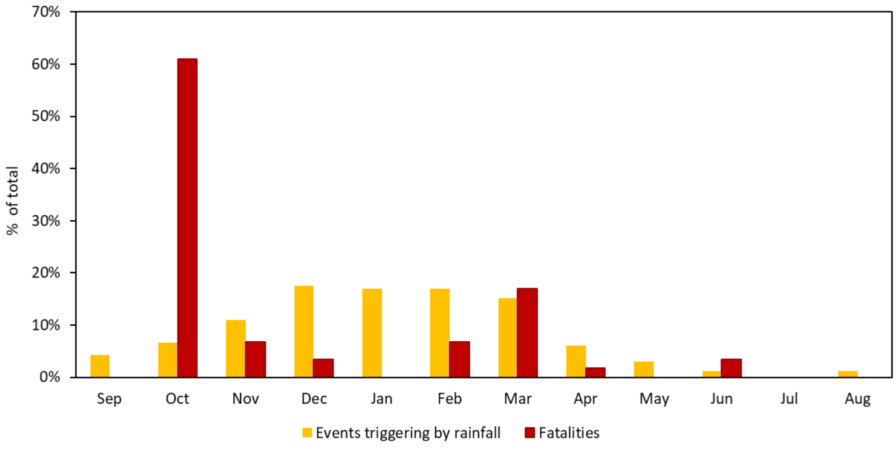

Figure 2.11 | Monthly distribution of landslide events triggering by rainfall and respective fatalities occurred on São Miguel Island in the period 1900–2020.

To gain better understanding of the influence of rainfall on the temporal trend of the number of landslide events, an analysis of the daily precipitation for the period 1900–2020 was conducted using data from the Ponta Delgada Meteorological Station (the only centenary station on São Miguel Island). Figure 2.12 shows the cumulative annual precipitation and the number of days per year with daily rainfall exceeding 65 mm. This threshold value is based on the rainfall intensity-duration threshold equation for landslide triggering calculated for the Povoação municipality (Zêzere et al. 2015), normalised by the Mean Annual Precipitation of Ponta Delgada Meteorological Station. The daily rainfall threshold of 65 mm was exceeded 29 times during the period 1900–1995 (0.3 per year in average). In the most recent period (1996–2020) the same threshold was exceeded 17 times (0.7 times per year in average). Notably, the year 1997 was an exceptional one, with the daily rainfall threshold exceeded 4 times. The accumulated annual precipitation does not show a clear trend. It is possible to identify an increase in the late 1930s that remains constant over the years, with drier and wetter years. The values of cumulative annual precipitation show a decrease over the years 2013 to 2020.

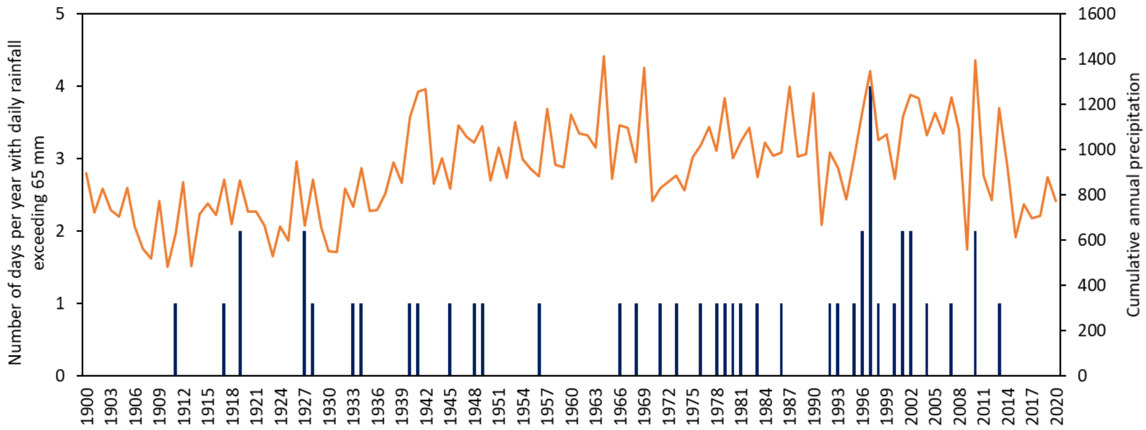

Figure 2.12 | Number of days per year with daily rainfall exceeding 65 mm (blue bars) and the cumulative annual precipitation (orange curve).

2.4.5 | Impact of landslide events

The landslide events catalogued in the NATHA database were responsible for 82 fatalities, 41 injuries, 305 people made homeless and 66 buildings partially or totally destroyed. The temporal distribution of fatalities caused by landslide events is shown in Figure 2.13a. In average, 0.7 fatalities were recorded per year and the ratio between deaths and total events (mortality index) is 0.35. The obtained ratio is strongly influenced by the outlier event of 31 October 1997. When this outlier event is excluded from the analysis, the mortality index drops to 0.22. The events with the highest number of fatalities occurred on 14 October 1942 and 31 October 1997 and were both triggered by very intense rainfall. The first event occurred in the parish of Furnas (Povoação municipality) and led to 7 fatalities. The second event took place in the parish of Ribeira Quente (Povoação municipality) and led to 29 fatalities.

Figure 2.13b shows the increasing number of fatalities per year on São Miguel Island, normalised by 10,000 inhabitants based on the number of residents per decade. Linear regression functions were computed for two periods: 1926–1995 and 1996–2020. The period 1900–1925 (no fatalities) and the events of 14 October 1942 and 31 October 1997 (outliers) were excluded from the analysis. The annual mortality increased by 0.03 fatalities/year/10,000 inhabitants during the period 1926–1995. In the most recent period (1996–2020), the annual mortality is twice as high increased by 0.06 fatalities/year/10,000 inhabitants.

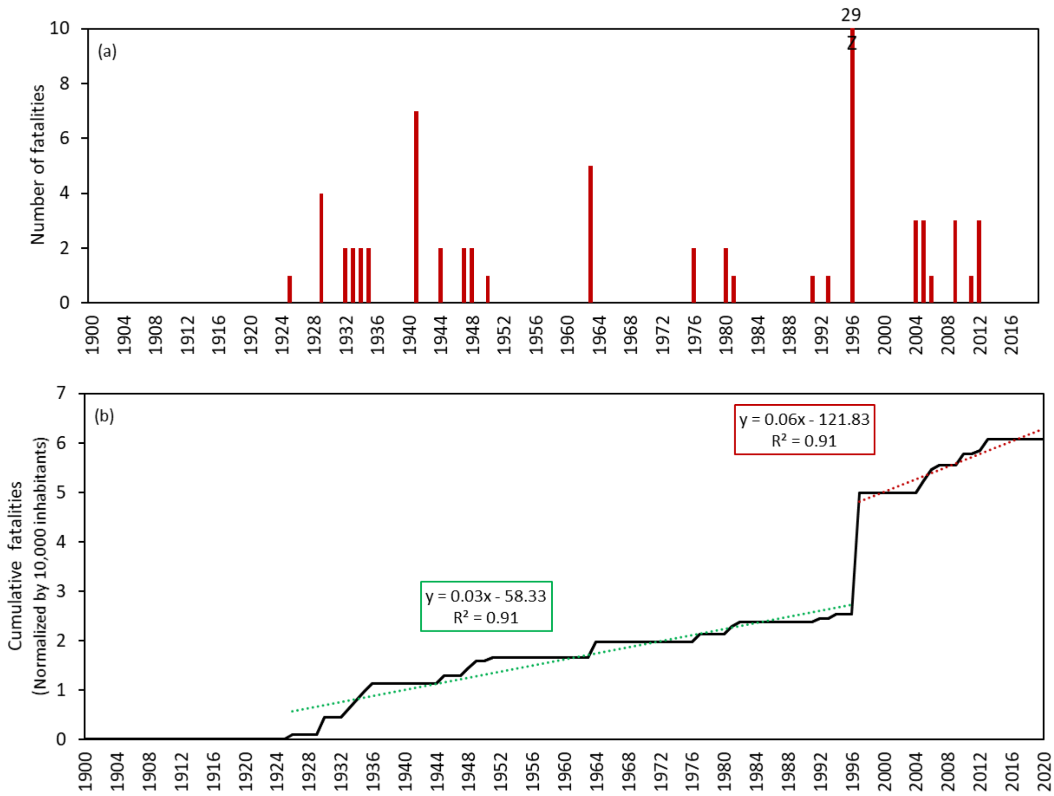

Figure 2.13 | (a) Temporal and (b) normalised cumulative distribution of fatalities caused by landslide events occurred on São Miguel Island.

The distribution of impact varies among the municipalities of São Miguel Island despite the relative similarity in the number of landslide events in Povoação, Ribeira Grande, and Ponta Delgada (Fig. 2.14). Povoação stands out with a high number of events that resulted in fatalities and significant damage. Specifically, Povoação recorded 48 fatalities, accounting for approximately 59% of the total fatalities documented in the database. Ponta Delgada stands out for the number of buildings destroyed and the number of people made homeless as a result of landslides. The other municipalities on the island registered a more limited impact.

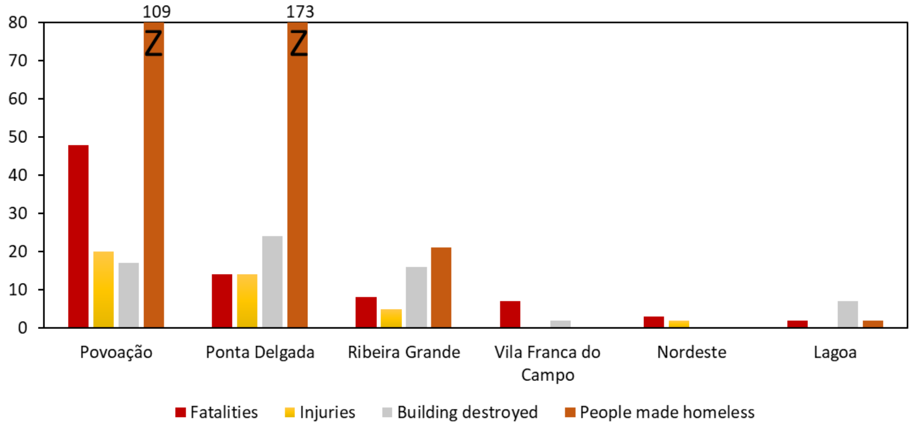

Figure 2.14 | Number of fatalities, injuries, buildings destroyed and people made homeless caused by landslide events in each municipality of São Miguel Island.

The type of impact caused by landslide events, as described by newspaper reports, is important to understand the variation of the number of events through time. Figure 2.15 shows the temporal distribution of landslide events according to their impact. For the period 1900–1995, the database contains 59 landslide events that causing road blockages (0.6 per year on average) and 40 events causing fatalities, injuries, buildings destroyed and people made homeless (0.4 per year on average). For the most recent period (1996–2020), the database contains 109 landslide events causing road blockages (4.4 per year on average) and 28 events causing fatalities, injuries, buildings destroyed and people made homeless (1.1 per year on average).

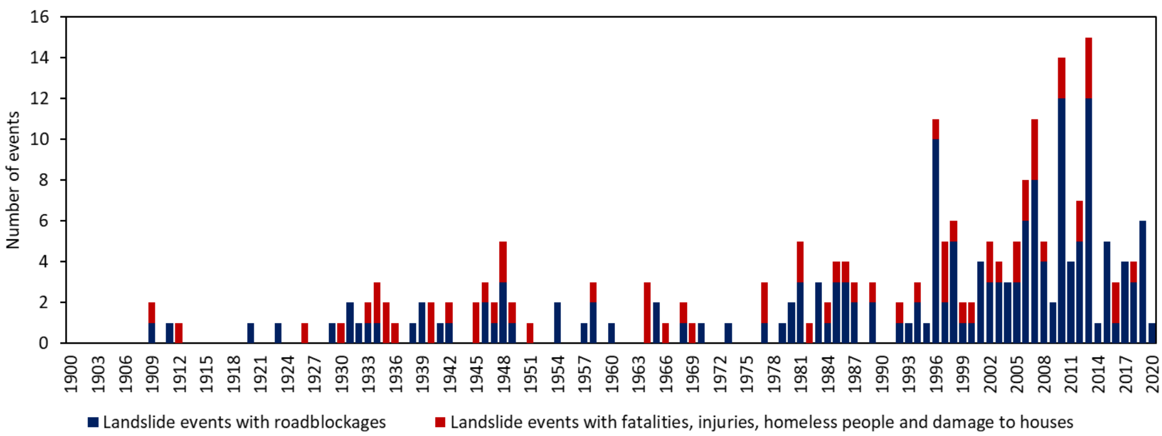

Figure 2.15 | Temporal distribution of landslide events according to their impact.

The F–N plot in Figure 2.16 illustrates the relationship between the frequency of landslide events and the corresponding number of fatalities on São Miguel Island. This plot serves as a tool for comparing the effects of natural disasters with established or acceptable criteria for societal risk assessment, as explained by (Guzzetti 2000). Based on the results and applying the most used risk acceptable criteria (Fell et al. 2005), it can be concluded that the societal risk associated with landslide events on São Miguel Island is considered unacceptable.

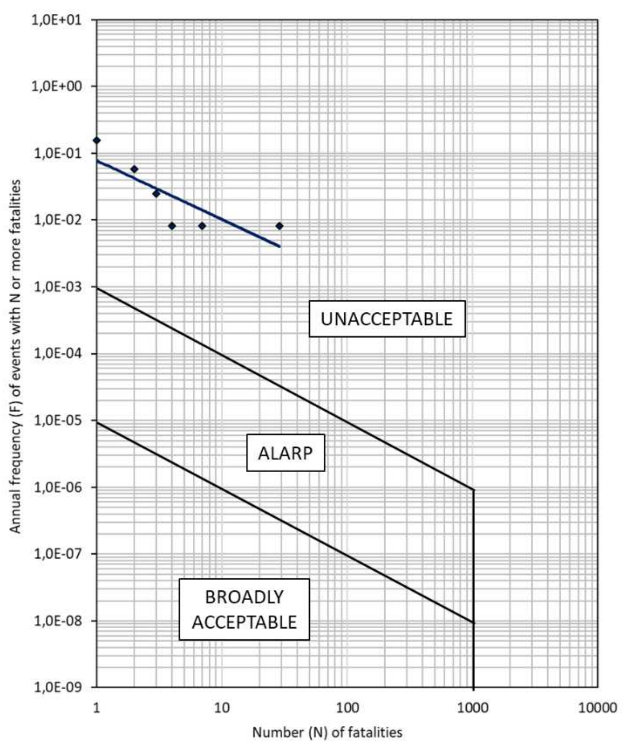

Figure 2.16 | Frequency vs consequences (F–N plot) for landslide events that caused fatalities on São Miguel Island.

2.5 | Discussion

The NATHA database was established in 2013 and serves as a repository for documental information regarding various natural hazards that have occurred in Azores. The data used in this work was collected by consulting approximately 55,500 regional and local newspapers. The temporal coverage of these newspapers is not uniform, and the period from 1900 to 2020 is not consistently represented in terms of the number of available newspapers. The *Açoriano Oriental* newspaper provides coverage for the entire studied period, while the *Correio dos Açores* newspaper has records starting from 1920 onwards. The early years of the time series are supported by the existence of six local newspapers, which contribute to the comprehensiveness of the data during that period. However, the data collection based on press archives have some limitations (Ibsen and Brunsden

1996, Cuesta et al. 1999, Guzzetti and Tonelli 2004): (i) many archives only record landslides with higher magnitude or that caused significant impact; (ii) the spatial coverage of the events is sometimes compromised, because the information sources do not describe the complete affected locations; (iii) it is not always possible to determine the triggering factor of the landslides, account for the costs or obtain the number of fatalities, injuries, homeless and destroyed infrastructures; (iv) changes in the quality and quantity of the news published by newspapers may have occurred along time, some related to the dictatorial regime of the country during the period 1933–1974; and (v) the journalist's experience and perception, as well as semantics in their descriptions introduce additional uncertainties.

A total of 236 landslide events were documented on the São Miguel Island during the period from 1900 to 2020, resulting in an average 1.9 events per year. The temporal distribution of events allows for the identification of two distinct periods: 1900–1995 and 1996–2020. The first period recorded a relatively low number of events (99), averaging 1.0 event per year. In contrast, the second, shorter in time, had a higher number of events (137), averaging 5.5 events per year. The results obtained are consistent with what has been observed in global landslide databases, which indicate an increase in the number of landslides in recent decades (Gómez et al. 2023).

The increasing number of landslide events seems to be related to a change in the precipitation regime. The analysis of daily rainfall showed that since 1996 the number of days exceeding the daily rainfall threshold of 65 mm was more than double in comparison to the initial period (0.3 per year in 1900–1995; 0.7 per year in 1996–2020). Given that rainfall is the primary trigger for landslides on São Miguel Island, this alteration in the rainfall pattern can, at least in part, account for the rising number of landslide events catalogued in the database. It is worth noting that the annual cumulative precipitation did not increase in the period 1996–2020, and therefore the increase in the number of events is due to the occurrence of extreme precipitation episodes, characterised by high intensity and short duration. This observation aligns with climate change scenarios that anticipate a heightened likelihood of extreme precipitation events (IPCC 2021). For instance, Ratnayake and Herath (2005) show that the increasing trend in rainfall intensity increases the number of landslides in Sri Lanka and Pereira et al. (2014) show that the temporal trend of landslide activity in the north of Portugal follows the rainfall regime. Furthermore, an analysis of the impact of the landslide events reported in newspapers revealed that the rising trend in the number of events during the most recent period (1996-2020) can be attributed in part to landslide events primarily resulting in road blockages. Although landslides events with fatalities, injuries, buildings destroyed and people made homeless also increased (0.4 events per year in 1900–1995; 1.1 events per year in 1996–2020), the landslide events that caused road blockages increased 7 times and correspond to 80% of catalogued events since 1996, while in the previous period they corresponded to 60% of all events. The increasing availability and dissemination of information, (e.g. coming from releases from the Regional Civil Protection Service, which was created in 1980), partially justify the increasing the number of landslide events that were reported by newspapers during the most recent period.

The spatial distribution of the landslide events showed differences between municipalities of São Miguel Island. Povoação, Ponta Delgada and Ribeira Grande municipalities have similar number of events in absolute terms, indicating a relatively higher occurrence in those areas. On the other hand, Vila Franca do Campo, Nordeste and Lagoa municipalities have a smaller number of events, indicating a lower frequency in those locations. The spatial distribution of these events across the municipalities normalised per unit area (10 km^2), further enhances the incidence of landslide events in Povoação. The high number of landslide events in Povoação is due to the geomorphology and geology, characterised by steep slopes, such as the inner walls of calderas volcanoes, fault scarps, sea cliffs, and stream valleys, mostly composed of non–cohesive materials (pumice deposits). Notably, this municipality has 53.6% of its area classified within the high and very high classes of landslide susceptibility (Marques 2013).

The rainfall was the dominant triggering factor along the island comprising over 70% of the events, similarly to what has been observed in numerous landslide national and international databases (e.g. Hadmoko et al. 2017, Lin and Wang 2018, Gómez et al. 2023). Landslide events induced by earthquakes are concentrated in the municipalities of Povoação, Ribeira Grande and Vila Franca do Campo, where the most seismicity on the São Miguel Island have been recorded (Silva et al. 2020). The low percentage of landslide events triggered by earthquakes is justified by the low frequency of earthquakes with magnitude and hypocentre location capable to trigger such events (Marques et al. 2006). Sea erosion has been responsible for several events in the municipalities of Povoação, Ponta Delgada, Ribeira Grande and Vila Franca do Campo. Landslide events prompted by storms with rough sea and strong waves have been caused damage to buildings and roads located near the sea cliffs. Landslide events triggered by anthropic actions have been occurred almost all municipalities and have been associated with activities such as mining and construction works, which have resulted in fatalities and/or injuries.

The impact caused by landslides totals 82 fatalities, 41 injuries, 305 people made homeless and 66 buildings partially or totally destroyed on São Miguel Island. Among the municipalities, Povoação stands out with a high number of events that resulted in fatalities and significant damage. Povoação recorded 48 fatalities, accounting for approximately 59% of the total fatalities documented in the database. This highlights the severity of the impact caused by landslide events in Povoação municipality compared to other areas on the island. The research conducted by Marques (2013) concludes that 22.6% of the buildings, 44.0% of the main roads and 26.7% of the secondary roads in Povoação are located in areas of high and very high landslide susceptibility, which highlights the existing high exposure in this municipality that contributes to consequences of landslide events.

2.6 | Conclusion

The NATHA (Natural Hazards in Azores) database is a repository of documents reporting natural events occurring in the Azores. This work aimed to analyse landslide events that occurred from 1900 to 2020, catalogued based on local and regional newspapers. The temporal distribution of the landslide events shows a higher concentration of events after 1996, which is explained by the shift in the precipitation regime that was characterised by the increasing number of days with more intense precipitation values in the most recent period. For the first time, this work demonstrates the influence of climate change on landslide occurrences in the Azores. The climate change scenarios presented in this study provide evidence of an expected increase in the probability of extreme rainfall events.

Irrespective of the impact caused, the increase in the number of events catalogued in the database in the most recent period (1996–2020) is mostly due to events that caused road blockages which can be explained by the increasing availability and dissemination of information, which increases the number of newspaper reports about this type of events. The spatial distribution of events reveals that the Povoação municipality is the most affected by landslide events. This is primarily attributed to its geology and geomorphology, which increase the likelihood of such events compared to other municipalities. The impact of landslide events varies significantly among the municipalities of São Miguel Island. Notably, the Povoação municipality stands out by the high impact of landslide events, which is explained by the exposure of its building, infrastructure and road network.

The landslide events predominantly occur during the rainiest months of the year, typically between November and March, with rainfall being the primary triggering factor on São Miguel Island. Cumulative monthly precipitation is not directly related to the occurrence of fatal events. Instead, these events are associated with the occurrence of extreme precipitation episodes, characterised by high intensity and short duration. The purpose of natural hazards databases is to prevent, reduce, and mitigate the risks associated with disasters. Stakeholders in civil protection and spatial planning should consider these databases to identify emergency management hotspots and select safe locations for future territorial expansion.

References

Bíl, M., Raška, P., Dolák, L. & Kubeček, J. (2021). CHILDA–Czech Historical Landslide Database. Natural Hazards and Earth System Sciences, 21, 2581–2596. https://doi.org/10.5194/nhess-21-2581-2021

Blais-Stevens, A., Castagner, A. & Behnia, P. (2015). Historical landslides that have resulted in fatalities in Canada (1771–2014) (Open File 7836). Geological Survey of Canada.

Booth, B., Croasdale, R. & Walker, G. P. L. (1978). A quantitative study of five thousand years of volcanism on S. Miguel, Azores. Philosophical Transactions of the Royal Society of London, 228, 271–319. https://doi.org/10.1098/rsta.1978.0018

Centre for Research on the Epidemiology of Disasters. (2022). EM-DAT: The International Disaster Database. http://www.emdat.be/

Cook, B. I., Mankin, J. S. & Anchukaitis, K. J. (2018). Climate change and drought: From past to future. Current Climate Change Reports, 4, 164–179. https://doi.org/10.1007/s40641-018-0093-2

Creighton, R. (2006). The Irish landslides database. In R. Creighton (Ed.), Landslides in Ireland (pp. 9–22). Geological Survey of Ireland.

Cuesta, M. J., Sánchez, M. J. & García, A. R. (1999). Press archives as temporal records of landslides in the North of Spain: Relationships between rainfall and instability slope events. Geomorphology, 30, 125–132. https://doi.org/10.1016/S0169-555X(99)00049-5

Cunha, A. (2003). The October 1997 landslides in São Miguel Island, Azores, Portugal. In J. Hervás (Ed.), *Lessons learnt from landslide disasters in Europe* (pp. 27–32). European Commission Joint Research Center.

Damm, B. & Klose, M. (2015). The landslide database for Germany: Closing the gap at national level. *Geomorphology, 249*, 82–93. https://doi.org/10.1016/j.geomorph.2015.03.021

Devoli, G. (2005). Collection of data on historical landslides in Nicaragua. In K. Sassa, H. Fukuoka, F. Wang & G. Wang (Eds.), *Landslides*. Springer. https://doi.org/10.1007/3-540-28680-2_29

Devoli, G., Strauch, W., Chávez, G. & Høeg, K. (2007). A landslide database for Nicaragua: A tool for landslide-hazard management. *Landslides, 4*, 163–176. https://doi.org/10.1007/s10346-006-0074-8

Duncan, A. M., Guest, J. E., Wallenstein, N. & Chester, D. K. (2015). The older volcanic complexes of São Miguel, Azores: Nordeste and Povoação. In J. L. Gaspar, J. E. Guest, A. M. Duncan, F. J. A. S. Barriga & D. K. Chester (Eds.), *Volcanic Geology of São Miguel Island (Azores Archipelago)* (Geological Society, London, Memoirs 44, pp. 147–153). https://doi.org/10.1144/M44.11

Elliott, A. & Kirschbaum, M. J. (2007). *The preliminary landslide history database of Utah, 1850–1978*. Utah Geological Survey.

Fell, R., Ho, K., Lacasse, S. & Leroi, E. (2005). A framework for landslide risk assessment and management. In O. Hungr, R. Fell, R. Couture & E. Eberhardt (Eds.), *Landslide risk management* (pp. 3–25). Taylor & Francis.

Fernandes, J. (2004). *Caracterização climática das ilhas de São Miguel e Santa Maria com base no Modelo CIELO* (Relatório de Estágio). University of the Azores.

Ferreira, T. (2000). *Caracterização da actividade vulcânica da ilha de S. Miguel (Açores): vulcanismo basáltico recente e zonas de desgaseificação. Avaliação de riscos* (PhD thesis). University of the Azores.

Ferreira, T., Gomes, A., Gaspar, J. L. & Guest, J. (2015). Distribution and significance of basaltic eruptive centres: São Miguel, Azores. In J. L. Gaspar, J. E. Guest, A. M. Duncan, F. J. A. S. Barriga & D. K. Chester (Eds.), *Volcanic Geology of São Miguel Island (Azores Archipelago)* (Geological Society, London, Memoirs 44, pp. 135–146). https://doi.org/10.1144/M44.10

Foster, C., Gibson, A. & Wildman, G. (2008). The new national landslide database and landslide hazard assessment of Great Britain. In K. Sassa (Ed.), *Proceedings of the First World Landslide Forum* (pp. 203–206). https://nora.nerc.ac.uk/id/eprint/4694

Froude, M. J. & Petley, D. N. (2018). Global fatal landslide occurrence from 2004 to 2016. *Natural Hazards and Earth System Sciences, 18*, 2161–2181. https://doi.org/10.5194/nhess-18-2161-2018

Frutuoso, G. (1981). Livro Quarto das *Saudades da Terra*. In G. Frutuoso (Ed.), *Saudades da Terra* (2ª ed., Vol. II, pp. 285–327). Instituto Cultural de Ponta Delgada.

Gaspar, J. L., Wallenstein, N., Coutinho, R., Ferreira, T., Queiroz, G., Pacheco, J., Guest, J., Tryggvason, E. & Malheiro, A. (1997). *Considerações sobre a ocorrência dos movimentos de massa registados na madrugada de 31 de Outubro de 1997 na Ilha de S. Miguel, Açores* (Documento Técnico-científico 14/CVARG/97). Centro de Vulcanologia e Avaliação de Riscos Geológicos.

Glade, T., Albini, P. & Francés, F. (2001). An introduction to the use of historical data in natural hazards assessment. In T. Glade, P. Albini & F. Francés (Eds.), *The use of historical data in natural hazard assessments* (pp. XVII–XXV). Kluwer Academic Publishers. https://doi.org/10.1007/978-94-017-3490-5

Guest, J. E., Gaspar, J. L., Cole, P. D., Queiroz, G., Duncan, A. M., Wallenstein, N., Ferreira, T. & Pacheco, J. M. (1999). Volcanic geology of Furnas Volcano, São Miguel, Azores. *Journal of Volcanology and Geothermal Research, 92*(1–2), 1–29. https://doi.org/10.1016/S0377-0273(99)00064-5

Guest, J. E., Pacheco, J. M., Cole, P. D., Duncan, A. M., Wallenstein, N., Queiroz, G., Gaspar, J. L. & Ferreira, T. (2015). The volcanic history of Furnas volcano, São Miguel, Azores. In J. L. Gaspar, J. E. Guest, A. M. Duncan, F. J. A. S. Barriga & D. K. Chester (Eds.), *Volcanic Geology of São Miguel Island (Azores Archipelago)* (Geological Society, London, Memoirs 44, pp. 125–134). https://doi.org/10.1144/M44.9

Guzzetti, F. (2000). Landslide fatalities and the evaluation of landslide risk in Italy. *Engineering Geology, 58*, 89–107. https://doi.org/10.1016/S0013-7952(00)00047-8

Guzzetti, F. & Tonelli, G. (2004). Information system on hydrological and geomorphological catastrophes in Italy (SICI): A tool for managing landslide and flood hazards. *Natural Hazards and Earth System Sciences, 4*, 213–232. https://doi.org/10.5194/nhess-4-213-2004

Gómez, D., García, E. F. & Aristizábal, E. (2023). Spatial and temporal landslide distributions using global and open landslide databases. *Natural Hazards, 117*, 25–55. https://doi.org/10.1007/s11069-023-05848-8

Hadmoko, D. S., Lavigne, F., Sartohadi, J., Gomez, C. & Daryono, D. (2017). Spatio-temporal distribution of landslides in Java and the triggering factors. *Forum Geografi, 31*, 1–15. https://doi.org/10.23917/forgeo.v31i1.3790

Herrera, G., Mateos, R. M., García-Davalillo, J. C., et al. (2018). Landslide databases in the Geological Surveys of Europe. *Landslides, 15*, 359–379. https://doi.org/10.1007/s10346-017-0902-z

Hilker, N., Ellis, M. A. & Hegg, C. (2009). The Swiss flood and landslide damage database 1972–2007. *Natural Hazards and Earth System Sciences, 9*, 913–925. https://doi.org/10.5194/nhess-9-913-2009

Holcombe, E. A., Beesley, M. E., Vardanega, P. J. & Sorbie, R. (2016). Urbanisation and landslides: Hazard drivers and better practices. *Proceedings of the Institution of Civil Engineers – Civil Engineering, 169*, 137–144. https://doi.org/10.1680/jcien.15.00044

Ibsen, M. L. & Brunsden, D. (1996). The nature, use and problems of historical archives for the temporal occurrence of landslides, with specific reference to the south coast of Britain, Ventnor, Isle of Wight. *Geomorphology, 15*, 241–258. https://doi.org/10.1016/0169-555X(95)00073-E

INE – Instituto Nacional de Estatística. (2021). *Censos 2021: XVI Recenseamento Geral da População; VI Recenseamento Geral da Habitação. Resultados provisórios.* Lisboa.

IPCC – Intergovernmental Panel on Climate Change. (2021). *Climate Change 2021: The Physical Science Basis. Contribution of Working Group I to the Sixth Assessment Report of the Intergovernmental Panel on Climate Change* (V. Masson-Delmotte, A. Zhai, S. L. Pirani, C. Connors, S. Péan, N. Berger, Y. Caud, L. Chen, M. I. Goldfarb, M. Gomis, K. Huang, E. Leitzell, J. B. R. Lonnoy, T. K. Matthews, T. Maycock, O. Waterfield, R. Yelekçi & B. Zhou, Eds.). Cambridge University Press. https://doi.org/10.1017/9781009157896

Jaedicke, C., Lied, K. & Kronholm, K. (2009). Integrated database for rapid mass movements in Norway. *Natural Hazards and Earth System Sciences, 9*, 469–479. https://doi.org/10.5194/nhess-9-469-2009

Jaupaj, O., Lamaj, M., Kulici, H., Jusufati, M., Plaku, E. & Gjeta, I. (2017). Landslide Inventory Map of Albania. In *Advancing Culture of Living with Landslides* (pp. 39–44). Springer. https://doi.org/10.1007/978-3-319-53498-5_5

Kalantzi, F., Doutsou, I. & Koukouvelas, I. (2010). Historical landslides in the Prefecture of Ioannina: Collection and analysis of data. *Bulletin Geological Society of Greece, 43*(3), 1350–1360. https://doi.org/10.12681/bgsg.11311

Kimuli, J. B., Di, B., Zhang, R., Wu, S., Li, J. & Yin, W. (2021). A multisource trend analysis of floods in Asia–Pacific 1990–2018: Implications for climate change in sustainable development goals. *International Journal of Disaster Risk Reduction, 59*, 102237. https://doi.org/10.1016/j.ijdrr.2021.102237

Kirschbaum, D., Stanley, T. & Zhou, Y. (2015). Spatial and temporal analysis of a global landslide catalog. *Geomorphology, 249*, 4–15. https://doi.org/10.1016/j.geomorph.2015.03.016

Knutson, T., Landsea, C. & Emanuel, K. (2010). Tropical cyclones and climate change: A review. In J. C. L. Chan & J. D. Kepert (Eds.), *Global perspectives on tropical cyclones: From science to mitigation* (pp. 243–284). World Scientific Publishing. https://doi.org/10.1142/9789814293488_0009

Köppen, W. (1936). Das geographische System der Klimate. In W. Köppen & G. Geiger (Eds.), *Handbuch der Klimatologie* (Vol. 1, pp. 1–44). Gebr. Borntraeger.

Li, W. Y., Liu, C., Hong, Y., Zhang, X. H., Wan, Z. M., Saharia, M., Sun, W. W., Yao, D. J., Chen, W., Chen, S., Yang, X. Q. & Yue, Y. (2016). A public cloud-based China's landslide inventory database (CsLID): Development, zone, and spatiotemporal analysis for significant historical events, 1949–2011. *Journal of Mountain Science, 13*, 1275–1285. https://doi.org/10.1007/s11629-015-3659-7

Lin, Q. & Wang, Y. (2018). Spatial and temporal analysis of a fatal landslide inventory in China from 1950 to 2016. *Landslides, 15*, 2357–2372. https://doi.org/10.1007/s10346-018-1037-6

Marques, R., Queiroz, G., Coutinho, R. & Zêzere, J. L. (2006). Actividade geomorfológica desencadeada pela crise sísmica de 2005 no Vulcão do Fogo (S. Miguel, Açores): Avaliação da susceptibilidade com recurso a regressão logística. *Publicações da Associação Portuguesa de Geomorfólogos, 5*, 47–61.

Marques, R. (2013). *Estudo de movimentos de vertente no concelho da Povoação (ilha de São Miguel, Açores): Inventariação, caracterização e análise da susceptibilidade* (PhD thesis). University of the Azores.

Marques, R., Zêzere, J. L., Gaspar, J. L. & Amaral, P. (2009). *Reconstituição e modelação probabilística da escoada detrítica de Vila Franca do Campo desencadeada pelo sismo de 22 de Outubro de 1522 (S. Miguel, Açores).* Publicações da Associação Portuguesa de Geomorfólogos, VI, 175–182.

Niculiță, M., Andrei, A. & Lupu, C. (2017). The landslide database of North–Eastern Romania. In M. Niculiță & M. C. Mărgărint (Eds.), *Proceedings of the Romanian Geomorphology Symposium* (Vol. 1, pp. 11–14). https://doi.org/10.15551/prgs.2017.81

Panwar, V. & Sen, S. (2020). Disaster damage records of EM–DAT and DesInventar: A systematic comparison. *Economics of Disasters and Climate Change, 4*, 295–317. https://doi.org/10.1007/s41885–019–00052–0

Pereira, S., Zêzere, J. L., Quaresma, I. D. & Bateira, C. (2014). Landslide incidence in the North of Portugal: Analysis of a historical landslide database based on press releases and technical reports. *Geomorphology, 214*, 514–525. https://doi.org/10.1016/j.geomorph.2014.02.032

Petley, D. N., Hearn, G. J., Hart, A., et al. (2007). Trends in landslide occurrence in Nepal. *Natural Hazards, 43*, 23–44. https://doi.org/10.1007/s11069–006–9100–3

Piacentini, D., Troiani, F., Daniele, G. & Pizziolo, M. (2018). Historical geospatial database for landslide analysis: The Catalogue of Landslide Occurrences in the Emilia–Romagna Region (CLOCkER). *Landslides, 15*, 811–822. https://doi.org/10.1007/s10346–018–0962–8

Queiroz, G. (1997). *Vulcão das Sete Cidades (S. Miguel, Açores) – História eruptiva e avaliação do hazard* (Doctoral dissertation). University of the Azores.

Queiroz, G., Gaspar, J. L., Guest, J. E., Gomes, A. & Almeida, M. H. (2015). Eruptive history and evolution of Sete Cidades volcano, São Miguel Island, Azores. In J. L. Gaspar, J. E. Guest, A. M. Duncan, F. J. A. S. Barriga & D. K. Chester (Eds.), *Volcanic Geology of São Miguel Island (Azores Archipelago)* (Vol. 44, pp. 87–104). Geological Society of London. https://doi.org/10.1144/M44.7

Ratnayake, U. & Herath, S. (2005). Changing rainfall and its impact on landslides in Sri Lanka. *Journal of Mountain Science, 2*, 218–224. https://doi.org/10.1007/BF02973195

Septer, D. (2007). *Flooding and landslide events, southern British Columbia 1808–2006.* Ministry of Environment, Province of British Columbia.

Silva, R. F., Marques, R. & Gaspar, J. L. (2018). Implications of landslide typology and predisposing factor combinations for probabilistic landslide susceptibility models: A case study in Lajedo Parish (Flores Island, Azores–Portugal). *Geosciences, 8*, 153. https://doi.org/10.3390/geosciences8050153

Silva, R., Carmo, R. & Marques, R. (2020). Characterization of the tectonic origins of historical and modern seismic events and their societal impact on the Azores

Archipelago, Portugal. *Geological Society Special Publications, 501*. https://doi.org/10.1144/SP501–2019–106

Silveira, D., Gaspar, J. L., Ferreira, T. & Queiroz, G. (2003). Reassessment of the historical seismic activity with major impact on S. Miguel Island (Azores). *Natural Hazards and Earth System Sciences, 3*, 1–8. https://doi.org/10.5194/nhess-3-615-2003

Van Den Eeckhaut, M. & Hervás, J. (2012). State of the art of national landslide databases in Europe and their potential for assessing landslide susceptibility, hazard and risk. *Geomorphology, 139–140*, 545–558. https://doi.org/10.1016/j.geomorph.2011.12.006

Van Den Eeckhaut, M., Hervás, J. & Montanarella, L. (2013). Landslide databases in Europe: Analysis and recommendations for interoperability and harmonisation. In C. Margottini, P. Canuti & K. Sassa (Eds.), *Landslide Science and Practice*. Springer. https://doi.org/10.1007/978-3-642-31325-7_4

Wallenstein, N. (1999). *Estudo da história recente e do comportamento eruptivo do vulcão do Fogo (S. Miguel, Açores). Avaliação preliminar do hazard* (Doctoral dissertation). University of the Azores.

Wallenstein, N., Duncan, A., Guest, J. E. & Almeida, M. H. (2015). Eruptive history of Fogo Volcano, São Miguel, Azores. In J. L. Gaspar, J. E. Guest, A. M. Duncan, F. J. A. S. Barriga & D. K. Chester (Eds.), *Volcanic Geology of São Miguel Island (Azores Archipelago)* (Vol. 44, pp. 105–123). Geological Society of London. https://doi.org/10.1144/M44.8

Zêzere, J. L., Pereira, S., Tavares, A., Bateira, C., Trigo, R., Quaresma, I., Santos, P., Santos, M. & Verde, J. (2014). DISASTER: A GIS database on hydro–geomorphologic disasters in Portugal. *Natural Hazards, 72*, 503–532. https://doi.org/10.1007/s11069–013–1018–y

Zêzere, J. L., Pereira, S., Oliveira, S., Marques, R. & Garcia, R. (2015). Rainfall thresholds for landslide activity in Portugal: A state of the art. *Environmental Earth Sciences, 73*, 2917–2936. https://doi.org/10.1007/s12665–014–3672–0

CHAPTER 3

3 | RAINFALL PATTERNS AND TRENDS ON SÃO MIGUEL ISLAND (AZORES, PORTUGAL): A HIERARCHICAL CLUSTERING AND TREND ANALYSIS APPROACH

Abstract

This study addressed rainfall patterns and trends on São Miguel Island (Azores, Portugal). Homogeneous rainfall areas were identified using Ward's hierarchical clustering method. The analysis was performed using monthly rainfall data from 21 rainfall stations, considering the climatological periods of 1978/79–2019/20 (full dataset), 1978/79–2009/10 (oldest sub-dataset), and 2010/11–2019/20 (latest sub-dataset). Four rainfall clusters were identified, with Mean Annual Precipitation (MAP) ranging from 835.8 mm in low-altitude areas to 2925.5 mm in regions with higher elevation. These clusters showed consistent patterns for the analysed periods, although some changes in their composition were observed when considering the oldest and latest sub-datasets. The correlation between altitude and rainfall was strong (R^2 up to 0.83), indicating an increase of approximately 196 mm of MAP per 100 m elevation gain. Moreover, no notable variation was observed between the island's windward and leeward slopes. Rainfall trend analysis using Mann–Kendall and Sen's slope tests revealed significant declines in both annual and seasonal rainfall in recent years. The strongest decreases occurred in autumn and winter, with trends as steep as −31.6 mm/year and −12.1 mm/year in autumn (both at the Fogo III station). Between the oldest and most recent periods, rainfall reductions reached up to 41% in autumn (P10) and 55% in winter (P10), particularly affecting clusters at lower and mid-altitudes. Although certain stations showed significant declines, the overall trend hints at a potential deviation from projections of global climate change models, as well as from trends identified in previous long-term rainfall studies. The predominantly positive phase of the North Atlantic Oscillation (NAO) observed in recent years has likely contributed, at least partially, to the decrease in the rainfall trend. Overall, the results provide a refined spatial and temporal characterisation of rainfall across São Miguel Island, improving the understanding of local climatic variability and offering valuable insights for regional water management and climate adaptation strategies.

Keywords: Cluster Analysis; Rainfall Trend; Rainfall Patterns; NAO; Azores

Manuscript published in *Climate*

Journal Impact Factor: 4.0; 5-Year Journal Impact Factor: 4.1

Silva, R. F., Marques, R., Zêzere, J. L. & Fragoso, M. (2025). Rainfall Patterns and Trends on São Miguel Island (Azores, Portugal): A Hierarchical Clustering and Trend Analysis Approach. Climate, 13(11), 238. https://doi.org/10.3390/cli13110238

3.1 | Introduction

Rainfall is considered the most important meteorological variable for studying regional climate (Frich et al. 2002; Novotny and Stefan 2007). Planning activities across various societal sectors, including agriculture, energy, water resources, and the hydrological cycle, requires a thorough understanding of the behaviour of this variable. Consequently, knowledge about spatial rainfall patterns is essential for the sustainable management of water resources and for detecting climate variability.

The spatial and temporal variability of rainfall represents one of the main challenges in climatological and hydrological analyses. Its understanding is hindered by the combined influence of multiple factors, which extend beyond local physiographic elements to include processes associated with atmospheric circulation and ocean–atmosphere interactions (Valdés-Pineda et al. 2015). In this context, the regionalisation of rainfall emerges as a fundamental tool, enabling the identification of homogeneous patterns and the reduction in the inherent complexity of climate data. A homogeneous rainfall region is an area with statistically similar long-term rainfall patterns (Lin et al. 2006). Various approaches have been employed in the scientific literature to examine spatial rainfall patterns, including L-moments (Guttman 1993; Modarres and Sarhadi 2011), k-means clustering (Isik and Singh 2008; Machiwal et al. 2017), regional frequency analysis (Medina-Cobo et al. 2017), harmonic analysis (Suhaila and Jemain 2009), spatial correlation functions (Şen and Habib 2001), multivariate regression (Sabziparvar et al. 2015), empirical orthogonal functions (Jebari et al. 2009; Santos et al. 2017), Pearson's correlation (Haines and Olley, 2017), support vector machines (Lin et al. 2017), and spatial interpolation (Gupta et al. 2017).

Cluster analysis has been widely applied in the literature for classification tasks (Jackson and Weinand 1995). Unlike many statistical methods that depend on predefined theoretical distributions, it groups the data based on observed similarities. Hierarchical and non-hierarchical clustering methods are used, with non-hierarchical methods being more prevalent. Hierarchical clustering arranges clusters hierarchically to reflect similarities or dissimilarities using either a top-down or bottom-up approach. Clusters are formed by repeatedly merging the closest objects based on the shortest distance, until all objects are joined. Ward's hierarchical method (Ward 1963) has frequently been used for categorising climatic and hydrologic data, consistently providing more accurate classification results compared to other methods (e.g. Masoodian 1998; Domroes et al. 1998; Unal et al. 2003; Martin et al. 2007; Lyra et al. 2014). Several studies have employed this method to identify clusters based on climatic variables.

Trends in time series have been identified using various statistical techniques, which are categorised into parametric and non-parametric tests (Zhang et al. 2006; Chen et al. 2007; Mirabbasi et al. 2020). Unlike parametric tests, which assume that the data are normally distributed, non-parametric tests make no such assumption (Sonali and Kumar

2013). Researchers in climatology, hydrology, and environmental sciences widely favour the non-parametric Mann-Kendall test (Mann 1945; Kendall 1976) for trend analysis. This test is often paired with Sen's slope estimator (Theil 1950; Sen 1968), another non-parametric method, to quantify the trend magnitude. Together, these methods offer valuable insights into the rate of change within a data series, enhancing the understanding of temporal dynamics.

Rainfall patterns in regions that are influenced by subtropical anticyclones exhibit complex relationships with altitude. Generally, rainfall increases with altitude because of orographic effects. However, this relationship is not always linear and can vary significantly among regions (Kumar and Santos 2015). Windward slopes typically receive more rainfall than leeward slopes because of the orographic effect: as moist air rises, it cools and condenses, forming clouds and rain on the wind-facing slopes, which leads to persistent rainfall patterns (Foresti et al. 2011). In contrast, leeward slopes tend to be drier, as the descending air warms and dries (Chen and Feng 2001).

The study of rainfall regimes in subtropical anticyclonic regions is fundamental to understanding climate dynamics, improving weather forecasting, and managing water resources. The Azores high-pressure system plays a significant role in modulating rainfall in various regions, including tropical Northeast Africa, Europe, and the Middle East (Iqbal et al. 2012; Rashid et al. 2012). Moreover, research on rainfall regimes in subtropical anticyclonic regions, such as the Azores, is crucial for understanding the impacts of climate change on rainfall patterns and aiding in the development of adaptation and mitigation strategies (Loo et al. 2014).

The characterisation of rainfall in the Azores remains relatively underexplored. Santos et al. (2004) assessed the potential impacts of climate change on the Azores and Madeira islands, focusing on variations in temperature and rainfall. De Lima et al. (2010) examined changes in rainfall patterns across Portugal, including the Azores, using long-term annual and monthly rainfall series. Based on long-term monthly rainfall series, Cropper and Hanna (2014) identified temporal trends and assessed inter-island variability, as well as the influence of large-scale atmospheric patterns across the Macaronesian archipelagos. Similarly, Hernández et al. (2016) analysed daily rainfall in Ponta Delgada (São Miguel Island) over the period of 1873–2012, examining its relationship with large-scale modes of climate variability. Across all studies, the North Atlantic Oscillation (NAO) emerges as the dominant large-scale driver of interannual rainfall variability in the Azores, consistently showing a negative correlation (Marques et al. 2008; Cropper and Hanna 2014; Hernández et al. 2016).

Building on these considerations, the main objective of this study was to analyse the spatial and temporal rainfall patterns on São Miguel Island (Azores, Portugal) using a combination of hierarchical clustering and trend analysis methods. To achieve this, the study focused on the following specific objectives: (i) identify homogeneous rainfall areas on the island using Ward's hierarchical clustering method; (ii) analyse rainfall trends and assess their significance using the Mann–Kendall test together with Sen's slope estimator; (iii) investigate the influence of the NAO on the temporal variability of rainfall by analysing the longest rainfall series available on the island; and (iv) study the rainfall distribution on the island in relation to the altitude under the broader influence of a subtropical anticyclone.

3.2 | Study Area and Climate Framework

The Azores archipelago, composed of nine volcanic islands in the North Atlantic Ocean (Figure 3.1a), includes São Miguel, the largest (744.6 km^2; 64 km long, 8–15 km wide). The island comprises seven morphological units with distinct geology and geomorphology (Figure 3.1b), including three active central volcanoes, Sete Cidades (Queiroz 1997; Queiroz et al. 2015), Fogo (Wallenstein 1999; Wallenstein et al. 2015), and Furnas (Guest et al. 1999, 2015) and two fissural volcanic systems, Picos (Ferreira 2000; Ferreira et al. 2015) and Congro (Booth et al. 1978; Guest et al. 1999). Elevation reaches 873 m at Sete Cidades, 949 m at Fogo, and 700 m at Furnas. The Picos Fissural Volcanic System forms gentle slopes below 300 m, while the Congro Fissural Volcanic System rises above 500 m. In the east, the extinct Povoação Volcano and Nordeste Complex (Duncan et al., 2015) form the island's oldest structures, with the highest elevation (1104 m) located there.

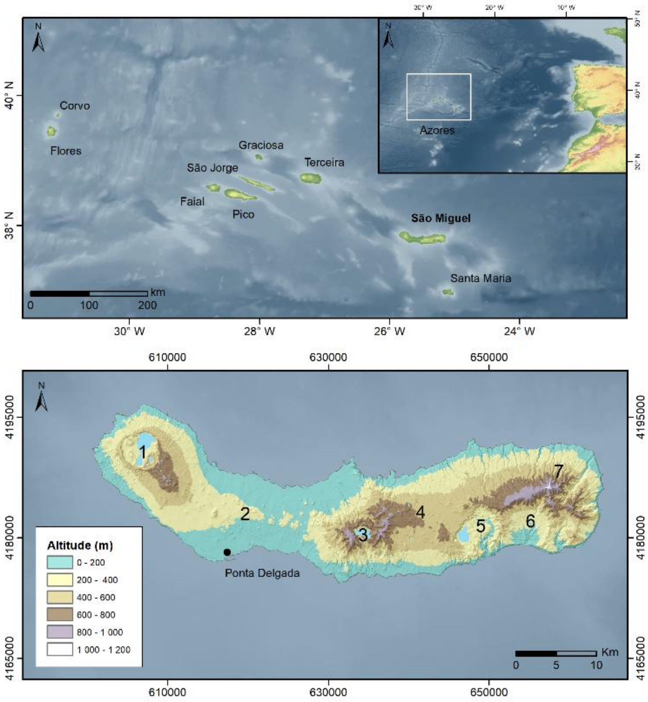

Figure 3.1 | Geographic location (a), altitude, and morphostructural units (b) of São Miguel Island: 1—Sete Cidades Volcano; 2—Picos Fissural Volcanic System; 3—Fogo Volcano; 4—Congro Fissural Volcanic System; 5—Furnas Volcano; 6—Povoacão Volcano; 7—Nordeste Volcanic Complex.

The archipelago is located in a zone of confrontation between tropical and polar air masses in the centre of the North Atlantic basin. Atmospheric circulation and the rainfall regime in the Azores region are primarily influenced by the variability of two main pressure systems: the Icelandic Low and the Azores Subtropical High (Azevedo 2001). During the cold season, the Icelandic Low intensifies, enhancing the activity of disturbances along the polar front and resulting in frequent rainy weather. In summer, the Azores High shifts northward, promoting more stable atmospheric conditions and a marked decrease in rainfall levels. The alternating dominance of these two pressure systems is illustrated in Figure 3.2, which displays the mean sea-level pressure fields (1991–2020) over the North Atlantic for January and July, highlighting the essential features of the seasonal climatic rhythm of the archipelago (see also Figure 3.3). This pressure dipole defines the North Atlantic Oscillation (NAO) (Hurrel et al. 2003).

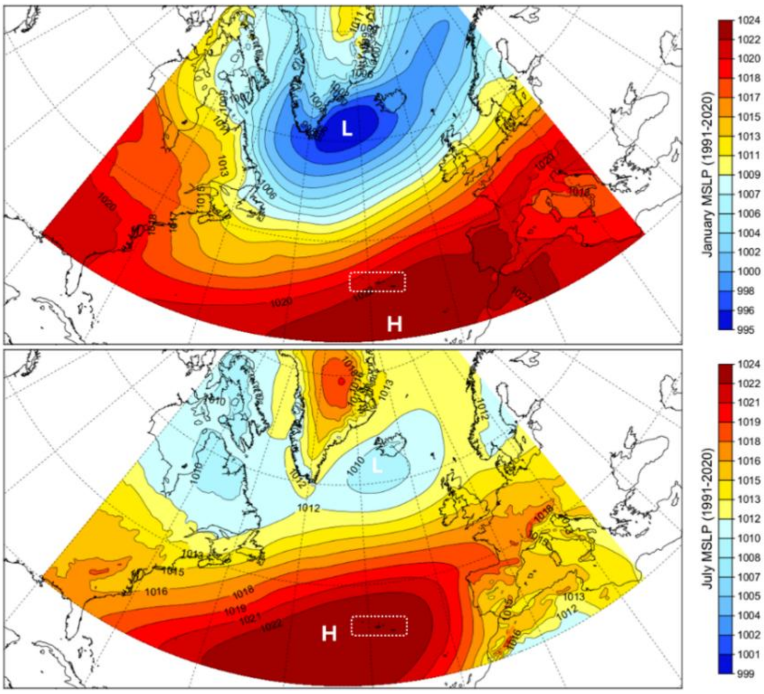

Figure 3.2 | Mean sea-level pressure (hPa) over the North Atlantic in January (top) and July (bottom). The Azores region is highlighted with a white dotted rectangle. The panels were generated by the authors using Climate Data Operators (CDOs; https://code.mpimet.mpg.de/projects/cdo, accessed on 20 May 2025) to compute average fields and Panoply (https://www.giss.nasa.gov/tools/panoply/, accessed on 20 May 2025) for map visualisation. Data source: Copernicus Climate Data Store—ERA5 daily statistics.

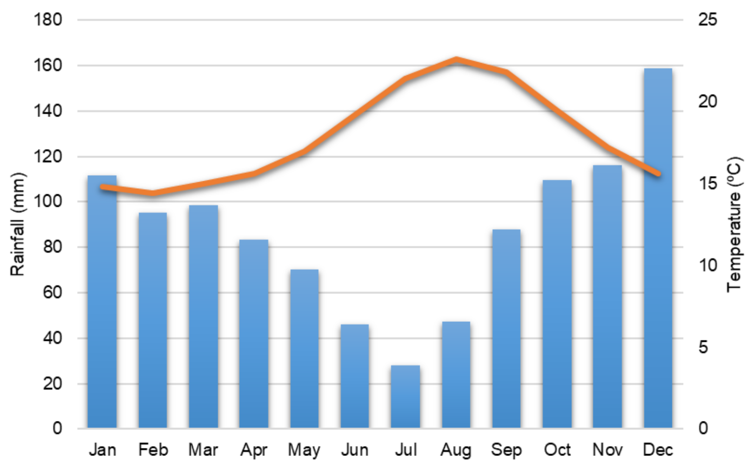

Figure 3.3 | Average monthly rainfall (blue bars) and average monthly temperature (orange line) at the Ponta Delgada meteorological station for the period of 1981–2010 (climate normal data from the Portuguese Institute for Sea and Atmosphere, IPMA, IP).

According to the Köppen classification, the Azores have a temperate (C-type) climate (Azevedo 2001; Carvalho et al. 2022), mainly Cfb, with some Csb areas along the coast (Chazarra et al. 2011). The monthly temperature range is low, with values ranging from 14.4 °C in February to 22.6 °C in August, resulting in an amplitude of around 8 °C (Figure 3.3). Rainfall is evenly distributed throughout the year, with a noticeable decrease in the summer months (Azevedo 2001). The monthly rainfall distribution shows a clear seasonal pattern, with the "rainiest season" spanning from October to March (Figure 3.3). In contrast, the summer months represent the "driest season", with the lowest rainfall levels typically occurring in July.

In Ponta Delgada, on average, rainfall occurs on approximately 122 days per year, consisting of 60 rain spells with an average duration of about 2 days. Each rain spell produces an average of 16 mm, with a mean rate of 7.9 mm/day. Around 42% of the annual total rainfall is due to rain spells lasting longer than 3 days (Hernández et al. 2016).

Based on the application of a climate simulation model for island environments (Azevedo 1996), São Miguel Island experiences a Mean Annual Precipitation (MAP) ranging from 1200 to 2000 mm near the coast, while in the interior high areas, it can reach as much as 4800 mm (Fernandes 2004). This gradient reflects the influence of prevailing westerly and northwesterly winds, shaped by the mid-latitude westerlies and the Azores High (Azevedo 2001). West- and northwest-facing slopes act as windward areas exposed to moist Atlantic air masses, while eastern and southeastern slopes lie in the leeward zone. Storms are most frequent in winter, though late-summer and autumn cyclones can also cause severe floods and landslides (Azevedo 2001).

Climatic diversity across the Azores results from the island's geomorphological and geological complexity. Several factors—such as central volcanoes; dismantled calderas; lakes; geological formations' alignment, including monogenetic cones along fracture zones; valleys, which are often associated with fault zones; ventilation corridors;

vegetation; and the altitude and orientation of slopes and sea cliffs—significantly contribute to local-scale climate differentiation on each island (Rodrigues 1992; Rodrigues 1995; Azevedo 1999; Brito 2004).

3.3 | Materials and Methods

3.3.1 | Rainfall Data Processing

The rainfall data used in this study were collected from 21 rainfall stations. The stations were selected based on the following criteria: (1) data availability from the owning entities and (2) the longest common data period (which corresponds to the climatological years between 1978/79 and 2019/2020). Out of 21 rainfall stations, 17 had data for the period between 1978/79 and 2019/2020, while the remaining 4 had data between 2010/11 and 2019/2020. Table 3.1 lists the rainfall stations, along with their respective altitudes, periods of record, and key descriptive statistics for the annual time series. The locations of these stations are illustrated in Figure 3.4.

Table 3.1 | Rainfall stations used in the analysis and descriptive statistics for the annual time series.

Nr.	Rainfall Station	Altitude (m)	Data Period	Nr. of Days $p \geq 1$ mm	Annual Rainfall (mm)			
					MAP	Min.	Max.	Standard Deviation
1	Mosteiros	21	2010/11–2019/20	106	838.2	540.5	1147.8	189.8
2	Sete Cidades	260	1978/79–2019/20	158	1797.5	833.6	2596.3	353.7
3	Candelária	201	2010/11–2019/20	109	753.6	614.7	1191.0	452.9
4	Capelas	377	2010/11–2019/20	140	1679.9	1358.7	2188.7	286.6
5	Santana	71	1978/79–2019/20	106	1135.3	671.1	1801.1	267.1
6	Ponta Delgada	20	1978/79–2019/20	120	1006.1	558.4	1620.9	218.5
7	Chã da Macela	308	2010/11–2019/20	137	1160.4	569.0	1548.2	263.9
8	Caldeira Velha	283	1978/79–2019/20	126	1562.9	386.6	2340.3	418.0
9	Salto do Cabrito	214	1978/79–2019/20	135	1675.6	606.1	2682.8	407.8
10	Lameiro	308	1978/79–2019/20	147	1666.4	985.4	2364.0	318.3
11	Fogo III	893	1978/79–2019/20	172	2384.5	964.7	4620.8	714.1

12	Lombo	580	1978/79–2019/20	156	2183.9	1116.0	3606.4	556.0
13	Praia	200	1978/79–2019/20	140	1831.2	928.3	3070.1	520.6
14	Monte Escuro	802	1978/79–2019/20	193	2963.0	1996.3	4186.0	547.1
15	Salga	290	1978/79–2019/20	136	1524.1	814.1	2340.4	326.6
16	Algarvia	340	1978/79–2019/20	141	1777.2	961.3	2659.7	387.9
17	Salto do Fojo	480	1978/79–2019/20	135	2276.8	1393.4	3049.2	417.2
18	Lagoa das Furnas	280	1978/79–2019/20	151	2127.4	1219.0	3762.4	557.0
19	Monte Simplício	320	1978/79–2019/20	130	1849.4	834.5	2734.0	485.3
20	Espigão da Ponte	934	1978/79–2019/20	201	2888.0	1567.5	8393.0	1181.3
21	Lomba da Erva	379	1978/79–2019/20	161	2224.1	1366.6	3039.3	419.7

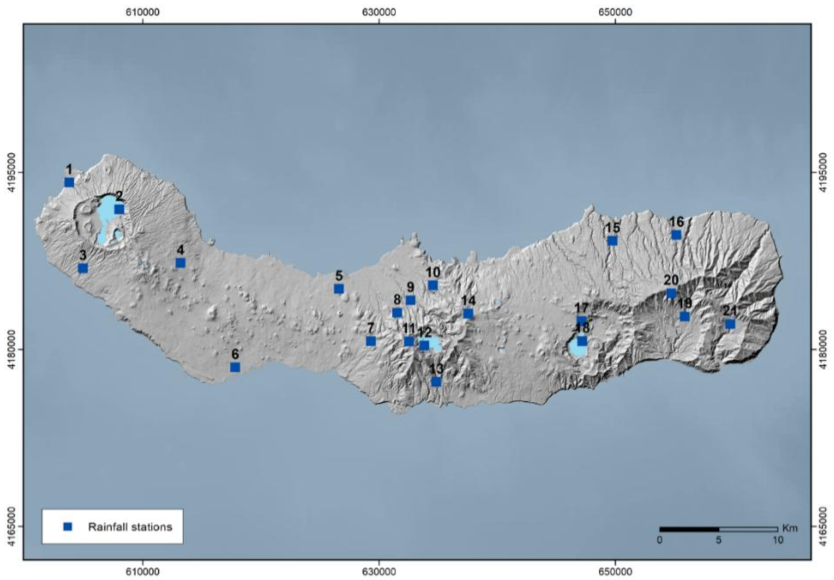

Figure 3.4 | Geographic locations of rainfall stations (numbers correspond to stations listed in Table 3.1).

Monthly rainfall data from each rainfall station were used in this study. The monthly data were aggregated into four three-month periods corresponding to the seasons: autumn (September, October, and November), winter (December, January, and February), spring (March, April, and May), and summer (June, July, and August). From these seasonal datasets, the 10th, 50th, and 90th percentiles were calculated. Additionally, annual rainfall totals and Mean Annual Precipitation (MAP) were computed for each rainfall station. Data quality was assessed through inspection for gaps or anomalies, with no inconsistencies detected. Normality was evaluated using the Shapiro–Wilk (e.g. Royston, 1982) and Kolmogorov–Smirnov (e.g. Deheuvels, 1981) tests, and homogeneity was verified through the Standard Normal Homogeneity Test (SNHT) (Alexandersson and Moberg 1997), Buishand range test (Buishand, 1982), Pettitt test (Pettitt, 1979), and Von Neumann ratio test (Von Neumann, 1941). Following Wijngaard et al. (2003), the series were classified as "useful", "doubtful", or "suspect" based on the number of tests rejecting the null hypothesis at the 1% significance level, thereby assessing their suitability for trend and variability analyses.

3.3.2 | Methods

This study was based on the analysis of three distinct temporal periods, determined by the available rainfall station coverage: (1) climatological years from 1978/79 to 2019/2020 (full dataset); (2) climatological years from 1978/79 to 2009/2010 (oldest sub-dataset); and (3) climatological years from 2010/11 to 2019/2020 (latest sub-dataset).

To classify the stations into homogeneous rainfall regions, hierarchical cluster analysis was performed using Ward's method (Ward 1963). This method minimises the total within-cluster variance, ensuring that elements that are grouped together show greater internal similarity than they do with other clusters. The squared Euclidean distance was used as a dissimilarity metric (Everitt and Dunn 1991). The number of clusters was validated using the Silhouette Coefficient, which quantifies how well each station fits within its assigned cluster (Wang et al. 2025).

Hierarchical clustering was performed in three steps to reflect the three temporal datasets: (i) clustering of 17 stations for the full period (1978/79–2019/2020); (ii) clustering of the same 17 stations for the oldest period (1978/79–2009/2010); and (iii) clustering of all 21 stations, including the more recent additions, for the period of 2010/11–2019/2020.

The hierarchical clustering of rainfall stations on São Miguel Island considered 13 variables: Mean Annual Precipitation (MAP) and the 10th, 50th, and 90th percentiles for each season. These percentiles were used in rainfall analysis to better understand the data distribution (Tsubo et al. 2007; Mazvimavi 2010). The 10th percentile (P10) represents frequently occurring low rainfall, helping identify dry periods. The 50th percentile (P50) corresponds to the median rainfall, providing a robust central measure that is unaffected by extreme values. The 90th percentile (P90) highlights high-rainfall events, which are crucial for assessing heavy rainfall conditions and extreme rainfall events. The data were normalised using the Z-score method, standardising the variables to have a mean of zero and a standard deviation of one, thus preventing differences in scale from influencing the clustering results. The Statistical Package for the Social

Sciences (IBM SPSS Statistics 30) software was used to derive hierarchical cluster groupings based on these variables.

The variation in the values of variables for each rainfall station within each cluster, as well as the variation between clusters for each of the three periods analysed, was calculated based on the average of each variable and the coefficient of variation (CV).

Rainfall trends were evaluated using the Mann–Kendall (M-K) test (Mann 1945; Kendall 1976) to assess trend significance and Sen's slope estimator (Theil 1950; Sen 1968) to determine the magnitude of trends. These non-parametric methods are widely recommended for environmental and hydrological time series, as they are robust to missing values and do not require a normal data distribution (World Meteorological Organization 2018; Sa'adi et al. 2019). The analysis of annual and seasonal rainfall trends was conducted using data from the 17 rainfall stations with the longest records, covering the climatological years of 1978/79–2019/20. Stations with data only for more recent periods were excluded, as their rainfall trend analysis would not be statistically representative. Annual rainfall trends were evaluated by analysing the total rainfall recorded for each climatological year at each station. Likewise, seasonal trends were assessed based on the accumulated rainfall for each season.

The correlation between the NAO and the annual and seasonal rainfall series for the same climatological period (1978/79–2019/20) was performed by calculating Spearman's correlation coefficients. Spearman's rank correlation and associated *p*-values capture monotonic relationships and are robust to non-normality and outliers, which are common in rainfall and climate index data (Wilks 2020). Statistical significance was determined at $p < 0.05$. The teleconnection index used was the Hurrel NAO index (PC-based), available at https://climatedataguide.ucar.edu/climate-data/hurrell-north-atlantic-oscillation-nao-index-pc-based (accessed on 12 November 2025) (Hurrel et al. 2003).

Although the relationship between altitude and rainfall is well known worldwide, the influence of altitude on the identified homogeneous rainfall station groups was also studied. To this end, linear regression graphs were constructed to examine the relationship between altitude and rainfall variables (MAP and the 10^{th}, 50^{th}, and 90^{th} percentiles) across the three considered temporal periods. In addition, Pearson correlation coefficients (r) and their corresponding significance levels (p-values) were calculated to assess the strength and reliability of these relationships.

3.4 | Results

3.4.1 | Analysis of Normalisation and Homogeneity Tests

The results of the Shapiro–Wilk and Kolmogorov–Smirnov normality tests, as well as the classification based on homogeneity tests applied to the annual rainfall time series, are summarised in Table 3.2. These statistics indicate that the null hypothesis of normality can be rejected for the Fogo III and Espigão da Ponte datasets. Although normality is a prerequisite for some of the subsequent homogeneity tests, all datasets were analysed. It should be noted that the results of the normality and homogeneity tests may affect the validity of the conclusions drawn from the subsequent trend tests and should be interpreted with caution.

While the majority of the datasets are classified as “useful”, some series may not be homogeneous over the entire recorded period. Specifically, the time series for Fogo III, Monte Simplício, and Espigão da Ponte were classified as “doubtful”. This could not be explained based on the available metadata. Moreover, the presence of a significant trend, such as a decreasing trend in a time series, can influence the results of homogeneity tests, potentially leading to their rejection, even in the absence of structural changes in the data (Lund et al. 2023). Consequently, for the Fogo III, Monte Simplício, and Espigão da Ponte time series, the results of the trend analysis over the full period should be interpreted with particular caution.

Table 3.2 | Statistics for the Shapiro–Wilk and Kolmogorov–Smirnov normality tests, applied to the annual rainfall time series. The results in bold indicate which series have normal distributions at a 5% significance level. The classification of the series is based on the results of the homogeneity tests.

Nr.	Rainfall Station	Data Period	Normality Tests		Classification Based on Homogeneity Tests
			Shapiro–Wilk	Kolmogorov–Smirnov	
2	Sete Cidades	1978/79–2019/20	**0.416**	**0.671**	Useful
5	Santana	1978/79–2019/20	**0.359**	**0.720**	Useful
6	Ponta Delgada	1978/79–2019/20	**0.435**	**0.885**	Useful
8	Caldeira Velha	1978/79–2019/20	**0.094**	**0.277**	Useful
9	Salto do Cabrito	1978/79–2019/20	**0.567**	**0.574**	Useful
10	Lameiro	1978/79–2019/20	**0.530**	**0.660**	Useful
11	Fogo III	1978/79–2019/20	0.012	**0.326**	Doubtful
12	Lombo	1978/79–2019/20	**0.828**	**0.978**	Useful
13	Praia	1978/79–2019/20	**0.470**	**0.756**	Useful
14	Monte Escuro	1978/79–2019/20	**0.329**	**0.972**	Useful
15	Salga	1978/79–2019/20	**0.555**	**0.785**	Useful
16	Algarvia	1978/79–2019/20	**0.990**	**0.996**	Useful
17	Salto do Fojo	1978/79–2019/20	**0.498**	**0.928**	Useful
18	Lagoa das Furnas	1978/79–2019/20	**0.057**	**0.697**	Useful

19	Monte Simplício	1978/79–2019/20	**0.122**	**0.609**	Doubtful
20	Espigão da Ponte	1978/79–2019/20	0.000	0.061	Doubtful
21	Lomba da Erva	1978/79–2019/20	**0.793**	**0.977**	Useful

3.4.2 | Clustering of Rainfall Stations and Statistical Analysis

Hierarchical clustering analysis based on Ward's method identified four main groups of rainfall stations with similar rainfall characteristics (Figure 3.5). The clustering structure was validated using the Silhouette Coefficient, calculated for k = 2 to k = 8, confirming that four clusters provide the most appropriate classification (Figure 3.6). The average silhouette values were consistently higher for k = 4 across the full dataset (0.55), the oldest sub-dataset (0.55), and the latest sub-dataset (0.48), indicating a good balance between cluster compactness and separation.

For the full dataset (Figure 3.5a), Cluster 1 comprises the stations of Santana and Ponta Delgada. Cluster 2 includes eight stations: Caldeira Velha, Salga, Monte Simplício, Praia, Lameiro, Salto do Cabrito, Algarvia, and Sete Cidades. Cluster 3 consists of five stations: Lombo, Salto do Fojo, Lomba da Erva, Lagoa das Furnas, and Fogo III. Lastly, Cluster 4 includes the stations of Monte Escuro and Espigão da Ponte.

In the oldest sub-dataset (Figure 3.5b), Clusters 1 and 2 remained unchanged, indicating temporal stability in the rainfall patterns of these stations. However, Clusters 3 and 4 underwent reconfiguration. Cluster 3 includes four stations (Lomba da Erva, Salto do Fojo, Lombo, and Lagoa das Furnas), while Cluster 4 includes three stations (Espigão da Ponte, Monte Escuro, and Fogo III). This shift reflects subtle changes in rainfall behaviour, particularly the migration of Fogo III from Cluster 3 to Cluster 4.

The latest sub-dataset (Figure 3.5c) exhibits a more pronounced reorganisation of the clusters. Cluster 1 expands to include four stations: Mosteiros, Ponta Delgada, Candelária, and Santana. Cluster 2 includes seven stations: Chã da Macela, Salga, Lameiro, Salto do Cabrito, Praia, Caldeira Velha, and Monte Simplício. Cluster 3 consists of eight stations: Lagoa das Furnas, Algarvia, Sete Cidades, Capelas, Fogo III, Lombo, Lomba da Erva, and Salto do Fojo. Cluster 4 maintains the same composition as in the full dataset, with the stations of Espigão da Ponte and Monte Escuro.

Out of the 21 stations analysed, 15 remained in the same cluster throughout the periods considered. Overall, Clusters 1 and 4 show a high degree of temporal stability, reflecting persistent rainfall regimes. In contrast, Clusters 2 and 3 exhibit greater variability, with changes in the number and composition of stations over time. Notably, after 2010, Algarvia and Sete Cidades migrated from Cluster 2 to Cluster 3, suggesting increased rainfall in these areas. The transitional behaviour of the Fogo III station, which shifted between Clusters 3 and 4, highlights the sensitivity of stations that are located in more exposed areas to slight variations in atmospheric circulation patterns.

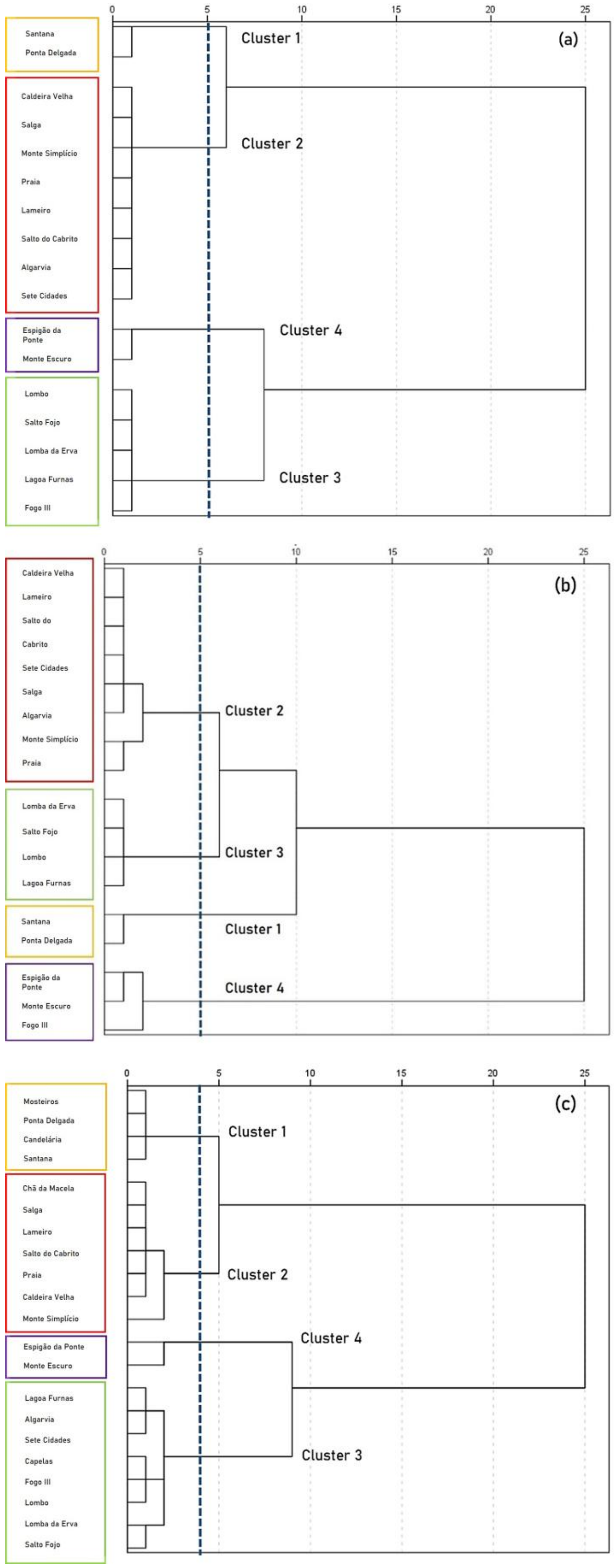

Figure 3.5 | Dendrogram with rainfall stations and their clusters for (a) the full dataset, (b) the oldest sub-dataset, and (**c**) the latest sub-dataset.

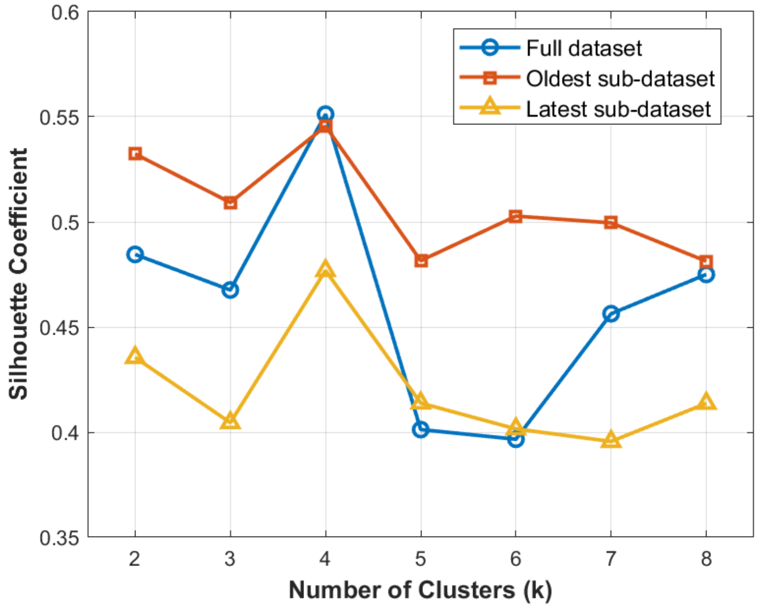

Figure 3.6 | Silhouette Coefficient for different numbers of clusters (k) for the full dataset, the oldest sub-dataset, and the latest sub-dataset.

The mean values of the variables used in the analysis (MAP, P10, P50, and P90) for each cluster are summarised in Table 3.3. The results highlight the variability in rainfall amounts across different clusters during each considered period. Significant variability in MAP is observed across the clusters. For the full dataset, Cluster 1 exhibits an average MAP of 1059.8 mm, whereas Cluster 4 shows a significantly higher average of 2925.5 mm. Clusters 2 and 3 record average MAP values of 1704.8 mm and 2229.6 mm, respectively. For the oldest sub-dataset, the pattern remains consistent: Cluster 1 maintains a lower average MAP of 1124.2 mm, while Cluster 2 is at 1800.9 mm, Cluster 3 at 2301.0 mm, and Cluster 4 at 2954.4 mm The latest sub-dataset reveals a reduction in overall MAP values and a decrease in the contrast between Clusters 1 and 2, with average MAP vales of 835.8 mm and 1292.6 mm, respectively. Meanwhile, Clusters 3 and 4 also show lower averages compared with previous periods, at 1762.0 mm and 2335.3 mm, respectively. This reduction may indicate a recent shift in rainfall distribution patterns, with a tendency towards drier conditions, especially in the lower-altitude clusters.

Table 3.3 | Mean values (mm) of rainfall variables for each cluster during the climatological years of 1978/79–2019/20, 1978/79–2009/10, and 2010/11–2019/20.

Dataset	**Full Dataset**				**Oldest Sub-Dataset**				**Latest Sub-Dataset**			
Climatological Years	**1978/79–2019/20**				**1978/79–2009/10**				**2010/11–2019/20**			
Variable	**Cluster 1**	**Cluster 2**	**Cluster 3**	**Cluster 4**	**Cluster 1**	**Cluster 2**	**Cluster 3**	**Cluster 4**	**Cluster 1**	**Cluster 2**	**Cluster 3**	**Cluster 4**
P10 Autumn	210.8	332.0	405.1	547.4	252.6	369.5	448.4	581.0	147.9	216.5	333.3	445.6
P50 Autumn	331.4	497.5	616.5	833.8	346.5	513.9	624.0	799.4	244.3	388.5	514.2	760.4
P90 Autumn	435.6	699.4	864.4	1158.1	449.6	712.0	878.0	1133.0	364.2	562.4	710.5	977.4
P10 Winter	194.8	313.4	443.9	553.4	234.0	398.3	525.4	593.7	104.5	215.6	232.8	405.5
P50 Winter	335.0	567.9	700.3	814.2	339.9	591.5	773.1	823.6	285.7	417.7	547.3	692.3
P90 Winter	559.9	855.0	1173.7	1365.2	577.5	874.2	1146.5	1384.5	387.0	665.8	809.4	1023.7
P10 Spring	128.9	215.8	301.6	422.6	131.1	233.9	298.5	426.8	106.6	182.3	281.1	379.2
P50 Spring	232.8	382.5	506.0	621.0	250.8	400.9	531.7	656.8	190.4	305.5	406.1	578.4
P90 Spring	394.7	635.3	888.8	1075.8	396.1	640.9	889.2	1061.7	285.7	425.6	619.7	694.0
P10 Summer	54.2	115.7	150.0	296.4	71.3	135.5	179.2	320.5	45.2	87.3	112.8	211.2
P50 Summer	111.2	199.4	276.1	423.2	115.1	214.6	268.8	424.2	79.5	153.1	205.1	331.9
P90 Summer	207.8	321.8	417.4	595.7	212.9	329.8	394.7	581.2	163.7	208.8	341.7	437.6
MAP	1070.6	1710.6	2239.4	2925.5	1124.2	1800.9	2301.0	2954.4	835.8	1292.6	1762.0	2335.3

The analysis of P10, P50, and P90 values reveals the seasonal fluctuation of rainfall, with higher values typically being recorded in winter, progressively decreasing through spring, and reaching their lowest level in summer. This seasonal trend corroborates the expected annual rainfall cycle. The P10 values are relatively uniform across all seasons and clusters, suggesting a uniformity in the lower limits of rainfall distribution. In contrast, P50 values, representing the median rainfall, show similar trends between clusters in winter and autumn; however, these values diverge significantly in summer, indicating more pronounced differences in median rainfall amounts within each cluster during the drier season. The P90 values, reflecting the upper limits of the rainfall distribution, exhibit significant variability between clusters, particularly in winter and autumn, highlighting the differences in extreme rainfall events across the clusters. During summer, however, differences in P90 values between clusters become less significant, which is consistent with the lower occurrence of extreme rainfall in the drier season.

The coefficient of variation (CV) values of the variables used in the analysis (MAP, P10, P50, and P90) within each cluster are summarised in Table 3.4, providing insights into intra-cluster homogeneity. For the full dataset, the rainfall stations in each cluster show high similarity, with CV values generally being less than 15%. Clusters 1 and 3 present lower CV values, indicating greater similarity between the stations within these clusters. In Cluster 2, the P10 variable shows higher CV values in autumn, winter, and summer (18.5%, 18.0%, and 19.3%, respectively). In Cluster 4, the greatest heterogeneity within the cluster is observed in the P10 variable for winter and summer (20.9% and 17.3%, respectively).

Table 3.4 | Coefficient of variation (CV) of rainfall variables for each cluster during the climatological years of 1978/79–2019/20, 1978/79–2009/10, and 2010/11–2019/20.

Dataset	**Full Dataset**				**Oldest Sub-Dataset**				**Latest Sub-Dataset**			
Climatological Years	**1978/79–2019/20**				**1978/79–2009/10**				**2010/11–2019/20**			
Variable	**Cluster 1**	**Cluster 2**	**Cluster 3**	**Cluster 4**	**Cluster 1**	**Cluster 2**	**Cluster 3**	**Cluster 4**	**Cluster 1**	**Cluster 2**	**Cluster 3**	**Cluster 4**
P10 Autumn	1.0%	18.5%	12.8%	8.6%	4.4%	9.2%	7.0%	6.1%	22.9%	32.9%	21.2%	5.4%
P50 Autumn	1.2%	5.0%	6.8%	4.0%	3.7%	5.7%	6.1%	9.7%	17.9%	18.1%	13.4%	7.5%
P90 Autumn	12.8%	9.3%	10.1%	5.2%	11.5%	8.0%	3.6%	9.8%	6.6%	19.0%	12.4%	6.6%
P10 Winter	7.5%	18.0%	7.6%	20.9%	2.8%	12.1%	9.0%	11.5%	22.6%	21.1%	36.3%	30.2%
P50 Winter	10.6%	7.4%	6.8%	11.2%	7.1%	8.2%	5.2%	10.4%	23.5%	21.8%	12.8%	37.0%
P90 Winter	7.4%	10.1%	5.6%	0.4%	11.4%	12.5%	2.7%	5.4%	13.5%	14.4%	10.9%	25.9%
P10 Spring	5.8%	11.4%	7.9%	11.0%	8.1%	20.4%	4.8%	15.4%	22.6%	35.8%	17.7%	1.6%
P50 Spring	5.1%	10.4%	8.1%	3.9%	2.3%	12.7%	9.8%	13.5%	5.5%	8.5%	11.9%	8.2%
P90 Spring	4.5%	8.9%	4.0%	9.6%	5.0%	10.8%	2.2%	11.9%	11.0%	8.5%	17.6%	9.5%
P10 Summer	6.9%	19.3%	13.6%	17.3%	12.6%	11.5%	13.3%	18.3%	25.1%	26.2%	17.9%	8.0%
P50 Summer	4.9%	7.0%	13.4%	4.5%	1.2%	7.6%	8.6%	11.2%	5.0%	23.4%	14.1%	2.4%
P90 Summer	14.5%	9.0%	12.8%	0.3%	17.5%	7.7%	5.6%	9.5%	27.3%	19.4%	23.4%	10.7%
MAP	8.5%	7.2%	4.4%	1.8%	8.2%	7.9%	2.5%	9.4%	8.1%	9.5%	7.9%	8.3%

For the oldest sub-dataset, the CV values remain generally low across clusters, indicating homogeneity among the rainfall stations that make up each cluster. Notably, in Cluster 1, the P90 in summer shows the highest CV value (17.5%), while in Cluster 2, the P10 in spring is the most different among the rainfall stations in the cluster (20.4%). In Cluster 3, the CV values are lower for all variables, reinforcing its homogeneity. Cluster 4 presents its highest CV values in P10 during spring and summer (15.4% and 18.3%, respectively).

In contrast, the latest sub-dataset shows generally higher CV values, frequently exceeding 15%, which reflects increased heterogeneity within clusters. In Cluster 1, the highest value is observed in the P90 variable for summer (27.3%). Cluster 2 exhibits the most variability in P10 during spring (35.8%). Cluster 3 shows the highest CV in P10 during winter (36.3%), and Cluster 4 exhibits the greatest variation in P50 during winter (37.0%). This rise in CV values corresponds to the inclusion of new rainfall stations into the clusters, whose differing characteristics contribute to increased heterogeneity within each group.

3.4.3 | Spatial Distribution of Rainfall Station Clusters

The spatial distribution of the rainfall station clusters provides valuable insights into the relationship between altitude and rainfall patterns across São Miguel Island. Figure 3.7 illustrates the spatial distribution of stations within each cluster for the full dataset, the oldest sub-dataset, and the latest sub-dataset, respectively, over the hypsometric map of São Miguel Island.

The analysis of the full dataset (Figure 3.7a) indicates that the geographical positioning of stations within Cluster 1 is confined to lower altitudinal zones, specifically below 150 m. Stations belonging to Cluster 2 are located at intermediate altitudes, ranging from 150 to 350 m. Stations within Cluster 3 are found at higher altitudes, between 350 and 800 m, with the notable exceptions of Lagoa das Furnas station, located inside the Furnas Volcano caldera, and Fogo III station, situated near the rim of the Fogo Volcano caldera. Despite their altitudes of 280 and 893 m, respectively, they are included in Cluster 3. Stations grouped into Cluster 4 are found at the highest altitudes on the island, exceeding 800 m. These results suggest that factors beyond altitude are influencing rainfall patterns.

For both the oldest and latest sub-datasets (Figure 3.7b,c), Cluster 1 consistently comprises stations located at the lowest altitudes, specifically between 0 and 150 m. Notably, the Candelária station, which is slightly higher at 201 m, is also included in this cluster in the latest sub-dataset (Figure 3.7c). Rainfall stations belonging to Cluster 2 are located within the intermediate altitude range of 150 to 350 m, whereas rainfall stations in Cluster 3 are generally found at higher altitudes, between 350 and 800 m, except

Lagoa das Furnas station. Despite its altitude of 280 m, it consistently remains within Cluster 3, as observed for the full dataset. The analysis of the latest sub-dataset shows that the Sete Cidades and Algarvia stations, located at altitudes of 260 m and 340 m, respectively, are included in Cluster 3 (Figure 3.7c), despite their altitudes aligning more closely with Cluster 2, underscoring the complex relationship between altitude, geographical factors, and rainfall distribution. Stations belonging to Cluster 4 are located at the highest altitudes on the island (above 800 m), with the latest sub-dataset including Fogo III station in Cluster 3, despite its altitude of 893 m (Figure 3.7c). This classification emphasises the complex interplay of topography and climate affecting rainfall distribution, suggesting that altitude is a significant, but not exclusive, determinant of rainfall distribution across São Miguel Island.

3.4.4 | Rainfall Trends

Figure 3.8 shows the evolution of the Mean Annual Precipitation (MAP) at four representative stations with the most pronounced decreasing rainfall trends—Santana (Cluster 1), Caldeira Velha (Cluster 2), Salto do Fojo (Cluster 3), and Monte Escuro (Cluster 4)—over the climatological years of 1978/79 and 2019/20. During the period corresponding to the oldest sub-dataset (1978/79 to 2009/10), all stations exhibit high interannual variability, reflecting the markedly unstable nature of the regional rainfall regime. However, in the most recent sub-dataset (2010/11 to 2019/20), a general reduction in MAP becomes evident.

Monte Escuro registers the highest annual totals yet shows a declining trend in the most recent decade, particularly with a reduced frequency of years with rainfall exceeding 3000 mm. At Salto do Fojo, the downward trend is more gradual but still evident, with several consecutive years over the last decade in which the rainfall is below the long-term average. At Caldeira Velha, a downward trend in rainfall has also been observed since 2009/10, with several consecutive years recording less than 1200 mm. Santana, while generally exhibiting a more stable pattern, also reveals subtle signs of decreasing rainfall, with an increasing number of recent years registering totals below 1000 mm.

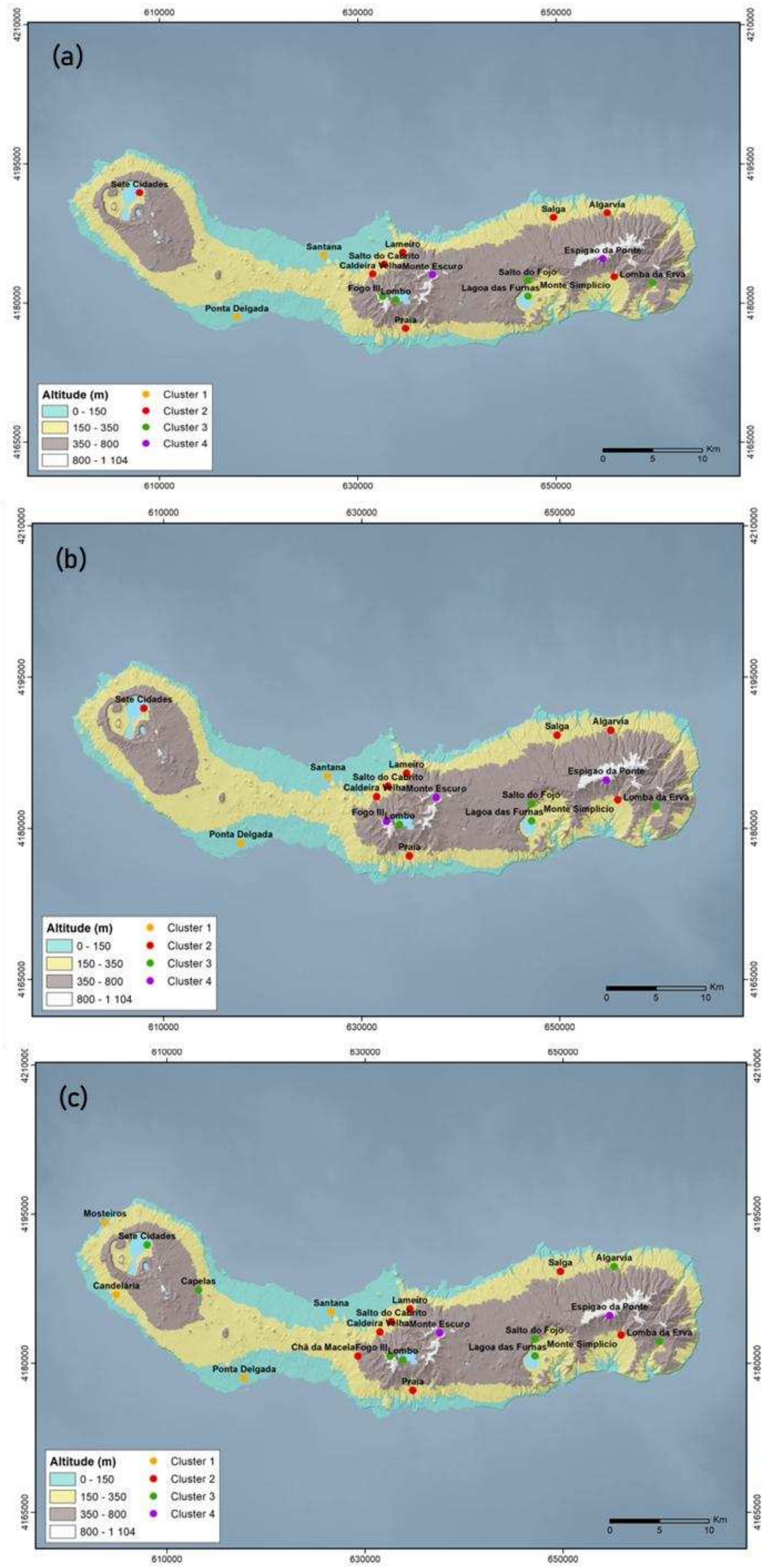

Figure 3.7 | Hypsometric map illustrating the distribution of rainfall station clusters for (a) the full dataset, (b) the oldest sub-dataset, and (c) the latest sub-dataset.

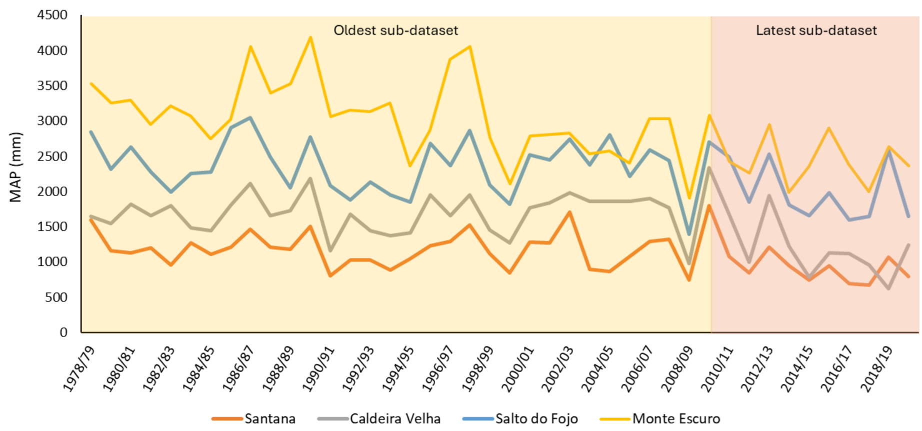

Figure 3.8 | Evolution of the Mean Annual Precipitation recorded between the climatological years 1978/79 and 2019/20 at the rainfall stations of Santana (Cluster 1), Caldeira Velha (Cluster 2), Salto do Fojo (Cluster 3), and Monte Escuro (Cluster 4).

The rate of change in the rainfall variable values between the oldest and latest sub-datasets is summarised in Table 3.5, which reveals a pronounced decrease in rainfall values, ranging from 20% to 30%. Nonetheless, differences are observed across variables and clusters. The MAP value exhibits a reduction of approximately 25% across the two sub-datasets. This reduction is most marked in Cluster 2, where it reaches −28.2%. The decrease in rainfall values during autumn is more pronounced in years with lower rainfall levels (P10), particularly in Clusters 1 and 2. In winter, there is a sharp decrease in rainfall in the driest years, ranging from −30% to −55%. In spring, the decrease in rainfall values is more pronounced in years with higher rainfall levels (P90) in all clusters, where the decreases are around −30%. The rates of change in summer are also high, particularly in years with lower levels of rainfall (P10), but yield a diminished impact, due to the season's typically lower rainfall compared with other periods of the year.

Table 3.5 | Rate of change in the value of rainfall variables between the oldest and latest sub-datasets.

Variable	Cluster 1	Cluster 2	Cluster 3	Cluster 4
P10 Autumn	−41.4%	−41.4%	−25.7%	−23.3%
P50 Autumn	−29.5%	−24.4%	−17.6%	−4.9%
P90 Autumn	−19.0%	−21.0%	−19.1%	−13.7%
P10 Winter	−55.3%	−45.9%	−55.7%	−31.7%
P50 Winter	−15.9%	−29.4%	−29.2%	−15.9%
P90 Winter	−33.0%	−23.8%	−29.4%	−26.1%
P10 Spring	−18.7%	−22.1%	−5.8%	−11.2%
P50 Spring	−24.1%	−23.8%	−23.6%	−11.9%
P90 Spring	−27.9%	−33.6%	−30.3%	−34.6%

P10 Summer	−36.6%	−35.6%	−37.1%	−34.1%
P50 Summer	−30.9%	−28.7%	−23.7%	−21.8%
P90 Summer	−23.1%	−36.7%	−13.4%	−24.7%
MAP	−25.7%	−28.2%	−23.4%	−21.0%

The Mann–Kendall test, paired with Sen's slope estimator, was used to identify rainfall trends at the 17 stations with data covering the period from 1978/79 to 2019/20. The outcomes, summarised in Table 3.6, reveal declining trends in rainfall on both the annual and seasonal scales, with autumn exhibiting the most significant decreases. Although visual inspection of the time series and slope estimates indicates decreasing rainfall at many stations, only 5 of the 17 stations showed statistically significant downward annual trends ($\alpha \leq 0.05$), highlighting the spatial heterogeneity of rainfall changes across the island. Figure 3.9 shows the spatial distribution of the annual rainfall trends obtained from the M-K test.

When analysing the rainfall data by clusters, distinct patterns and trends emerge across different regions, underscored by significant changes in rainfall measurements. In Cluster 1, autumn registered the most significant decreases, specifically in Santana (−3.71 mm/year **) and Ponta Delgada (−3.43 mm/year **), pointing to a trend towards drier autumns and an overall reduction in annual rainfall, with Santana being particularly affected. Cluster 2 is characterised by significant reductions, with Monte Simplício showing a notable annual decrease (−19.18 mm/year *). Caldeira Velha exhibits significant decreases in autumn (−6.91 mm/year **), a trend that is also observed at Sete Cidades (−4.19 mm/year *), Lameiro (−4.06 mm/year *), and Salto do Cabrito (−3.96 mm/year *). Moreover, Monte Simplício reveals significant decreases in winter (−7.77 mm/year *) and spring (−5.37 mm/year **), indicating localised environmental changes affecting rainfall patterns. Cluster 3 is highlighted by the severe annual rainfall reduction at Fogo III (−31.57 mm/year ***), along with a considerable decrease at Salto do Fojo (−13.04 mm/year *). This cluster shows the most pronounced rainfall decline across all seasons, especially at Fogo III, with significant reductions in autumn (−12.08 mm/year ***), winter (−10.01 mm/year **), spring (−5.87 mm/year *), and summer (−6.14 mm/year ***). In Cluster 4, Monte Escuro and Espigão da Ponte both show significant annual decreases in rainfall (−25.55 mm/year *** and −21.34 mm/year **, respectively). Monte Escuro also experiences substantial reductions in autumn, spring, and summer (−9.11 mm/year **, −7.10 mm/year *, and −3.57 mm/year *, respectively), while Espigão da Ponte experiences a notable decrease in summer (−4.05 mm/year *). These stations exhibit significant negative variations during summer when compared with other clusters, indicating pronounced seasonal influences on rainfall patterns.

Table 3.6 | Sen's slope estimator of the annual and seasonal rainfall trends (numerical values, mm/year) and respective levels of significance according to the M–K Test.

Cluster	Rainfall Station	Q_{Annual}	Q_{Autmun}	Q_{Winter}	Q_{Spring}	Q_{Summer}
1	Ponta Delgada	−3.70	**−3.43 ****	−1.13	−0.73	0.20
	Santana	−7.19	**−3.71 ****	−1.56	−0.95	−0.57
2	Caldeira Velha	−12.21	**−6.91 ****	−1.78	−3.04	**−3.15 ***
	Salga	−1.88	−1.15	0.50	0.10	−0.64
	Monte Simplício	**−19.18 ***	−4.27	**−7.77 ***	**−5.37 ***	−1.16
	Praia	−10.75	−2.86	−3.16	**−3.79 ***	−0.66
	Lameiro	−7.05	**−4.06 ***	−0.40	−1.21	−0.35
	Salto Cabrito	−7.91	**−3.96 ***	−2.53	−1.23	**−2.30 ***
	Sete Cidades	−0.81	**−4.19 ***	−0.34	0.13	1.06
	Algarvia	2.68	−1.64	−1.22	0.40	0.25
3	Lombo	−9.70	−1.98	−6.39	−1.54	−0.11
	Lagoa Furnas	−9.44	**−4.17 ***	−2.16	−3.25	−1.05
	Fogo III	**−31.57 *****	**−12.08 *****	**−10.01 ****	**−5.87 ***	**−6.14 *****
	Lomba da Erva	−9.05	−3.21	−2.87	−3.09	−0.66
	Salto Fojo	**−13.04 ***	−3.36	−4.23	−3.18	−1.32
4	Monte Escuro	**−25.55 *****	**−9.11 ****	−5.12	**−7.10 ***	**−3.57 ***
	Espigão da Ponte	**−21.34 ****	−2.95	−6.75	−5.02	**−4.05 ***

*** trend at α = 0.001 level of significance; ** trend at α = 0.01 level of significance; * trend at α = 0.05 level of significance.

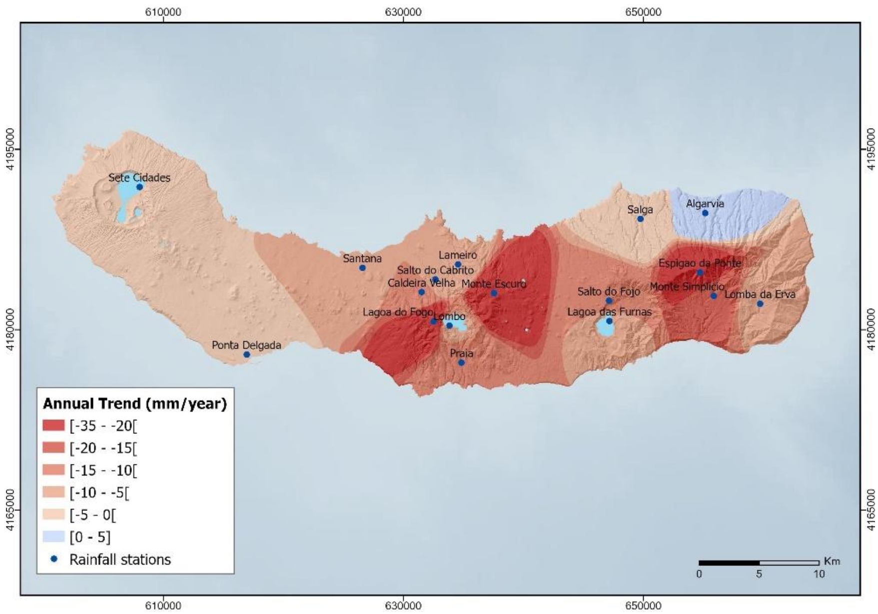

Figure 3.9 | Spatial distribution of the annual rainfall trends (mm/year), determined by the M–K test.

3.4.5 | NAO–Rainfall Relationship

Across the 17 rainfall stations, the Spearman rank correlations reveal a broadly consistent negative association between the Hurrell PC-based NAO index and rainfall, particularly for annual totals and for the autumn season (Table 3.7).

During autumn, correlations remain predominantly negative and statistically significant at several stations, such as Lomba da Erva (ρ = −0.46, p < 0.01), Monte Simplício (ρ = −0.43, p < 0.01), Salto Fojo (ρ = −0.44, p < 0.01), and Espigão da Ponte (ρ = −0.41, p = 0.01).

By contrast, winter correlations are generally weaker and mostly non-significant (−0.1 to −0.2), while spring and summer correlations are low and spatially inconsistent. At the annual scale, most stations exhibit negative coefficients, several of which are statistically significant at the 95% confidence level, notably at Salto do Cabrito (ρ = −0.46, p < 0.01), Ponta Delgada (ρ = −0.38, p = 0.01), Sete Cidades (ρ = −0.33, p = 0.03), Monte Simplício (ρ = −0.33, p = 0.04), Lagoa das Furnas (ρ = −0.35, p = 0.02), and Lomba da Erva (ρ = −0.33, p = 0.04).

Table 3.7 | Spearman rank correlation coefficients between annual and seasonal rainfall and the Hurrell PC-based NAO index. Values in bold indicate statistical significance at p < 0.05.

Rainfall Station	Annual	Autumn	Winter	Spring	Summer
Lagoa Furnas	**−0.35**	−0.26	−0.14	−0.10	0.27
Lombo	−0.26	−0.28	−0.13	0.14	0.06
Santana	−0.27	−0.28	−0.06	0.12	**0.44**
Sete Cidades	**−0.33**	−0.24	−0.11	0.29	0.23
Algarvia	−0.24	**−0.38**	−0.11	0.15	0.28
Caldeira Velha	−0.30	−0.18	−0.16	0.02	0.29
Espigão da Ponte	0.09	**−0.41**	−0.09	0.11	**0.38**
Fogo III	−0.12	−0.13	−0.26	0.10	**0.37**
Lameiro	−0.28	−0.25	−0.17	0.16	**0.40**
Lomba da Erva	**−0.33**	**−0.46**	−0.28	0.16	0.04
Monte Escuro	−0.03	0.03	−0.22	0.01	**0.61**
Monte Simplício	**−0.33**	**−0.43**	−0.20	0.02	0.05
Praia	−0.06	−0.28	−0.12	0.13	0.29
Salga	−0.16	−0.20	−0.08	0.26	0.22
Salto Cabrito	**−0.46**	**−0.35**	−0.23	0.08	**0.38**
Salto Fojo	−0.30	**−0.44**	−0.17	0.04	0.28
Ponta Delgada	**−0.38**	−0.18	−0.17	0.05	**0.32**

These six stations are illustrated in Figure 3.10, which presents scatter plots of annual rainfall versus the NAO index, with data points from the latest sub-dataset (2010–2020) highlighted in red. In general, years with higher NAO values correspond to lower annual rainfall totals. The MAP values in the latest sub-dataset are consistently lower than would be expected.

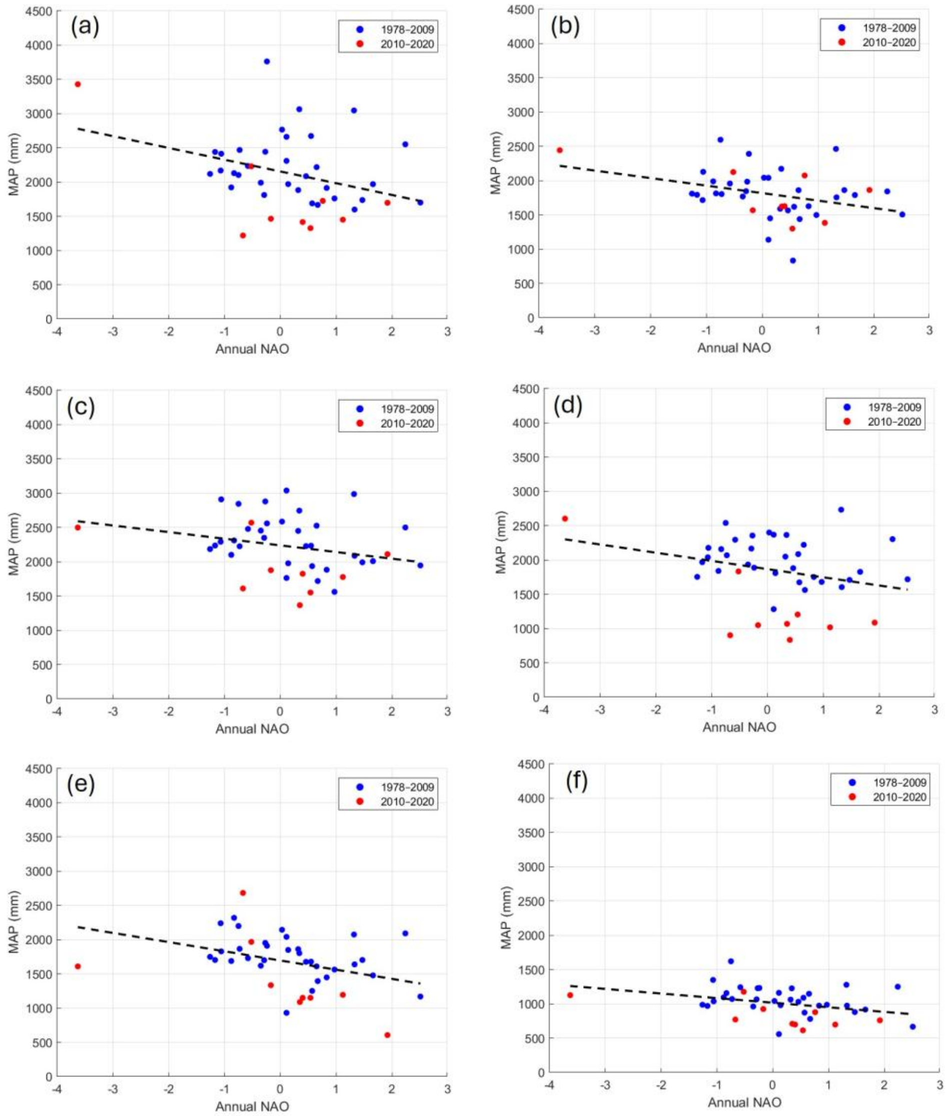

Figure 3.10 | Scatterplots of MAP versus annual NAO index for (a) Lagoa das Furnas, (b) Sete Cidades, (c) Lomba da Erva, (d) Monte Simplício, (e) Salto do Cabrito, and (f) Ponta Delgada. The trend line is dotted.

3.4.6 | Altitude-Rainfall Relationship

Analysing rainfall’s correlations with altitude provides an insightful examination of the interplay between rainfall metrics and altitude across different climatological periods. As expected, the linear regression analysis, presented in Figures 3.11 and 3.12, indicates a strong correlation between the various rainfall variables and altitude, highlighting the influence of altitude on rainfall distribution.

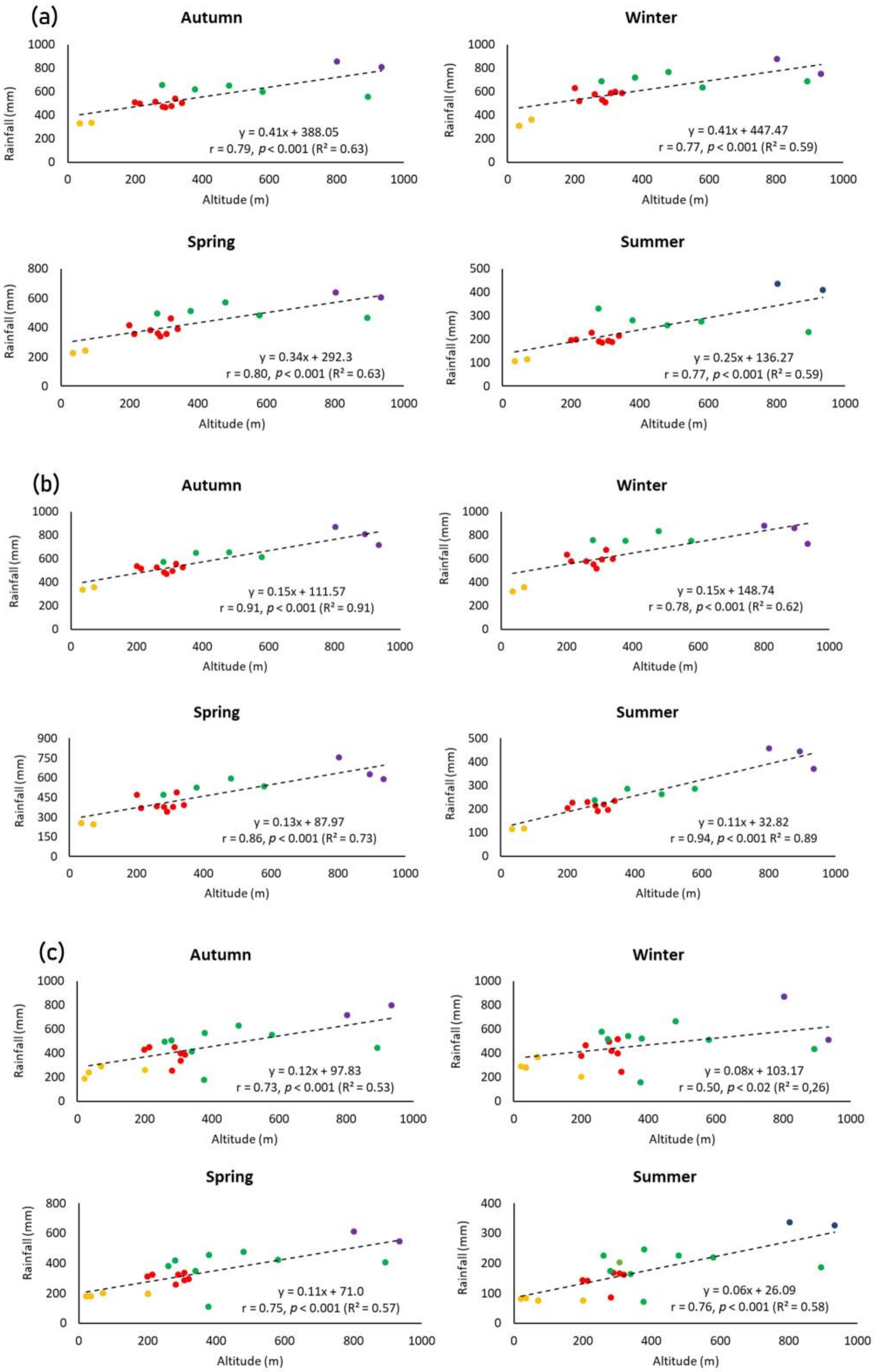

Figure 3.11 | Correlation of the P50 variable with altitude across clusters in every season for (a) the full dataset, (b) the oldest sub-dataset, and (c) the latest sub-dataset. The trend line is dotted.

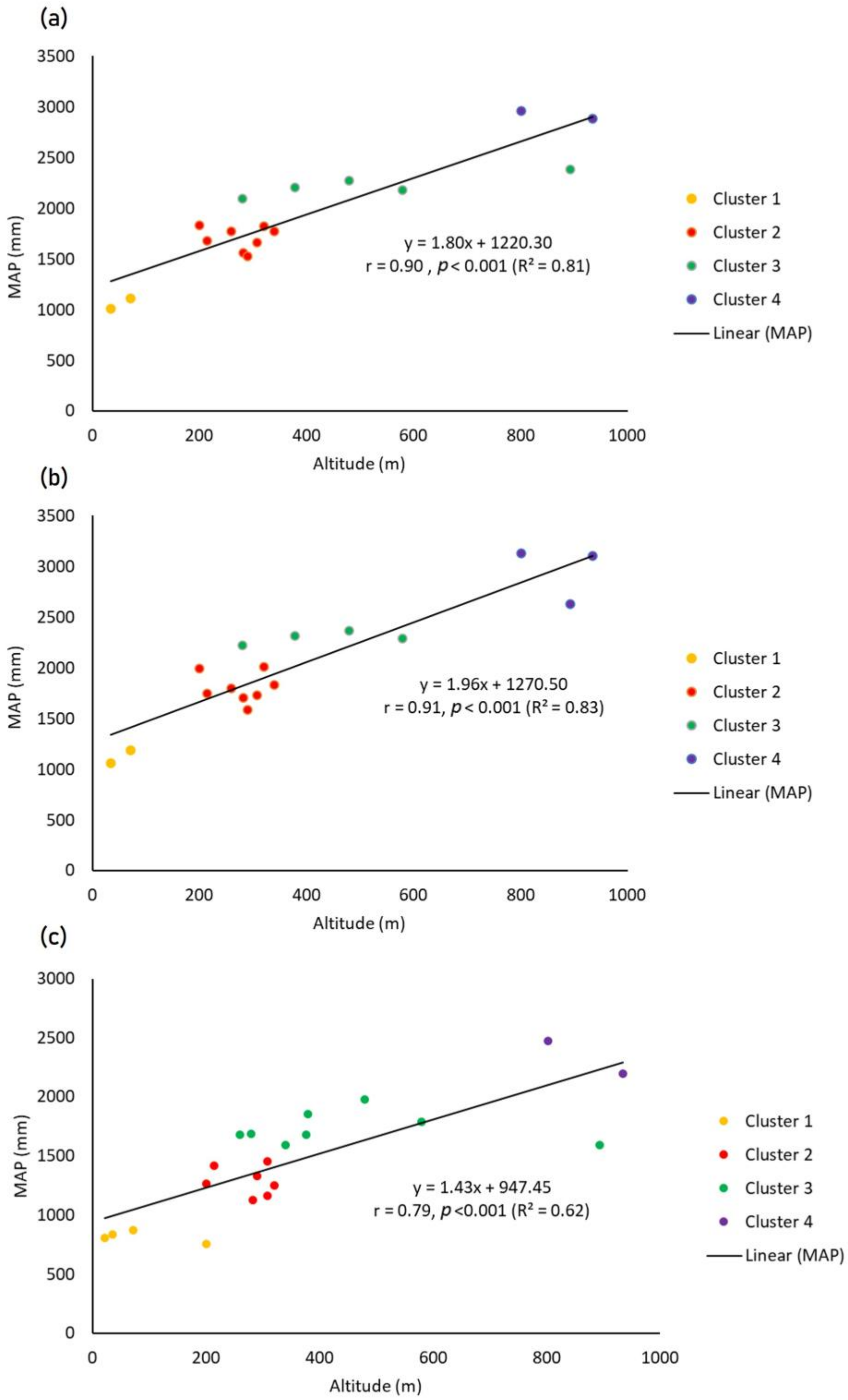

Figure 3.12 | Correlation of Mean Annual Precipitation (MAP) with altitude across clusters for (a) the full dataset, (b) the oldest sub-dataset, and (c) the latest sub-dataset. The trend line is dotted.

Based on the analysis of the P50 variable (Figure 3.11), a positive correlation with altitude is observed across all datasets, with stronger relationships occurring in autumn and summer. Winter and spring show a weaker, though still significant, correlation. For the P10 and P90 variables, the results indicate the same behaviour. This observation suggests the presence of additional physiographic factors, such as the existence of central volcanoes, dismantled calderas, and lakes; geological formations' alignment; ventilation corridors; vegetation; and the orientation of slopes and sea cliffs, which contribute to the variability of the variables beyond that caused by altitude, which can all play significant roles in determining the intensity and distribution of high-magnitude rainfall events.

For the full dataset, the correlation coefficient between MAP and altitude is 0.81, indicating a strong positive relationship. The linear regression model suggests that MAP increases by approximately 180 mm for every 100 m of elevation gain (Figure 3.12a). The spatial distribution of MAP illustrates the altitude influence, with rainfall accumulation ranging from 1120 mm at sea level to 3209 mm at the highest altitude on the island (Figure 3.13a), reflecting a clear altitudinal gradient in rainfall.

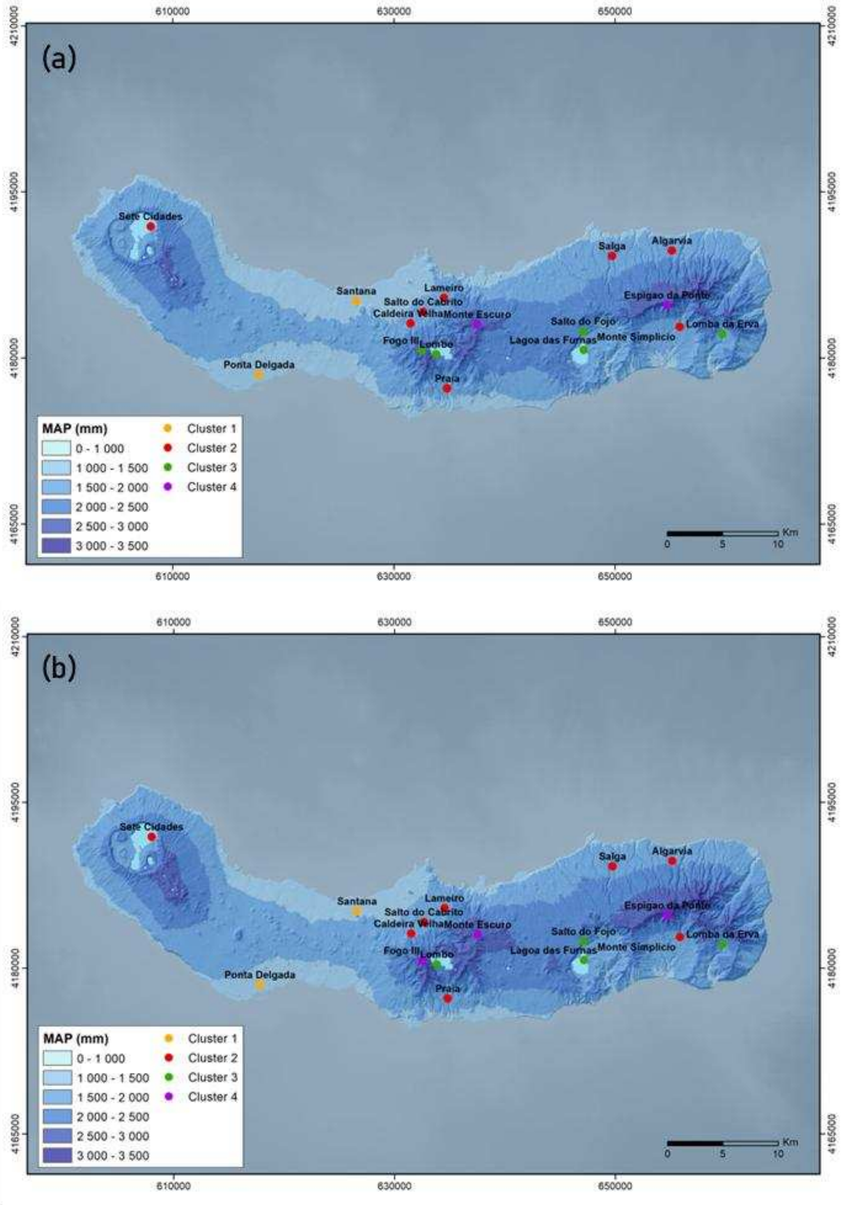

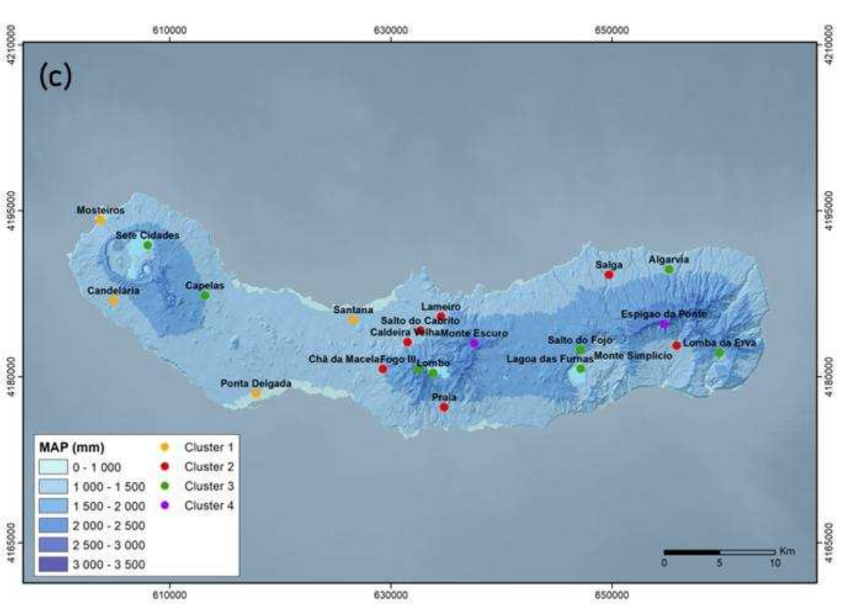

Figure 3.13 | Spatial distribution of Mean Annual Precipitation (MAP) and the locations of rainfall station clusters for (a) the full dataset, (b) the oldest sub-dataset, and (c) the latest sub-dataset.

In the oldest sub-dataset, the correlation coefficient increases slightly to 0.83, suggesting an even stronger altitude influence, with a 196 mm increase in MAP per 100 m elevation gain (Figure 3.12b) and rainfall ranging from 1270 mm at sea level to 3444 mm at the highest points on the island (Figure 3.13b).

In the latest sub-dataset, the correlation coefficient is 0.62, indicating a slightly weaker but still significant relationship between MAP and altitude. Notably, the rate of increase in rainfall with elevation gain decreases, with MAP rising 144 mm per 100 m altitude gain (Figure 3.12c). Rainfall values range from 947 mm at sea level to 2537 mm at the highest altitudes (Figure 3.13c), reflecting an overall reduction in rainfall at higher elevations.

3.5 | Discussion

The cluster analysis, based on rainfall data from the climatological years of 1978/79 to 2019/20, and the two sub-datasets (1978/79 to 2009/10 and 2010/11 to 2019/20), identified four distinct groups of rainfall stations that reflect the spatial and temporal rainfall distribution on São Miguel Island. This analysis provides significant insights into the dynamics of rainfall, highlighting both the constancy and variability of rainfall patterns across the studied period.

The analysis reveals a notable consistency in the clustering of stations over the years, with specific stations being recurrently grouped together, underscoring the stability of rainfall patterns. However, changes in cluster composition were observed when focusing on the oldest and latest sub-datasets, reflecting the variability and evolving rainfall dynamics within the studied timeframe. The greater heterogeneity of rainfall station characteristics within each cluster in the latest sub-dataset, compared with the other periods considered, suggests that longer timeframes—such as the full dataset or the oldest sub-dataset—are more suitable for clustering, yielding more consistent and robust results. In addition, the shorter duration of the latest sub-dataset (10 years) limits the statistical power of trend analyses, making any observed changes during this period more tentative and less conclusive from a climatological standpoint. Furthermore, the shorter duration of the most recent data subset (10 years) limits the statistical power. However, this shorter time window allowed the inclusion of additional rainfall stations that began operating after 2010, thereby improving the spatial coverage and representativeness of the clustering analysis. Similar approaches have been applied in regional studies using shorter time periods to assess emerging climate signals and short-term hydroclimatic variability (Spinoni et al. 2015).

Although the clusters are referred to as “homogeneous rainfall regions,” some internal variability remains within each group, as indicated by the coefficients of variation, particularly in the most recent sub-dataset. Therefore, the term “homogeneous” should be interpreted in a statistical sense, referring to the grouping of stations with broadly similar rainfall regimes and temporal behaviour, rather than complete uniformity.

Rainfall stations within each cluster are generally located at similar altitudes, although exceptions indicate that factors other than altitude influence rainfall distribution, as observed in other regions worldwide (Rianna et al. 2015; Mahindawansha et al. 2022). On São Miguel, the complex volcanic morphology plays a major role in shaping local rainfall patterns. Stations located within or near volcanic calderas, such as Lagoa das Furnas, Fogo, and Sete Cidades, often record higher rainfall totals than nearby stations at comparable altitudes. This is likely explained by the geomorphological setting of these depressions, where steep caldera rims and elevated relief enhance orographic uplift and moisture condensation. Consequently, the clustering results reflect not only the altitudinal gradient but also the combined effects of volcanic topography and local atmospheric circulation on rainfall distribution across the island.

A significant finding of this study is the variability in Mean Annual Precipitation (MAP) across clusters, coupled with evident seasonal variations. These results align with the expected annual rainfall cycle on the island, with higher values typically being recorded in winter and lower values in summer. Seasonal variations in the variables are consistent with the island’s climatic pattern, in which winter is the wettest season and summer is the driest. Seasonal fluctuations in P10, P50, and P90 values align with the island’s climate, with P10 values being relatively uniform across seasons and clusters, while P50 and P90 show important differences, especially during the wettest months. These variables play a crucial role in cluster differentiation.

Temporal analysis comparing the two sub-datasets unveils a decrease in rainfall in the most recent period. Previous long-term studies based on the centennial rainfall series of São Miguel Island indicate that MAP values were higher during the more recent periods of those records. This pattern was demonstrated by Hernández et al. (2016) for the period of 1943–2012 and by Cropper and Hanna (2014) for the period of 1981–2010. However, the results of this study reveal a reduction in rainfall that was not detected in these earlier long-term analyses, suggesting that the rainfall decline is mainly concentrated in the period after 2010.

Trend analyses for the climatological years of 1978/79–2019/20, using the M–K test and Sen's slope estimator, indicate predominantly decreasing trends in annual and seasonal rainfall; however, statistically significant declines were only detected at a subset of stations. Autumn displays the most pronounced reductions across multiple stations and clusters, indicating a systemic shift towards drier autumns on São Miguel Island. Cluster-based analysis further reveals spatial variations in these trends. Notably, Cluster 1 experiences a marked decrease in autumn rainfall, particularly in Santana and Ponta Delgada, indicating a shift towards drier conditions. Cluster 2 shows notable reductions in several seasons, with Monte Simplício experiencing significant declines in annual and winter rainfall. Cluster 3, notably at Fogo III, suffers drastic reductions in rainfall across all seasons, likely with severe ecological and hydrological implications. Similarly, Cluster 4, which includes Monte Escuro and Espigão da Ponte, shows significant annual and seasonal rainfall declines. These findings underscore the critical need for understanding regional rainfall trends to mitigate potential negative effects on ecosystems and water resources.

Climate change scenarios for the Azores predict an increase in winter rainfall and a reduction in summer rainfall (PRAC 2019). However, some of the observed reductions in rainfall, especially during autumn and winter, appear to contrast with these climate projections. Nonetheless, the limited spatial significance of these trends calls for further investigation before definitive conclusions are drawn. Climate change projections suggest that subtropical anticyclones will undergo changes in intensity and location. It is expected that the anticyclones over the North Pacific, South Atlantic, and South Indian Oceans will weaken, while the subtropical anticyclone over the North Atlantic will intensify (He et al. 2017). The decreasing rainfall trend observed in this study could be linked to this intensification, driven by increased tropospheric static stability resulting from changes in diabatic heating patterns (He et al. 2017). Additionally, expansion of the Azores High during the 20th century, driven by the increase in greenhouse gas concentrations, has decreased rainfall in winter, a trend that is expected to continue in the coming years with global warming (Cresswell-Clay et al. 2022). This expansion also contributes to decreasing rainfall on the Eastern Iberian Peninsula (Miró et al. 2023).

Across São Miguel, annual rainfall maintains the expected negative association with the PC-based NAO; however, the pronounced drying of the latest sub-dataset occurs even under neutral or negative NAO phases. This suggests that additional climate drivers, such as the East Atlantic pattern, the Scandinavian pattern, or broader North Atlantic

SST anomalies, may also be influencing recent rainfall behaviour (Rodrigo 2021; Comas-Bru et al. 2014). A more detailed investigation of these teleconnections is therefore warranted to fully understand the observed downward trend.

The obtained results show a strong positive relationship between station altitude and rainfall, with rainfall increasing consistently with altitude. However, the strength of this relationship has decreased in recent years, suggesting that the altitude–rainfall dependency may not be strictly linear and could be modulated by additional factors. This differs from other regions that are influenced by subtropical anticyclones, where rainfall does not always increase with altitude (Rodwell and Hoskins 2001; Lopes 2015; Söllheim et al. 2024).

Furthermore, the identified clusters and rainfall patterns suggest that there are no clear differences between windward and leeward slopes, unlike in many other regions, where the windward side typically receives more rain (Peñate et al. 2013; Van Den Hende et al. 2021). The limited orographic contrast between the windward and leeward slopes can be attributed to the island's small size and its west–east alignment, which offers little resistance to the prevailing winds. These factors, combined with moderate topographic gradients, restrict the development of heavy rain shadow effects.

3.6 | Conclusions

This study explored the spatial and temporal patterns of rainfall on São Miguel Island (Azores) in the period of 1978/79–2019/20. Consistent patterns in rainfall distribution were identified across four clusters, although some changes in cluster composition were observed in the most recent period (2010/11–2019/20). A notable finding was the significant variability in rainfall metrics across different clusters, with each cluster exhibiting distinct Mean Annual Precipitation (MAP) values. Seasonal variations in rainfall distribution were also evident, with higher values typically being recorded in winter and lower values in summer, reflecting the island's characteristic annual rainfall pattern.

The spatial distribution of rainfall stations within each cluster, relative to altitude, suggests a strong correlation between elevation and rainfall patterns on São Miguel Island. However, some exceptions to this trend were observed, indicating the influence of additional factors beyond altitude. These anomalies, such as stations appearing in unexpected clusters, can be attributed to local geographic or environmental features, including the presence of volcanic calderas.

The trend analysis provided critical insights, indicating decreasing trends in both annual and seasonal rainfall at several locations on the island. However, statistically significant reductions were detected at only a limited number of stations (5 out of 17 at the annual scale). Notably, autumn exhibited the most consistent and significant decrease across several stations and clusters, suggesting a shift towards drier conditions. These findings provide preliminary evidence of changing rainfall patterns on São Miguel Island, while highlighting the need for continued monitoring and long-term datasets to robustly assess climate trends. Given the diverse topographical and climatic conditions across the Azores islands, expanding this analysis to include the entire archipelago would provide a more comprehensive understanding of regional rainfall trends and their potential implications. Across the island, rainfall also maintains the expected negative association with the NAO, particularly in autumn and for annual totals. However, the most recent decade consistently shows lower rainfall even under neutral or negative NAO phases. This suggests that the recent drying trend cannot be explained by the NAO alone and may reflect the influence of additional atmospheric modes over the North Atlantic.

The integration of cluster and trend analysis not only enabled the identification of previously unrecognised rainfall patterns but also introduced a novel methodological approach in the context of the Azores. The identification of homogeneous rainfall regions and the analysis of temporal trends can also support the optimisation of the monitoring network, facilitating the strategic installation and maintenance of rainfall stations in key areas. By revealing evolving climatic dynamics and proposing a replicable methodological model, this work represents a significant advancement in the scientific understanding of climate variability in the Azores and offers practical tools for sustainable land and risk management.

References

Alexandersson, H. & Moberg, A. (1997). Homogenization of Swedish temperature data. Part I: Homogeneity test for linear trends. *International Journal of Climatology, 17*, 25–34. https://doi.org/10.1002/(SICI)1097-0088(199701)17:1%3C25::AID-JOC103%3E3.0.CO;2-J

Azevedo, E. B. (1996). *Modelação do clima insular à escala local – Modelo CIELO aplicado à Ilha Terceira* (Doctoral dissertation). University of the Azores.

Azevedo, E. B. (2001). Condicionantes dinâmicas do clima no arquipélago dos Açores: Elementos para o seu estudo. *Açoreana, 9*(3), 309–317.

Azevedo, E. B., Pereira, L. S. & Itier, B. (1999). Modeling the local climate in island environments: Water balance applications. *Agricultural Water Management, 40*, 393–403. https://doi.org/10.1016/S0378-3774(99)00012-8

Booth, B., Croasdale, R. & Walker, G. P. L. (1978). A quantitative study of five thousand years of volcanism on S. Miguel, Azores. *Philosophical Transactions of the Royal Society of London, 228*, 271–319. https://doi.org/10.1098/rsta.1978.0018

Brito, R. S. (2004). *São Miguel – a Ilha Verde. Estudo Geográfico (1950–2000)* (2nd ed.). Ponta Delgada.

Buishand, T. A. (1982). Some methods for testing the homogeneity of rainfall records. *Journal of Hydrology, 58*, 11–27. https://doi.org/10.1016/0022-1694(82)90066-X

Carvalho, F. S., Meirelles, M. G., Henriques, D. V., Navarro, P. V. & Vasconcelos, H. C. (2022). Climate change and the increase of extreme events in Azores. In *Climate Change Management* (pp. 349–365). https://doi.org/10.1007/978-3-031-09879-6_20

Chazarra, A., Baceló, A. M., Pires, V., Cunha, S., Silva, A., Marques, J., Carvalho, F., Mendes, M., Neto, J. & Mendes, L. (2011). *Climate Atlas of the Archipelagos of the Canary Islands, Madeira and the Azores*. State Meteorological Agency of Spain & Institute of Meteorology, Lisbon.

Chen, H., Guo, S., Xu, C. & Singh, V. P. (2007). Historical temporal trends of hydro-climatic variables and runoff response to climate variability and their relevance in water resource management in the Hanjiang Basin. *Journal of Hydrology, 344*(3–4), 171–184. https://doi.org/10.1016/j.jhydrol.2007.06.034

Chen, Y.-L. & Feng, J. (2001). Numerical simulations of airflow and cloud distributions over the windward side of the Island of Hawaii. Part I: The effects of trade-wind inversion. *Monthly Weather Review, 129*(5), 1117–1134. https://doi.org/10.1175/1520-0493(2001)129%3C1117:NSOAAC%3E2.0.CO;2

Cresswell-Clay, N., Ummenhofer, C. C., Thatcher, D. L., Wanamaker, A. D., Denniston, R. F., Asmerom, Y. & Polyak, V. J. (2022). Twentieth-century Azores High expansion unprecedented in the past 1,200 years. *Nature Geoscience, 15*(7), 548–553. https://doi.org/10.1038/s41561-022-00971-w

Cropper, T. E. & Hanna, E. (2014). An analysis of the climate of Macaronesia, 1865–2012. *International Journal of Climatology, 34*(3), 604–622. https://doi.org/10.1002/joc.3710

De Lima, M. I. P., Carvalho, S. C. P. & De Lima, J. L. M. P. (2010). Investigating annual and monthly trends in precipitation structure: An overview across Portugal. *Natural Hazards and Earth System Sciences, 10*(11), 2429–2440. https://doi.org/10.5194/nhess-10-2429-2010

Deheuvels, P. A. (1981). Kolmogorov–Smirnov type test for independence and multivariate samples. *Revue Roumaine de Mathématiques Pures et Appliquées, 26*, 213–226.

Domroes, M., Kaviani, M. & Schaefer, D. (1998). An analysis of regional and intra-annual rainfall variability over Iran using multivariate statistical methods. *Theoretical and Applied Climatology, 61*, 151–159. https://doi.org/10.1007/s007040050060

Duncan, A. M., Guest, J. E., Wallenstein, N. & Chester, D. K. (2015). The older volcanic complexes of São Miguel, Azores: Nordeste and Povoação. In J. L. Gaspar, J. E. Guest, A. M. Duncan, F. J. A. S. Barriga & D. K. Chester (Eds.), *Volcanic geology of São Miguel Island (Azores Archipelago)* (Vol. 44, pp. 147–153). Geological Society of London, Memoirs. https://doi.org/10.1144/M44.11

Comas-Bru, L. & McDermott, F. (2014). Impacts of the EA and SCA patterns on the European twentieth century NAO–winter climate relationship. *Quarterly Journal of the Royal Meteorological Society, 140*, 354–363. https://doi.org/10.1002/qj.2158

Everitt, B. S. & Dunn, G. (1991). *Applied multivariate analysis*. Edward Arnold. https://doi.org/10.1002/9781118887486

Fernandes, J. (2004). *Caracterização climática das ilhas de São Miguel e Santa Maria com base no Modelo CIELO* (Internship report). University of the Azores.

Ferreira, T. (2000). *Caracterização da actividade vulcânica da ilha de S. Miguel (Açores): Vulcanismo basáltico recente e zonas de desgaseificação. Avaliação de riscos* (Doctoral dissertation). University of the Azores.

Ferreira, T., Gomes, A., Gaspar, J. L. & Guest, J. (2015). Distribution and significance of basaltic eruptive centres: São Miguel, Azores. In J. L. Gaspar, J. E. Guest, A. M. Duncan, F. J. A. S. Barriga & D. K. Chester (Eds.), *Volcanic geology of São Miguel Island (Azores Archipelago)* (Vol. 44, pp. 135–146). Geological Society of London, Memoirs. https://doi.org/10.1144/M44.10

Foresti, L., Pozdnoukhov, A. & Kanevski, M. (2011). Data-driven exploration of orographic enhancement of precipitation. *Advances in Science and Research, 6*(1), 129–135. https://doi.org/10.5194/asr-6-129-2011

Frich, P., Alexander, L. V., Della-Marta, P., Gleason, B., Haylock, M., Klein Tank, A. M. G. & Peterson, T. (2002). Observed coherent changes in climatic extremes during the second half of the twentieth century. *Climate Research, 19*, 193–212. https://doi.org/10.3354/cr019193

Guest, J. E., Gaspar, J. L., Cole, P. D., Queiroz, G., Duncan, A. M., Wallenstein, N., Ferreira, T. & Pacheco, J. M. (1999). Volcanic geology of Furnas Volcano, São Miguel, Azores. *Journal of Volcanology and Geothermal Research, 92*(1–2), 1–29. https://doi.org/10.1016/S0377-0273(99)00064-5

Guest, J. E., Pacheco, J. M., Cole, P. D., Duncan, A. M., Wallenstein, N., Queiroz, G., Gaspar, J. L. & Ferreira, T. (2015). The volcanic history of Furnas volcano, São Miguel, Azores. In J. L. Gaspar, J. E. Guest, A. M. Duncan, F. J. A. S. Barriga & D. K. Chester (Eds.), *Volcanic Geology of São Miguel Island (Azores Archipelago)* (Mem. 44, pp. 125–134). Geological Society of London. https://doi.org/10.1144/M44.9

Gupta, A., Kamble, T. & Machiwal, D. (2017). Comparison of ordinary and Bayesian kriging techniques in depicting rainfall variability in arid and semi-arid regions of north-west India. *Environmental Earth Sciences, 76*(512). https://doi.org/10.1007/s12665-017-6814-3

Guttman, N. B. (1993). The use of L-moments in the determination of regional rainfall climates. *Journal of Climate, 6*, 2309–2325. https://doi.org/10.1175/1520-0442(1993)006<2309:TUOLMI>2.0.CO;2

Haines, H. A. & Olley, J. M. (2017). The implications of regional variations in rainfall for reconstructing rainfall patterns using tree rings. *Hydrological Processes, 31*, 2951–2960. https://doi.org/10.1002/hyp.11238

He, C., Wu, B., Zou, L. & Zhou, T. (2017). Responses of the summertime subtropical anticyclones to global warming. *Journal of Climate, 30*(16), 6465–6479. https://doi.org/10.1175/JCLI-D-16-0529.1

Hernández, A., Kutiel, H., Trigo, R. M., Valente, M. A., Sigró, J., Cropper, T. & Santo, F. E. (2016). New Azores archipelago daily rainfall dataset and its links with large-scale modes of climate variability. *International Journal of Climatology, 36*, 4439–4454. https://doi.org/10.1002/joc.4642

Hurrell, J. W., Kushnir, Y., Ottersen, G. & Visbeck, M. (2003). An overview of the North Atlantic Oscillation. In J. W. Hurrell, Y. Kushnir, G. Ottersen & M. Visbeck (Eds.), *The North Atlantic Oscillation: Climatic significance and environmental impact*. American Geophysical Union. https://doi.org/10.1029/134GM01

Iqbal, M. J., Khan, F. & Hameed, S. (2012). Influence of Azores High pressure on Middle Eastern rainfall. *Theoretical and Applied Climatology, 111*(1–2), 211–221. https://doi.org/10.1007/s00704-012-0648-4

Jackson, I. J. & Weinand, H. (1995). Classification of tropical rainfall stations: A comparison of clustering techniques. *International Journal of Climatology, 15*(9), 985–994. https://doi.org/10.1002/joc.3370150905

Jebari, S., Berndtsson, R., Uvo, C. & Bahri, A. (2009). Regionalizing fine time-scale rainfall affected by topography in semi-arid Tunisia. *Hydrological Sciences Journal, 52*(6), 1199–1215. https://doi.org/10.1623/hysj.52.6.1199

Kendall, S. (1976). *Time series*. Oxford University Press.

Kumar, S. & Santosh, S. (2015). Temporal and spatial dynamics of rainfall in Satluj River Basin, Himachal Pradesh, India. *International Letters of Chemistry, Physics and Astronomy, 54*, 150–165. https://doi.org/10.56431/p-6p2zo2

Lin, G. F. & Chen, L. H. (2006). Identification of homogeneous regions for regional frequency analysis using the self-organizing map. *Journal of Hydrology, 324*, 1–9. https://doi.org/10.1016/j.jhydrol.2005.09.009

Lin, G. F., Chang, M. J. & Wu, J. T. (2017). A hybrid statistical downscaling method based on the classification of rainfall patterns. *Water Resources Management, 31*(1), 377–401. https://doi.org/10.1007/s11269-016-1532-2

Loo, Y. Y., Billa, L. & Singh, A. (2014). Effect of climate change on seasonal monsoon in Asia and its impact on the variability of monsoon rainfall in Southeast Asia. *Geoscience Frontiers, 6*(6), 817–823. https://doi.org/10.1016/j.gsf.2014.02.009

Lopes, S. (2015). *Clima e ordenamento do território no Funchal* (PhD thesis). University of Lisbon.

Lund, R. B., Beaulieu, C., Killick, R., Lu, Q. & Shi, X. (2023). Good practices and common pitfalls in climate time series changepoint techniques: A review. *Journal of Climate, 36*(23), 8041–8057. https://doi.org/10.1175/JCLI-D-22-0954.1

Lyra, G. B., Oliveira-Júnior, J. F. & Zeri, M. (2014). Cluster analysis applied to the spatial and temporal variability of monthly rainfall in Alagoas state, Northeast of Brazil. *International Journal of Climatology, 34*, 3546–3558. https://doi.org/10.1002/joc.3926

Machiwal, D., Dayal, D. & Kumar, S. (2017). Long-term rainfall trends and change points in hot and cold arid regions of India. *Hydrological Sciences Journal, 62*(7), 1050–1066. https://doi.org/10.1080/02626667.2017.1303705

Mahindawansha, A., Jost, M. & Gassmann, M. (2022). Spatial and temporal variations of stable isotopes in precipitation in the mountainous region, North Hesse. *Water, 14*(23), 3910. https://doi.org/10.3390/w14233910

Mann, H. B. (1945). Non-parametric test against trend. *Econometrica, 13*, 245–259.

Marques, R., Zêzere, J. L., Trigo, R., Gaspar, J. & Trigo, I. (2008). Rainfall patterns and critical values associated with landslides in Povoação County (São Miguel Island, Azores): Relationships with the North Atlantic Oscillation. *Hydrological Processes, 22*, 478–494. https://doi.org/10.1002/hyp.6879

Martin, T. N., Storck, L. & Dourado Neto, D. (2007). Simulação estocástica da radiação fotossinteticamente ativa e da temperatura do ar por diferentes métodos. *Pesquisa Agropecuária Brasileira, 42*(9), 1211–1219. https://doi.org/10.1590/S0100-204X2007000900001

Masoodian, S. A. (1998). *An analysis of tempo-spatial variation of rainfall in Iran* (Doctoral dissertation). University of Isfahan.

Mazvimavi, D. (2010). Investigating changes over time of annual rainfall in Zimbabwe. *Hydrology and Earth System Sciences, 14*(12), 2671–2679. https://doi.org/10.5194/hess-14-2671-2010

Medina-Cobo, M. T., García-Marín, A. P., Estévez, J., Jiménez-Hornero, F. J. & Ayuso-Muñoz, J. L. (2017). Obtaining homogeneous regions by determining the generalized fractal dimensions of validated daily rainfall data sets. *Water Resources Management, 31*(7), 2333–2344. https://doi.org/10.1007/s11269-017-1653-2

Mirabbasi, R., Ahmadi, F. & Jhajharia, D. (2020). Comparison of parametric and non-parametric methods for trend identification in groundwater levels in Sirjan plain aquifer, Iran. *Hydrology Research, 51*(6), 1455–1477. https://doi.org/10.2166/nh.2020.041

Miró, J. J., Estrela, M. J., Corell, D., Gómez, I. & Luna, M. Y. (2023). Precipitation and drought trends (1952–2021) in a key hydrological recharge area of the eastern Iberian Peninsula. *Atmospheric Research, 286*, 106695. https://doi.org/10.1016/j.atmosres.2023.106695

Modarres, R. & Sarhadi, A. (2011). Statistically-based regionalization of rainfall climates of Iran. *Global and Planetary Change, 75*(1–2), 67–75. https://doi.org/10.1016/j.gloplacha.2010.10.009

Novotny, E. V. & Stefan, H. G. (2007). Stream flow in Minnesota: Indicator of climate change. *Journal of Hydrology, 334*(3–4), 319–333. https://doi.org/10.1016/j.jhydrol.2006.10.011

Peñate, I., Rodríguez, G., Cianca, A. & Martín-González, J. M. (2013). Scaling properties of rainfall and desert dust in the Canary Islands. *Nonlinear Processes in Geophysics, 20*(6), 1079–1094. https://doi.org/10.5194/npg-20-1079-2013

Pettitt, A. N. (1979). A non-parametric approach to the change-point problem. *Applied Statistics, 28*(2), 126–135. https://doi.org/10.2307/2346729

Programa Regional para as Alterações Climáticas (PRAC) (2019). *Decreto Legislativo Regional n.º 30/2019/A*. Diário da República n.º 229/2019, Série I. Assembleia Legislativa da Região Autónoma dos Açores.

Queiroz, G. (1997). *Vulcão das Sete Cidades (S. Miguel, Açores) – História eruptiva e avaliação do hazard* (PhD thesis). University of the Azores.

Queiroz, G., Gaspar, J. L., Guest, J. E., Gomes, A. & Almeida, M. H. (2015). Eruptive history and evolution of Sete Cidades volcano, São Miguel Island, Azores. In J. L. Gaspar, J. E. Guest, A. M. Duncan, F. J. A. S. Barriga & D. K. Chester (Eds.), *Volcanic Geology of São Miguel Island (Azores Archipelago)* (Mem. 44, pp. 87–104). Geological Society of London. https://doi.org/10.1144/M44.7

Rashid, S. A., Iqbal, M. J. & Hussain, M. A. (2012). Impact of north–south shift of Azores High on summer precipitation over northwest Europe. *International Journal of Geosciences, 3*(5), 992–999. https://doi.org/10.4236/ijg.2012.325099

Rianna, M., Montesarchio, V., Napolitano, F. & Ubertini, L. (2015). A preliminary analysis of rainfall spatial distribution at catchment scale. In *AIP Conference Proceedings* (Vol. 1648, Issue 1). AIP Publishing. https://doi.org/10.1063/1.4912478

Rodrigues, R. (1992). *Avaliação das disponibilidades hídricas da ilha de São Miguel (Açores)* (Rel. 217/92 – NHHF). Laboratório Nacional de Engenharia Civil.

Rodrigues, R. (1995). *Hidrologia de ilhas vulcânicas* (Dissertação para obtenção do grau de Especialista). Laboratório Nacional de Engenharia Civil.

Rodwell, M. J. & Hoskins, B. J. (2001). Subtropical anticyclones and summer monsoons. *Journal of Climate, 14*(15), 3192–3211. https://doi.org/10.1175/1520-0442(2001)014<3192:SAASM>2.0.CO;2

Rodrigo, F. S. (2021). *Exploring combined influences of EA and NAO on the temperature–precipitation relationship in the Iberian Peninsula*. Geosciences, 11, 211. https://doi.org/10.3390/geosciences11050211

Royston, P. (1982). An extension of Shapiro and Wilk's W test for normality to large samples. *Applied Statistics, 31*, 115–124. https://doi.org/10.2307/2347973

Sa'adi, Z., Shahid, S., Ismail, T., Chung, E. S. & Wang, X. J. (2019). Trends analysis of rainfall and rainfall extremes in Sarawak, Malaysia using modified Mann–Kendall test. *Meteorology and Atmospheric Physics, 131*, 263–277. https://doi.org/10.1007/s00703-017-0564-3

Sabziparvar, A. A., Movahedi, S., Asakereh, H., Maryanaji, Z. & Masoodian, S. A. (2015). Geographical factors affecting variability of rainfall regime in Iran. *Theoretical and Applied Climatology, 120*(1–2), 367–376. https://doi.org/10.1007/s00704-014-1174-3

Santos, F. D., Valente, M. A., Miranda, P. M. A., Aguiar, A., Azevedo, E. B., Tomé, A. R. & Coelho, F. (2004). Climate change scenarios in the Azores and Madeira Islands. *World Resource Review, 16*(4), 473–491.

Sen, P. K. (1968). Estimates of the regression coefficient based on Kendall's tau. *Journal of the American Statistical Association, 63*, 1379–1389. https://doi.org/10.2307/2285891

Şen, Z. & Habib, Z. (2001). Monthly spatial rainfall correlation functions and interpretations for Turkey. *Hydrological Sciences Journal, 46*(4), 525–535. https://doi.org/10.1080/02626660109492848

Söllheim, Á. L. L., Suarez, P. M. & Hernández, F. G. (2024). The digital climate atlas of the Canary Islands: A tool to improve knowledge of climate and temperature and precipitation trends in the Atlantic islands. *Climate Services, 34*, 100487. https://doi.org/10.1016/j.cliser.2024.100487

Sonali, P. & Nagesh Kumar, D. (2013). Review of trend detection methods and their application to detect temperature changes in India. *Journal of Hydrology, 476*, 212–227. https://doi.org/10.1016/j.jhydrol.2012.10.034

Spinoni, J., Naumann, G., Vogt, J. V. & Barbosa, P. (2015). The biggest drought events in Europe from 1950 to 2012. *Journal of Hydrology: Regional Studies, 3*, 509–524. https://doi.org/10.1016/j.ejrh.2015.01.001

Suhaila, J. & Jemain, A. A. (2009). A comparison of the rainfall patterns between stations on the East and the West coasts of Peninsular Malaysia using the smoothing model of rainfall amounts. *Meteorological Applications, 16*(3), 391–401. https://doi.org/10.1002/met.137

Theil, H. (1950). A rank-invariant method of linear and polynomial regression analysis. I, II, III. *Nederlands Akad Wetensch Proc Ser A, 53*, 386–392, 521–525, 1397–1412.

Tsubo, M., Walker, S. & Hensley, M. (2005). Quantifying risk for water harvesting under semi-arid conditions: Part I. Rainfall intensity generation. *Agricultural Water Management, 76*(2), 77–93. https://doi.org/10.1016/j.agwat.2005.01.008

Unal, Y., Kindap, T. & Karaca, M. (2003). Redefining the climate zones of Turkey using cluster analysis. *International Journal of Climatology, 23*(9), 1045–1055. https://doi.org/10.1002/joc.910

Valdés-Pineda, R., Pizarro-Tapia, R., Valdés, J. B. & Diaz, H. F. (2015). Analysis of spatio-temporal changes in annual and seasonal precipitation variability in South America–Chile and related ocean–atmosphere circulation patterns. *International Journal of Climatology, 36*(8), 2979–3001. https://doi.org/10.1002/joc.4532

Van Den Hende, C., Nyssen, J., Van Schaeybroeck, B., Van Vooren, S., Van Ginderachter, M. & Termonia, P. (2021). Analysis of rain-shadows in the Ethiopian Mountains using climatological model data. *Climate Dynamics, 56*(5–6), 1663–1679. https://doi.org/10.1007/s00382-020-05554-2

Von Neumann, J. (1941). Distribution of the ratio of the mean square successive difference to the variance. *Annals of Mathematical Statistics, 12*(4), 367–395. https://doi.org/10.1214/aoms/1177731677

Wallenstein, N. (1999). *Estudo da história recente e do comportamento eruptivo do vulcão do Fogo (S. Miguel, Açores). Avaliação preliminar do "hazard"* (PhD dissertation). University of the Azores.

Wallenstein, N., Duncan, A., Guest, J. E. & Almeida, M. H. (2015). Eruptive history of Fogo Volcano, São Miguel, Azores. In J. L. Gaspar et al. (Eds.), *Volcanic Geology of São Miguel Island (Azores Archipelago)* (pp. 105–123). Geological Society of London. https://doi.org/10.1144/M44.8

Ward, J. H., Jr. (1963). Hierarchical grouping to optimize an objective function. *Journal of the American Statistical Association, 58*, 236–244. https://doi.org/10.2307/2282967

Wijngaard, J. B., Klein-Tank, A. M. G. & Können, G. P. (2003). Homogeneity of 20th century European daily temperature and precipitation series. *International Journal of Climatology, 23*, 679–692. https://doi.org/10.1002/joc.906

Wilks, D. S. (2020). *Statistical methods in the atmospheric sciences* (4th ed.). Academic Press.

World Meteorological Organization. (2018). *Guide to climatological practices* (2nd ed.).

Zhang, Q., Liu, C., Xu, C., Xu, Y. & Jiang, T. (2006). Observed trends of annual maximum water level and streamflow during past 130 years in the Yangtze River basin, China. *Journal of Hydrology, 324*(1), 255–265. https://doi.org/10.1016/j.jhydrol.2005.09.023

CHAPTER 4

4 | A NEW APPROACH FOR DEVELOPING COMBINED EMPIRICAL RAINFALL-TRIGGERED LANDSLIDE THRESHOLDS: APPLICATION TO SÃO MIGUEL ISLAND (AZORES, PORTUGAL)

Abstract

Landslides, often triggered by intense or prolonged rainfall, pose significant risks to communities and infrastructure. Identifying accurate rainfall thresholds is crucial for predicting landslide events and developing effective early warning systems. This study, conducted on São Miguel Island (Azores), aimed to improve the predictive capability of rainfall thresholds by integrating both rainfall preparatory and rainfall trigger thresh-olds. Using data from 61 landslide events and rainfall measurements recorded at four stations between 1977 and 2020, the study applied the Generalised Extreme Value (GEV) distribution with Maximum Likelihood Estimation (MLE) to identify the cumulative rainfall–duration pair with the highest return period for each event, thereby establishing a preparatory threshold. The trigger threshold was determined by analysing the rainfall amount recorded on the day of the event while also accounting for the duration of the preparatory rainfall period. The final threshold combines both the preparatory and trigger thresholds, and an event is detected when both thresholds are exceeded. Preparatory thresholds showed similar patterns across the stations, with Sete Cidades and Furnas recording the highest cumulative rainfall values, while Santana and Ponta Del-gada exhibited lower thresholds. The trigger thresholds at Furnas reflected the highest daily rainfall intensities. The analysis also indicated that the rainfall intensity required to trigger landslides decreases with increasing durations of the antecedent rainfall. Performance of the thresholds using ROC metrics revealed that the combined threshold outperformed the preparatory threshold alone by reducing false positives (FPs) and improving predictive accuracy. In all cases, the combined threshold demonstrated superior performance in detecting landslide events, highlighting its effectiveness in land-slide prediction. This study provides a detailed analysis of rainfall thresholds for landslides on São Miguel Island and underscores the advantages of the combined threshold approach for improving landslide prediction and supporting the development of robust early warning systems.

Keywords: Landslide; Combined Rainfall Threshold; São Miguel Island; Azores

Manuscript published in *Water*

Journal Impact Factor: 3.5; 5-year Journal Impact Factor: 3.6

Silva, R.F., Marques, R. & Zêzere, J.L. (2026). A New Approach for Developing Combined Empirical Rainfall-Triggered Landslide Thresholds: Application to São Miguel Island (Azores, Portugal) Water, 18(6), 673. https://doi.org/10.3390/w18060673

4.1 | Introduction

Rainfall is one of the most important factors triggering landslides (e.g. Guzzetti et al. 2007; Petley 2012). For the same region, the triggering of different types of landslides can be related to different critical hydrological conditions for failure due to the diversity of triggering conditions and physical phenomena involved (e.g. Zêzere et al. 2015; Caine 1980). Although there have been previous studies trying to identify the amount of rainfall required for landslide triggering, the work of Caine (1980) was the first to propose global minimum thresholds for triggering shallow landslides, using a power-law equation based on rainfall intensity-duration conditions. Since then, the identification of rainfall thresholds has been the focus of numerous scientific studies (e.g. Guzzetti et al. 2007; Guzzetti et al. 2008; Segoni et al. 2018; Gonzalez et al. 2024), frequently in relation to the development of landslide early warning systems.

Rainfall thresholds can be defined using physical (process-based, conceptual) or empirical (historical, statistical) approaches (e.g. Bogaard et al. 2018; Frattini et al. 2009). Empirical models, which are the focus of this study, rely on historical records of instability events and statistical analysis of rainfall data. Intensity-duration (ID) thresholds are the most common in the literature (e.g. Guzzetti et al. 2008, Brunetti et al. 2010; Staley et al. 2013; Ma et al. 2015) and relate the total rainfall of an event to the instantaneous rainfall. These ID thresholds cover a wide range of rainfall durations and intensities, with most thresholds covering the intervals of 1 to 100 h and 1 to 200 mm/h. These thresholds exhibit asymptotic behaviour during very short rainfall durations (Guzzetti et al. 2007). Rainfall thresholds based on the amount of rainfall during landslide triggering events have been defined using different rainfall variables including: (i) daily rainfall (R), (ii) antecedent rainfall; (iii) cumulative event rainfall (E); and (iv) normalised cumulative event rainfall. The latter type of threshold states that landslides are likely to occur, or occur frequently, if the total rainfall during a rainfall event exceeds a predetermined percentage of the Mean Annual Precipitation (MAP) (Guzzetti et al. 2007). Normalisation allows one to compare thresholds across different areas, since in most cases, regional and local thresholds are specific to each area (Dahal et al. 2008).

Empirical ID thresholds are used to predict landslide occurrence based on a pow-er-law equation. This approach is based on two main assumptions (Marin 2020): (i) the probability of landslide initiation increases non-linearly with the intensity of rainfall, identified by a threshold value that, when reached or exceeded, indicates a high probability of these events being triggered; (ii) as the duration of rainfall increases, the intensity required to trigger landslides decreases. For these ID thresholds to be effective predictors, they must meet specific criteria: accurately represent the rainfall intensities that trigger landslide events; be activated at the correct time or shortly after; and minimise both the instances of landslides occurring below the threshold (false negatives) and conditions exceeding the threshold that do not result in landslides (false positives). Traditionally, their definition has been subjective, making them difficult to replicate and compare results across different studies. A common approach is the "lower limit" (LL) method (e.g. Vaz et al. 2018), which defines the threshold as the lowest rainfall intensity that resulted in landslide events. While this method provides a conservative estimate, it is prone to a large number of false positives.

Recent advances incorporate soil moisture and hydrological information into hydrometeorological thresholds, improving the predictive performance by accounting for pre-conditioning factors that enhance slope susceptibility (Palau et al. 2023). Studies show that integrating modelled soil moisture from reanalysis datasets can substantially reduce false alarms while maintaining detection accuracy (Palazzolo et al. 2025). Additionally, machine learning techniques are better suited to capturing nonlinear relationships than traditional empirical models, with hybrid artificial intelligence methods demonstrating superior accuracy (Ebrahim et al. 2025). Beyond traditional empirical and physical approaches, probabilistic methods have been developed to quantify landslide occurrence uncertainty more rigorously (Zhang et al. 2025). Hybrid artificial intelligence models, including support vector machines, random forests, and deep learning approaches, consistently demonstrate higher predictive accuracy than simpler empirical models by capturing nonlinear dynamics often missed by traditional approaches (Ebrahim et al. 2025). Recent advances in the field also suggest that combining multiple complementary threshold types may offer improved prediction performance compared to traditional single-threshold approaches (Nocentini et al. 2023).

Despite this progress, operational challenges persist: false alarms reduce public confidence, while missed alarms represent critical failures with potential risk to human life. Recent research has therefore focused on optimising these dual objectives through multi-source validation and calibration procedures that explicitly minimise false alarm rates while maintaining acceptable detection performance (Nocentini et al. 2023). In this study, we propose the use of two thresholds that, when combined, maximise landslide event prediction while reducing the number of false positives compared to the traditional single-threshold approach. To achieve this, six steps were established: (i) identify the landslide events that occurred within the area of influence of four rainfall stations during the 44-year period 1977–2020; (ii) define a cumulative rainfall-duration ($R_{cum} - D$) function corresponding to the best discrimination between days with and without landslides (preparatory threshold); (iii) define a 1-day rainfall intensity-duration ($I_{D1} - D$) function, using the same criteria, based on the rainfall recorded on the day of the event (trigger threshold); (iv) assess the performance of the preparatory and combined thresholds using a back-analysis method; (v) normalise the rainfall thresholds by the MAP; and (vi) estimate the monthly probability of exceedance and return period of the combined thresholds. This methodology is expected to enhance the precision and reliability of rainfall thresholds in predicting landslides.

4.2 | Study Area

4.2.1 | Geology and Climate

The Azores are located in the North Atlantic Ocean, at the meeting point of the Eurasian, African, and North American tectonic plates (Figure 4.1a). This complex geo-dynamic setting results in recurrent seismic and volcanic activity (Gaspar et al. 2015), which often triggers significant landslide events. However, rainfall-triggered landslides are the most prevalent geological hazard in the region, driven by the physical, mechanical, and hydrological properties of volcanic materials as well as the island's geomorphology.

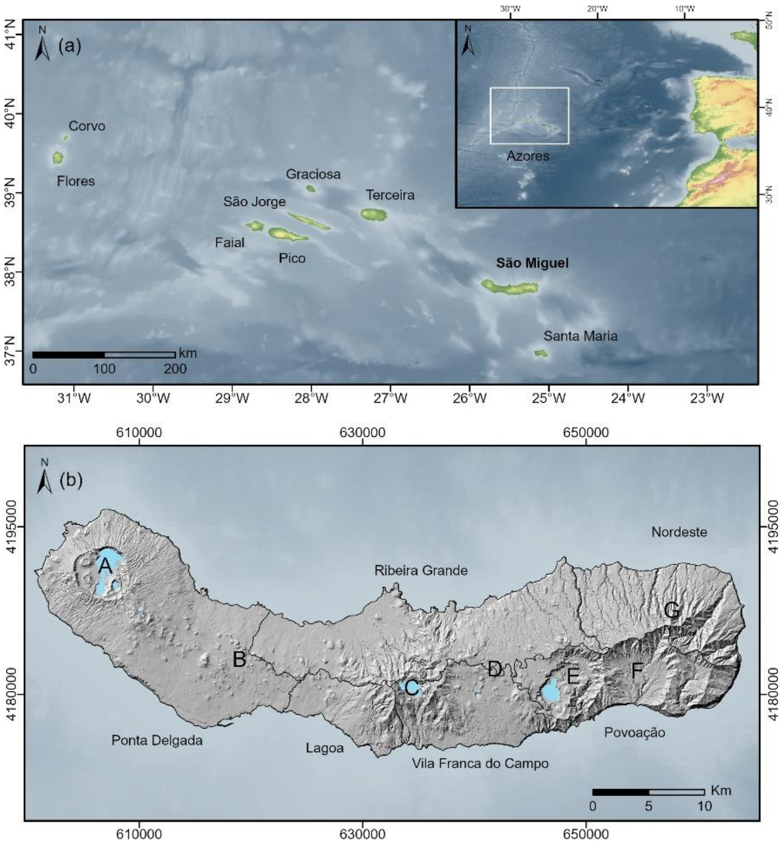

Figure 4.1 | (a) Geographical position and (b) municipalities (black lines) and morphostructural units of São Miguel Island: A—Sete Cidades Volcano; B—Picos Fissural Volcanic System; C—Fogo Volcano; D—Congro Fissural Volcanic System; E—Furnas Volcano; F— Povoacão Volcano; and G—Nordeste Volcanic Complex.

São Miguel Island spans 744.6 km^2, with elevations ranging from sea level to 1143 m a.s.l. Administratively, it is divided into 6 municipalities, comprising a total of 64 parishes (Figure 4.1b). The island has three active central volcanoes with summit calderas: Sete Cidades (Queiroz et al. 2015), Fogo (Wallenstein et al. 2015), and Furnas (Guest et al. 2015) (Figure 4.1b). Landslides are prevalent in several morphological formations characterised by steep slopes, including the inner walls of caldera volcanoes, fault scarps, coastal cliffs, and stream valleys (Marques et al. 2015). These formations are predominantly composed of non-cohesive materials, such as pumice deposits.

The central volcanoes are linked by two fissural volcanic systems: Picos (Ferreira et al. 2015) and Congro (Guest et al. 1999). Extensive outcrops of basaltic lava flows and scoria heavily influence the morphology of the Picos Fissural Volcanic System, which is characterised by mild slopes and a limited drainage network. Landslides in this area primarily concentrate along the coastal cliffs (Marques et al. 2015). Scoria cones and their associated lava flows are the primary features of the Congro Fissural Volcanic System, which also includes pumice cones, domes, and maars. The entire region is blanketed by thick pumice fallout deposits from the explosive eruptions of the Fogo and Furnas Volcanoes. Positioned as an elevated zone in the axial area, with elevations surpassing 500 m above sea level, gentle slopes ascend towards the north and south coastlines. Landslides are prevalent in this region, particularly along coastal cliffs and within deep narrow valleys (Marques et al. 2015).

The Nordeste Volcanic System and Povoação Volcano (Duncan et al. 2015) represent the island's earliest geological formations. The Nordeste Volcanic System is characterised by a shield volcano primarily comprised of basaltic lavas, which underwent extensive erosion during and after volcanic activity. Conversely, Povoação Volcano initially formed as a lava shield, followed by explosive trachytic activity and subsequent caldera collapse. Landslides in the Nordeste Volcanic System are concentrated in areas where weathered basaltic lava flows intersect steep slopes and deep narrow valleys experiencing intense fluvial erosion. In Povoação Volcano, landslides are linked to non-cohesive materials, mainly pumice, which underwent significant erosion both during and after volcanic activity (Marques et al. 2015).

The climate of the Azores is essentially influenced by the geographical location of the islands (Azevedo 2001). Rainfall is distributed across the year, with a notable reduction during the summer period. The annual rainfall pattern exhibits distinct seasonal variations, with the "wettest period" occurring from October to March. Conversely, the summer months constitute the "driest period", with July typically experiencing the lowest levels of rainfall (Figure 4.2).

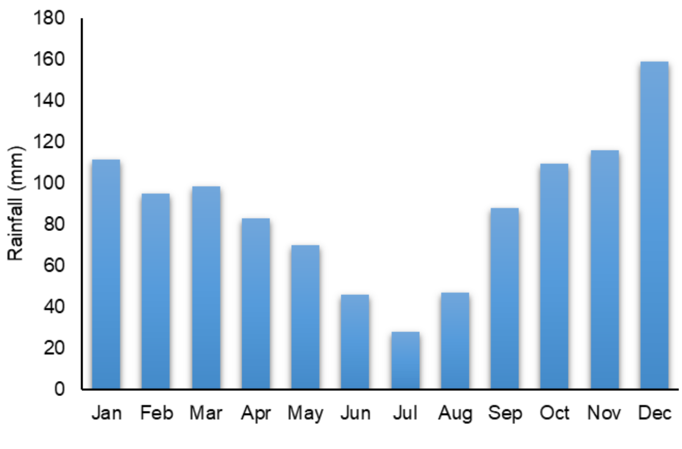

Figure 4.2 | Average monthly rainfall at the Ponta Delgada meteorological station for the period of 1981–2010 (climate normal data from the Portuguese Institute for Sea and Atmosphere).

The fluctuation in yearly rainfall patterns is associated with the archipelago's proximity to the North Atlantic Subtropical Anticyclone, commonly referred to as the Azores High (Hernández et al. 2016; Carvalho et al. 2023). Mean Annual Precipitation (MAP) ranges from approximately 800–1000 mm in low-altitude coastal areas to more than 2900 mm at higher elevations, with extreme annual totals locally exceeding 4000 mm in the central volcanic highlands (Silva et al. 2025). Rainfall shows a strong positive correlation with altitude, with average increases of about 180–200 mm per 100 m of elevation gain, which reflects the dominant influence of orographic forcing (Silva et al. 2025).

Long-term trend analyses reveal a general decrease in both annual and seasonal rainfall over recent decades, particularly after 2010 (Silva et al. 2025). The most pronounced reductions are observed in autumn and winter. Stormy periods are more frequent in winter, although late summer and autumn can also experience them due to sporadic cyclones and tropical storms passing near the archipelago (Azevedo 2001). These weather systems, often in their weakening stages, can produce some of the most intense storms affecting the Azores, potentially triggering significant and destructive hydro-geomorphological events.

4.2.2 | Landslide Incidence

Landslides have historically resulted in numerous fatalities and substantial socio-economic disruption on São Miguel Island (Silva et al. 2024). The most devastating incident took place on 31 October 1997, when intense rainfall triggered nearly 1000 shallow landslides (Marques et al. 2008; Marques 2013; Marques et al. 2015) and caused 29 fatalities in the village of Ribeira Quente.

Marques et al. (2015) carried out a systematic inventory of landslides on São Miguel Island based on the interpretation of high-resolution geo-referenced digital orthophoto maps, supplemented with topographic data. The photointerpretation was conducted at the 1:1000 scale, identifying slope instabilities through morphological changes, vegetation patterns, and modifications to surface drainage conditions. The inventory includes 9890 landslide scars, represented as polygons in a GIS environment, with a total planimetric area of approximately 13.16 km^2 (Figure 4.2).

Landslides on São Miguel Island predominantly consist of shallow translational slides and soil slips, which frequently evolve into debris flows (Marques et al. 2015). Most landslides are typically narrow—rarely wider than 30–40 m—and originate on steep slopes where the slip surfaces generally do not exceed depths of 2–3 m. Most failures initiate near the crest of steep slopes and often extend downslope across the full length of the slope, effectively defining the total area of depletion. These slopes are commonly composed of unsaturated, cohesionless pyroclastic materials, where matric suction plays a critical role in slope stability by contributing apparent cohesion and enhancing shear strength (Amaral 2010; Amaral et al. 2009).

The spatial distribution of landslides shows a clear concentration along the flanks of the island's young central volcanoes and along coastal sea cliffs (Figure 4.3). These regions are typified by vertical caldera walls, steep inclines, deeply incised valleys, and fault scarps, all covered by unconsolidated pyroclastic deposits from recent explosive eruptions—conditions highly conducive to landslide activity (Marques et al. 2015). In the eastern part of the island, the Nordeste Volcanic System also exhibits significant landslide occurrence due to the presence of deep gullies incised into thick, weathered lava flows. Notably, larger landslides tend to occur on slopes with extended slope lengths, especially those associated with deeply entrenched, narrow valleys, further emphasising the role of topography in landslide susceptibility (Marques et al. 2015).

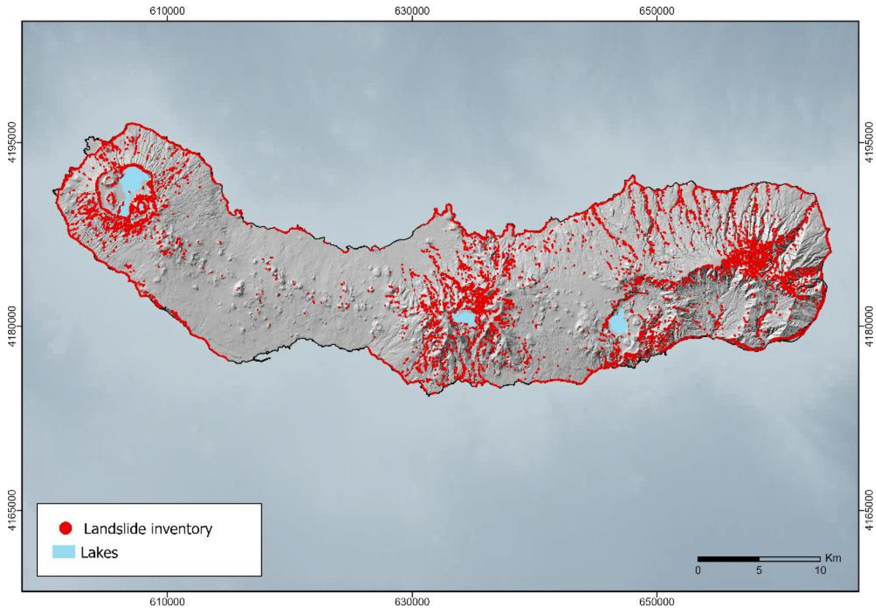

Figure 4.3 | Landslide inventory of São Miguel Island carried out by Marques et al. (2015).

4.2.3 | Previous Thresholds Studies in Study Area

On São Miguel Island, rainfall is the main trigger for landslides (Silva et al. 2024). Over the past few years, researchers have studied the correlation between rainfall and landslides in this region. In a study conducted by Marques et al. (2008), the role of rainfall in triggering landslides in Povoação (São Miguel Island) was assessed. The researchers re-constructed both the absolute and calibrated antecedent rainfall data. For each landslide event, they identified the critical combinations of rainfall accumulation and duration, which were subsequently used to establish the corresponding thresholds. Building on this work, Marques et al. (2010) established the foundation for the implementation of an empirical landslide warning system in

Povoação (ELEWS-Pov). This system automates the reconstructing of the absolute accumulated rainfall for various durations, enabling the real-time monitoring of meteorological conditions. Researchers have also examined the connection between the North Atlantic Oscillation (NAO) and landslide occurrence in the Azores. Marques et al. (2008) identified an inverse relationship between landslides in the Povoação region and the NAO index. However, this relationship was less evident than the one observed in the northern area of Lisbon, Portugal (Zêzere et al. 2005). Zêzere et al. (2015) compared several empirical rainfall thresholds established for different Portuguese regions, examining thresholds for the Lisbon area, Douro Valley, NW Mountains, and Povoação on São Miguel Island. More recently, Marques et al. (2021a; 2021b) developed an early warning system to generate alerts and alarms based on empirical rainfall thresholds. This application was designed to mitigate land-slide risks during the construction of a semi-tunnel on the only road leading to Ribeira Quente, located on São Miguel Island.

4.3 | Data and Methods

4.3.1 | Landslide Events

In this study, a landslide event is defined by the date of slope instability and may include multiple individual landslides. The landslide events were extracted from the NATHA database (Marques 2013), which was constructed through a systematic review of daily and weekly newspapers published on São Miguel Island between 1900 and 2020 (Silva et al. 2024). The available information is generally limited to the date, landslide type, and its reported impacts. Furthermore, in the NATHA database, location data are most often provided only at the parish level (the smallest administrative unit).

Although the type of landslide is occasionally unspecified, the most frequent types are shallow slides and debris flows (Figure 4.4). On São Miguel Island, landslide events are widespread throughout the climatological year but are concentrated in the rainiest months of the year, particularly between December and March, which account for 67% of the total landslide events.

Figure 4.4 | Examples of landslides on São Miguel Island: (a) debris flow that caused 29 fatalities in 1997; (b) shallow landslide that caused one fatality in 2012; (c) shallow landslide that destroyed access to a beach in 2013; and (d) rockfall that blocked a road in 2013.

Table 4.1 summarises the 61 landslide events considered in this study. For each event, the table presents the date, affected municipality, spatial extent, and the estimated number of individual landslides. The affected municipality corresponds to the municipality or municipalities where landslides were recorded during a given event. The spatial extent is defined as the cumulative area of the parishes affected by each event. The number of landslides represents the estimated total of individual landslides that occurred during each event.

Table 4.1 | Date, affected municipality, spatial extent and estimated number of landslides for each recorded landslide event.

Date	Affected Municipality	Spatial Extent (km^2)	No. of Landslides		
			<10	10–1000	>1000
10 February 1979	Ponta Delgada, Povoação	66.9	x		
9 April 1980	Ribeira Grande, Povoação	59.4		x	
27 November 1980	Ponta Delgada, Ribeira Grande, Povoação	88.4		x	
1 January 1982	Ponta Delgada, Povoação	43.9	x		
2 March 1983	Ponta Delgada, Povoação	56.3		x	
22 December 1983	Povoação	34.4	x		

23 December 1983	Ponta Delgada	18.2	x		
3 March 1984	Ponta Delgada, Ribeira Grande, Povoação	45.2		x	
8 February 1985	All municipalities	285.5		x	
13 February 1986	Lagoa, Vila Franca do Campo, Ribeira Grande	34.4	x		
3 September 1986	Povoação, Nordeste	26.2	x		
24 January 1987	Ribeira Grande	4.7	x		
8 October 1993	Povoação, Nordeste	20.1	x		
12 December 1994	Ponta Delgada, Ribeira Grande, Lagoa	21.6	x		
24 December 1995	Povoação	34.4	x		
21 October 1996	Ribeira Grande, Povoação	106.3		x	
15 December 1996	Povoação	110.3		x	
30 December 1996	Ponta Delgada, Lagoa, Vila Franca do Campo, Povoação	202.9		x	
2 January 1997	Ponta Delgada, Vila Franca do Campo	23.5	x		
10 September 1997	Lagoa, Povoação	9.1	x		
11 September 1997	Ponta Delgada	12.3	x		
31 October 1997	Vila Franca do Campo, Povoação, Nordeste	224.7			x
14 December 1997	Ponta Delgada, Ribeira Grande, Nordeste	100.6		x	
15 December 1997	Povoação	99.0		x	
26 January 1998	Ribeira Grande, Lagoa, Vila Franca do Campo, Povoação	200.3		x	
1 October 1998	Povoação, Nordeste	146.3		x	
29 November 2000	Ribeira Grande, Lagoa, Vila Franca do Campo	10.8	x		
30 November 2000	Povoação	43.5	x		
7 January 2001	Ribeira Grande, Povoação	12.8	x		
4 March 2001	Ribeira Grande, Vila Franca do Campo	10.8	x		
5 March 2001	Povoação, Nordeste	123.2		x	
19 December 2001	All municipalities	645.8		x	
11 January 2002	Ponta Delgada	8.7	x		
11 February 2002	Ribeira Grande	77.1		x	
13 February 2002	Ponta Delgada, Vila Franca do Campo, Povoação	104.6		x	
30 October 2002	Povoação, Nordeste	123.2		x	
15 December 2002	Ponta Delgada, Povoação	60.0	x		

10 April 2003	Vila Franca do Campo, Povoação	81.1		x
11 April 2003	Ponta Delgada	85.4		x
6 March 2005	Ribeira Grande, Povoação	82.2		x
8 March 2005	Povoação	23.2	x	
18 March 2005	Ribeira Grande, Lagoa, Povoação	103.3		x
17 June 2005	Povoação	34.4	x	
13 November 2006	Ribeira Grande, Nordeste	77.1		x
15 December 2006	Ponta Delgada, Ribeira Grande, Nordeste	86.3		x
13 November 2007	Povoação	60.6	x	
18 November 2007	Ponta Delgada, Vila Franca do Campo, Povoação	129.3		x
13 February 2010	Ribeira Grande	12.7	x	
15 December 2010	Povoação	9.0	x	
2 January 2011	Ponta Delgada	2.9	x	
15 October 2011	Ponta Delgada	14.8	x	
11 May 2012	Ponta Delgada	5.6	x	
28 February 2013	Ponta Delgada	16.9	x	
14 March 2013	Povoação, Nordeste	45.8		x
18 March 2013	Ponta Delgada, Povoação	21.3	x	
9 December 2013	Ribeira Grande	12.8	x	
11 May 2015	Ponta Delgada, Ribeira Grande, Povoação	92.5		x
15 January 2016	Ponta Delgada, Ribeira Grande	25.1	x	
23 January 2016	Ponta Delgada, Vila Franca do Campo, Nordeste	41.4		x
22 August 2019	Povoação	35.7	x	
28 January 2020	Ribeira Grande, Povoação	200.3		x

4.3.2 | Rainfall Data

The rainfall data used in this study were collected from four rainfall stations (analysed by Silva et al. 2025): three owned by the Government of the Autonomous Region of the Azores (GRAA) and one by the Portuguese Institute for Sea and Atmosphere (IPMA). These rainfall stations were selected for their long time series of daily rainfall data, their representative coverage of the island's rainfall distribution and morphostructural units; and the extensive catalogue of landslide events within their areas of influence. Unfortunately, hourly rainfall records in the Azores are only available from 2012 onward, covering just 16% of the landslide events listed in Table 4.1. Moreover, most of these events lack precise timing information. These limitations prevented the use of hourly precipitation data for establishing rainfall thresholds for landslide triggering. Indeed, a long-term rainfall time series, together with a comprehensive landslide event catalogue, are essential requirements for developing robust rainfall thresholds for landslide triggering using probabilistic approaches.

Details regarding the altitude, MAP, data periods and ownership of rainfall stations are provided in Table 4.2. The distribution of MAP and the location of these rainfall stations are illustrated in Figure 4.5.

Table 4.2 | Rainfall stations used in the analysis.

Station	Altitude (m)	MAP (mm)	Data Period	Owner
Sete Cidades	260	1797.5	1977/78–2019/2020	GRAA
Santana	71	1135.3	1977/78–2019/2020	GRAA
Ponta Delgada	20	1006.1	1977/78–2019/2020	IPMA
Furnas	280	2127.4	1977/78–2019/2020	GRAA

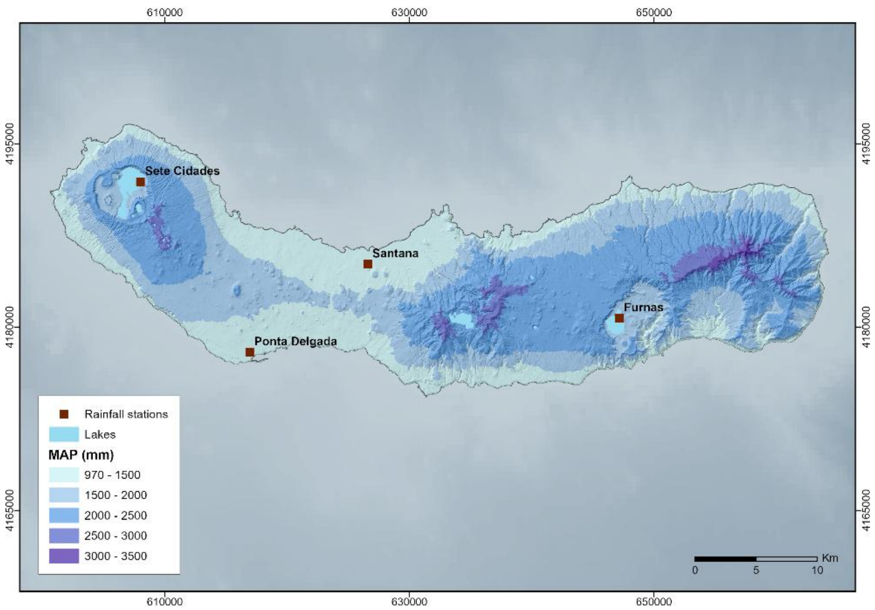

Figure 4.5 | Geographic location of rainfall stations and the distribution of the MAP (mm).

The method of selecting reference rainfall stations for defining rainfall thresholds, based on the nearest rainfall station, remains one of the simplest and most widely used approach (Segoni et al. 2018). Since landslide events in the NATHA database are typically geolocated only at the parish level (the smallest administrative division), spatial analysis was limited to this resolution. To address this, four areas of influence were defined around the rainfall stations by grouping nearby parishes (within a 10 km radius), considering both geographic and geomorphologic context (Figure 4.6). Each landslide event was then associated with the nearest rainfall station within these areas. When a landslide event extended across two or more areas of influence, this overlap was accounted for in the analysis. Landslide events occurring outside the defined areas of influence were excluded from the analysis.

The area of influence of the Sete Cidades rainfall station essentially corresponds to the Sete Cidades Volcano and covers an area of 112.1 km^2. The Ponta Delgada and Santana rainfall stations represent areas of influence within the Picos Fissural Volcanic System, to the south and north, respectively, with areas of 85.4 km^2 and 77.1 km^2. The area of influence of Furnas rainfall station mainly corresponds to the Furnas and Povoação Volcanoes and the southwestern part of the island, covering an area of 123.2 km^2. Overall, 346.8 km^2 (47%) of the island lie outside the areas of influence defined for the four selected rainfall stations.

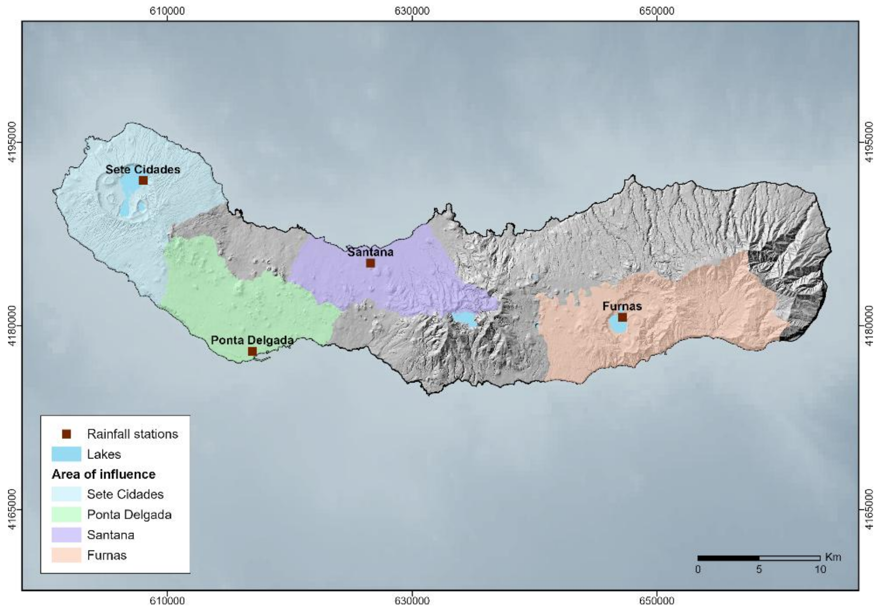

Figure 4.6 | Areas of influence of each reference rainfall station.

Figure 4.7 presents a summary of the steps used in this study to define the preparatory and trigger thresholds. In the workflow diagram, green boxes represent the input data, grey rectangles correspond to the processing steps, blue trapezoids indicate intermediate outputs, and yellow boxes represent the final outputs. The reconstruction of cumulated rainfall in this study follows the methodology proposed by Zêzere et al. (2005). The daily rainfall data recorded on the rainfall stations were organised by climatological year, which spans from September to August. Rainfall daily data from the climatological years 1977/78 to 2019/2020 were considered, corresponding to the period from 1 September 1977 to 31 August 2020. This approach was chosen instead of the hydrological year (October–September) because the rainfall regime in the study area justifies it. By starting the analysis in September, following the typically dry months of July and August, the complete transition to the wet season is captured in each climatological year.

For each data period from each rainfall station, the cumulated antecedent rainfall was calculated over various durations. Field observations on São Miguel Island indicate that typically a water table is generally absent close to the ground surface at most landslide sites. The rapid variation and evolution of pore pressures at the top of the slope are not directly linked to the evolution and elevation of the groundwater level. Therefore, the water infiltration process and the development of a percolation front are considered the main triggering mechanisms for landslides (Amaral et al. 2009). In this context, durations from 1 to 20 consecutive days were considered.

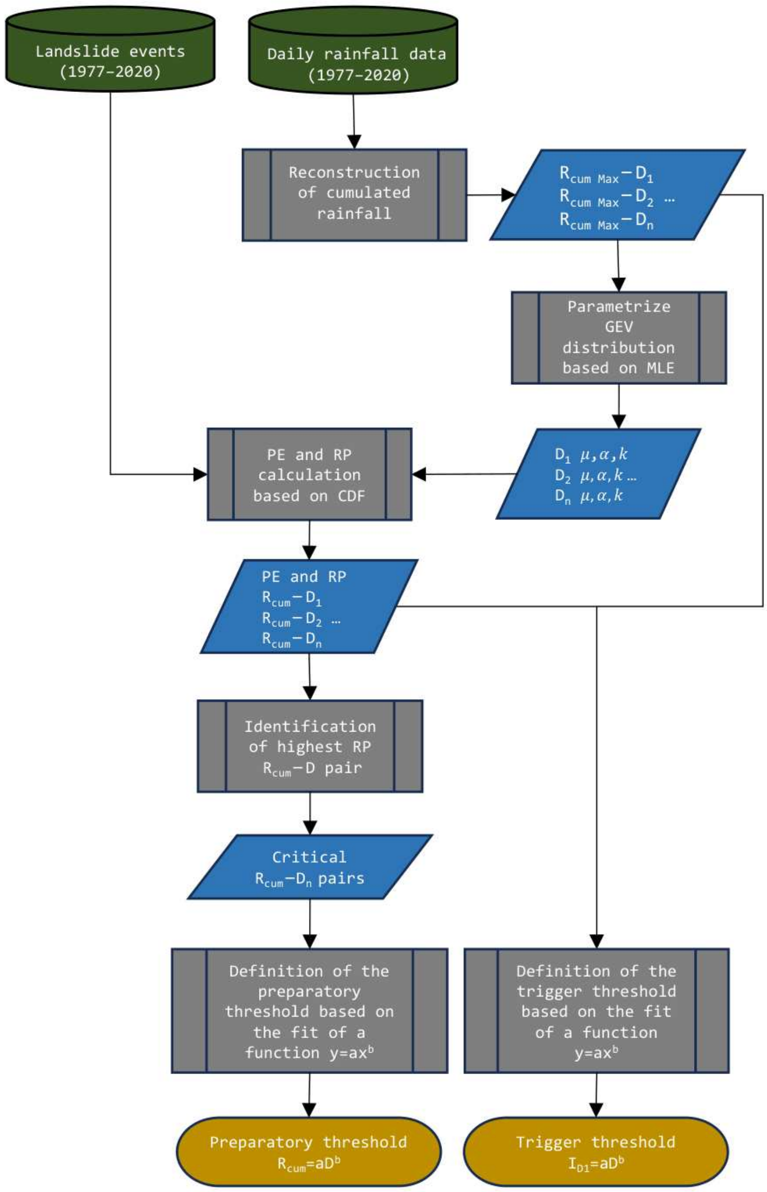

Figure 4.7 | Workflow for defining preparatory and trigger thresholds.

4.3.3 | Generalised Extreme Value (GEV) Distribution

Extreme value analysis allows for predictions of future extreme event probabilities based on historical data (El Adlouni et al. 2007). One common method used in extreme value analysis is the block maxima approach, which involves modelling a sequence of maximum values taken from blocks (or periods) of equal duration. In this study, the maximum annual rainfall values, for all the cumulated rainfall periods considered, were extracted and analysed using the generalised extreme value (GEV) distribution (Coles 2001). The Generalised Extreme Value (GEV) distribution comprises three distinct categories: type I (Gumbel distribution), type II (Fréchet distribution), and type III (Weibull distribution). Let X denote the annual maximum cumulative rainfall for a given duration D, obtained using the block maxima approach. The variable X is assumed to follow a Generalised Extreme Value (GEV) distribution. The probability density function (PDF) for the GEV is represented as Equation (1):

$$f(x,\mu,\sigma,\xi) = \begin{cases} \frac{1}{\sigma}\left[1+\xi\left(\frac{x-\mu}{\sigma}\right)^{-\frac{1}{\xi}-1}\right] exp\left[-\left(1+\xi\frac{x-\mu}{\sigma}\right)^{-\frac{1}{\xi}}\right], \xi \neq 0 \\ \frac{1}{\sigma} exp\left[-\left(\frac{x-\mu}{\sigma}\right)\right] exp\left[-exp\left(-\frac{x-\mu}{\sigma}\right)\right] \quad , \xi = 0 \end{cases} \quad (1)$$

The cumulative distribution function (CDF), resultant from the integration of the PDF, is given by Equation (2):

$$F(x,\mu,\sigma,k) = \begin{cases} exp\left[-\left(1+k\frac{x-\mu}{\sigma}\right)^{-\frac{1}{\xi}}\right], \xi \neq 0 \\ exp\left[-exp\left(-\frac{x-\mu}{\sigma}\right)\right] \quad , \xi = 0 \end{cases} \quad (2)$$

where μ is the location parameter, σ is the scale parameter and ξ is the shape parameter. The three scenarios are as follows: (i) when $\xi = 0$, resulting in the Extreme Value type I distribution; (ii) when $\xi < 0$, yielding the Extreme Value type II distribution; and (iii) when $\xi > 0$, producing the Extreme Value type III distribution (Chow et al. 1988). In each of these cases, the value of α remains positive.

4.3.4 | Parameter Estimation

The GEV parameters were estimated using the Maximum Likelihood Estimation (MLE) method. The goal of MLE is to find the values of μ, σ, ξ that maximise the likelihood function. This is typically achieved by taking the natural logarithm of the likelihood function (log-likelihood) and then applying optimisation techniques to maximise it. For $\xi \neq 0$, the likelihood function is given by Equations (3) and (4) (Coles 2001; Clarke 2013):

$$l(\mu, \sigma, \xi) = -n \, log \, \sigma - (1 + \xi) \sum_{i=1}^{n} z_i - \sum_{i=1}^{n} \exp(-z_i) \, , \qquad \xi \neq 0, \tag{3}$$

where:

$$z_i = \frac{1}{\xi} log \left[1 + \xi \frac{(x - \mu)}{\sigma} \right], 1 + \xi \left(\frac{x - \mu}{\sigma} \right) > 0 \; for \; i = 1, 2, \dots, n \tag{4}$$

If ξ = 0, the GEV distribution reduces to the Gumbel distribution, and the resulting log-likelihood function is given by Equation (5):

$$l(\mu, \sigma) = -n \, log \, \sigma - \sum_{i=1}^{n} exp \left[-\left(\frac{x - \mu}{\sigma} \right) \right] - \sum_{i=1}^{n} \left[-\left(\frac{x - \mu}{\sigma} \right) \right] \tag{5}$$

Coles (2001) notes that ML estimates exhibit typical asymptotic behaviours when $\xi \geq -0.5$. When $\xi = [-1, -0.5]$, ML estimates are attainable but lack standard asymptotic properties. For $\xi < -1$, ML estimates are non-existent, and for $\xi > 0.5$, second and higher moments are not definable. Additionally, MLE introduces minimal bias for sample sizes ranging from 30 to 100. However, caution is advised when estimating parameters near ξ = 0, as emphasised by Kotz and Nadarajah (2000).

3.5. Probability of Exceedance and Return Period

The temporal probability of a landslide event is estimated by the probability that the rainfall event will exceed the defined rainfall threshold (Jaiswal et al. 2010; Tien Bui et al. 2013; Afungang et al. 2016). The Probability (p) of Exceedance the specified rainfall threshold within a given year is determined by applying Equation (6):

$$p = 1 - F(x) \tag{6}$$

where $F(x)$ is the cumulative distribution function.

Due to the extension of the results for all four stations and multiple durations, the corresponding graphical representations of the PDF and CDF/Probability of Exceedance curves are provided in the Supplementary Materials (Figures S1–S4).

The return period (RP) is the average time between events that exceed a particular threshold. It is calculated as the reciprocal of the probability of exceedance, as shown in Equation (7):

$$RP = \frac{1}{1 - F(x)} \tag{7}$$

For each landslide event, the cumulated rainfall–duration ($R_{cum} - D$) pair with the highest RP was selected. This approach ensures that the rarest (most extreme) rainfall periods are chosen for each event, allowing for the maximum distinction between rainfall periods associated with landslide events and those not related with landslide events, similar to the criteria used by Marques et al. (2008) and Zêzere et al. (2005, 2015).

Based on the $R_{cum} - D$ pair for each landslide event, a preparatory threshold was plotted, corresponding to the best distinction between days with recorded landslides and days without landslides. The parameters of the preparatory threshold were adjusted so that all landslide events remained above the function while minimising the number of false positives.

For values of $D > 1$, the R_{cum} values tend to attenuate the importance of the rainfall recorded on the day of the landslide event (R_{D1}), and this problem worsens with increasing duration. To address this issue, a function relating rainfall intensity on the day of the landslide event (I_{D1}) and the duration (D) was tested, and a trigger threshold was also defined, aiming to achieve the best distinction between days with recorded landslides and days without landslides, considering the previously established criteria.

The combined rainfall threshold responsible for triggering landslides corresponds, therefore, to a combination of two distinct power functions: the preparatory threshold and the trigger threshold, with the parameter α shared by both functions. Landslide triggering conditions are detected when the preparatory threshold is exceeded for a certain $R_{cum} - D$ pair and, simultaneously, for the same rainfall duration, the trigger threshold is exceeded, thus properly emphasising the rainfall intensity recorded on the day of the event.

The MAP from the 44 years of rainfall records was used to normalise the amount and intensity of the calculated thresholds, by computing the ratio between the amount and intensity of rainfall and the MAP.

The monthly probability of exceedance and return period of the combined thresholds are calculated by first determining the maximum rainfall values for all durations in each month of each year, followed by fitting the GEV distribution to the maximum rainfall data for each month and duration. Finally, the combined probabilities of exceedance for different months and durations are obtained by multiplying the probability of exceedance of the preparatory and trigger thresholds.

4.3.5 | Criteria for Thresholds Validation

The receiver operating characteristic (ROC) analysis was used to assess the performance of empirical rainfall thresholds. These analytical techniques can also be applied for calibrating rainfall thresholds (e.g. Staley et al. 2013; Mathew et al. 2014; Zêzere et al. 2015). To avoid an overestimation of threshold performance due to the large proportion of non-rainy days, only days with daily rainfall ≥ 10 mm were considered in the validation procedure. This approach follows recommendations in the literature (e.g. Piciullo et al. 2020), which suggest excluding non-rainfall days when computing confusion matrix elements and ROC-based performance metrics. By restricting the analysis to rainfall days above this threshold, the validation focuses on meteorologically relevant conditions for landslide triggering, resulting in a more conservative and realistic assessment of predictive capability.

The confusion matrix evaluates prediction accuracy by classifying outcomes as true positives (TPs), false negatives (FNs), true negatives (TNs), and false positives (FPs). For rainfall thresholds, TPs are landslides exceeding the threshold, FNs are landslides below the threshold, TNs correspond to non-landslide rainfall conditions below the threshold, and FPs are non-landslide conditions exceeding the threshold (Beguería 2006). Furthermore, this study employed four ROC metric functions outlined by Staley et al. (2013), as illustrated in Figure 4.8 and Equations (8)–(11). The proportion of correctly identified landslide occurrences based on the threshold is referred to as the true positive rate (TP_{rate}). The false positive rate (FP_{rate}) represents the percentage of rainfall events exceeding the threshold for which no landslide occurrence data are reported. The false alarm rate (FA_{rate}) represents the proportion of incorrect predictions in relation to the total number of rainfall events exceeding the specified threshold. The threat score (TS) is used to assess the threshold for optimising correct predictions while minimising the false positive (FP) and false negative (FN) rates.

	Landslide Observed	No Landslide Observed
Above Threshold	True Positive (TP)	False Positive (FP)
Below Threshold	False Negative (FN)	True Negative (TN)

$$TP_{rate} = \frac{TP}{TP + FN}, [0, 1] \tag{8}$$

$$FP_{rate} = \frac{FP}{FP + TN}, [0, 1] \tag{9}$$

$$FA_{rate} = \frac{FP}{TP + FP}, [0, 1] \tag{10}$$

$$TS = \frac{TP}{TP + FN + FP}, [0, 1] \tag{11}$$

Figure 4.8 | Confusion matrix illustrating the four possible outcomes of a binary classification model and the metrics used to assess classifier performance in ROC analysis.

4.4 | Results and Discussion

4.4.1 | Thresholds for Landslide

Over the 44-year study period, a total of 61 landslide events were recorded. For each event, the rainfall duration (D), the cumulated rainfall (R_{cum}), and the 1-day rainfall intensity (I_{D1}) were calculated. The respective return periods (RPs) and the combined return period were determined for each landslide event, following the methodology described in the previous section. The results were grouped by the four rainfall stations considering their respective areas of influence (Tables 4.3–4.6).

Table 4.3 | Landslide events triggered by rainfall within the influence area of the Sete Cidades rainfall station.

Date	D (Days)	R_{cum} (mm)	I_{D1} (mm/day)	RP R_{cum} (Years)	RP I_{D1} (Years)	Combined RP (Years)
10 February 1979	12	232.2	42.7	2.0	1.0	2.0
1 January 1982	7	116.2	39.5	1.1	1.0	1.1
2 March 1983	1	172.1		15.3		15.3
23 December 1983	2	200.2	119.0	8.3	3.9	32.3
3 March 1984	8	208.0	52.7	2.2	1.0	2.2
30 December 1996	20	244.0	40.0	1.2	1.0	1.2
2 January 1997	19	244.5	35.0	1.3	1.0	1.3
11 September 1997	2	101.0	76.0	1.4	1.3	1.8
14 December 1997	1	90.0		1.8		1.8
19 December 2001	1	127.0		4.9		4.9
11 January 2002	17	339.2	47.5	3.6	1.0	3.6
13 February 2002	2	92.0	49.0	1.2	1.0	1.2
15 December 2002	2	89.8	69.2	1.2	1.2	1.4
15 December 2006	1	211.4		36.3		36.3
18 November 2007	1	100.4		2.3		2.3
15 October 2011	20	183.9	32.0	1.0	1.0	1.0
11 May 2012	1	65.4		1.1		1.1
28 February 2013	4	111.6	50.9	1.2	1.0	1.2
18 March 2013	8	232.3	65.5	3.0	1.1	3.3
15 January 2016	3	177.1	102.3	3.7	2.5	9.2
23 January 2016	15	390.2	69.4	6.9	1.2	8.1

Table 4.4 | Landslide events triggered by rainfall within the influence area of the Ponta Delgada rainfall station.

Date	*D* (Days)	R_{cum} (mm)	I_{D1} (mm/day)	RP R_{cum} (Years)	RP I_{D1} (Years)	Combined RP (Years)
27 November 1980	1	81.3		3.9		3.9
23 December 1983	2	116.3	84.0	5.7	4.2	24.0
3 March 1984	8	130.1	41.5	2.4	1.2	2.9
8 February 1985	7	139.3	38.4	3.3	1.1	3.8
12 December 1994	1	56.0		1.7		1.7
30 December 1996	20	321.3	62.6	17.2	2.1	36.3
19 December 2001	1	100.0		7.0		7.0
11 April 2003	9	93.6	29.5	1.2	1.0	1.2
2 January 2011	19	255.5	31.9	6.1	1.0	6.4
11 May 2015	12	143.4	57.8	1.9	1.8	3.5
15 January 2016	4	57.0	34.1	1.1	1.1	1.2
23 January 2016	12	120.0	35.5	1.4	1.1	1.5

Table 4.5 | Landslide events triggered by rainfall within the influence area of the Santana rainfall station.

Date	*D* (Days)	R_{cum} (mm)	I_{D1} (mm/day)	RP R_{cum} (Years)	RP I_{D1} (Years)	Combined RP (Years)
9 April 1980	16	149.7	23.5	1.2	1.0	1.2
27 November 1980	1	88.0		3.6		3.6
3 March 1984	8	176.0	47.7	3.6	1.1	4.0
8 February 1985	7	157.2	53.5	3.0	1.2	3.7
24 January 1987	19	266.6	45.9	5.1	1.1	5.5
12 December 1994	1	87.7		3.6		3.6
21 October 1996	1	138.9		13.3		13.3
14 December 1997	1	54.2		1.3		1.3
26 January 1998	18	161.6	28.4	1.2	1.0	1.2
29 November 2000	1	83.6		3.2		3.2
4 March 2001	8	121.0	35.2	1.4	1.0	1.4
19 December 2001	1	124.4		9.7		9.7
11 February 2002	1	51.4		1.2		1.2
6 March 2005	1	115.8		7.9		7.9
18 March 2005	14	223.6	32.6	3.5	1.0	3.5

13 November 2006	1	51.4		1.2		1.2
15 December 2006	1	53.0		1.2		1.2
13 February 2010	8	191.4	59.6	5.2	1.5	7.7
9 December 2013	9	148.0	40.9	1.8	1.0	1.9
11 May 2015	12	212.2	79.2	3.8	2.8	10.4
15 January 2016	9	124.4	39.6	1.3	1.0	1.3
28 January 2020	1	45.5		1.1		1.1

Table 4.6 | Landslide events triggered by rainfall within the influence area of the Furnas rainfall station.

Date	***D*** **(Days)**	R_{cum} **(mm)**	I_{D1} **(mm/day)**	**RP** R_{cum} **(Years)**	**RP** I_{D1} **(Years)**	**Combined RP (Years)**
10 February 1979	19	368.3	66.0	2.1	1.1	2.3
9 April 1980	16	249.0	63.0	1.2	1.1	1.3
27 November 1980	1	172.8		10.1		10.1
1 January 1982	8	201.6	64.2	1.5	1.1	1.6
2 March 1983	1	76.6		1.2	1.2	1.2
22 December 1983	1	119.7		2.9		2.9
3 March 1984	3	222.6	112.0	6.1	2.4	14.7
8 February 1985	7	204.6	90.7	1.7	1.5	2.6
13 February 1986	1	73.6		1.2		1.2
3 September 1986	1	161.6		7.8		7.8
8 October 1993	1	142.6		5.0		5.0
24 December 1995	13	330.1	57.2	2.5	1.0	2.6
21 October 1996	1	97.6		1.8		1.8
15 December 1996	1	96.8		1.7		1.7
30 December 1996	20	432.6	64.8	3.0	1.1	3.3
10 September 1997	1	100.5		1.9		1.9
31 October 1997	1	220.0		28.7		28.7
15 December 1997	2	148.4	96.6	2.5	1.7	4.4
26 January 1998	18	386.5	94.6	2.5	1.7	4.2
1 October 1998	1	160.0		7.5		7.5
30 November 2000	5	284.2	152.2	6.7	6.3	42.2
7 January 2001	1	102.4		2.0		2.0
5 March 2001	8	225.1	48.5	1.9	1.0	1.9

19 December 2001	1	138.2		4.5		4.5
13 February 2002	2	133.5	80.5	2.0	1.3	2.6
30 October 2002	1	128.0		3.5		3.5
15 December 2002	2	156.3	119.9	2.9	2.9	8.5
10 April 2003	9	230.4	64.6	1.8	1.1	1.9
6 March 2005	1	149.8		5.9		5.9
18 March 2005	14	431.4	90.8	5.7	1.5	8.8
8 March 2005	4	241.6	60.8	5.3	1.1	5.5
17 June 2005	1	192.8		16.0		16.0
13 November 2007	12	306.8	97.4	2.4	1.8	4.2
18 November 2007	17	455.9	110.1	5.0	2.3	11.5
8 January 2010	1	136.0		4.2		4.2
15 December 2010	13	498.0	87.0	13.0	1.4	18.7
14 March 2013	18	458.8	115.2	4.5	2.6	11.8
18 March 2013	19	431.0	41.9	3.3	1.0	3.3
11 May 2015	12	309.1	70.4	2.4	1.1	2.8
22 August 2019	2	85.3	67.6	1.1	1.1	1.3
28 January 2020	2	74.2	60.7	1.1	1.1	1.1

The abundance of landslide events varies among the stations, reflecting the interplay of specific topographic, geomorphological, and geological factors combined with local rainfall patterns. Sete Cidades and Furnas influence areas concentrated most of the events, accounting for 38.7% and 45.2% respectively, which suggests that these areas have a higher landslide activity.

For all meteorological stations, two distinct rainfall patterns could be recognised as being associated with landslide activity: (i) short-duration, high-intensity rainfall and (ii) long-duration, low-intensity rainfall. Landslide events characterised by short-duration and high-intensity rainfall typically occur during storms or convective weather events (e.g. the 31 October 1997 landslide event in the Furnas rainfall station influence area; Table 4.5). These events are linked to lower values of R_{cum}, which indicates that less demanding cumulative rainfall is required for preparation, but higher I_{D1} values, which signal more demanding high intensity conditions on the day of the event. In contrast, landslide events typically associated with long-duration rainfall periods are generally triggered by the accumulation of rainfall over extended periods (up to 20 consecutive days), which saturates the soil and destabilises slopes (e.g. the 30 December 1996 landslide event in the Sete Cidades rainfall station influence area; Table 4.2). These events are characterised by higher R_{cum} values, indicating the importance of prolonged rainfall in preparing the slopes for failure, but lower I_{D1} values, indicating less demanding high intensity conditions on the day of the event. The distinction between these two rainfall patterns underscores the complex interplay between rainfall characteristics and landslide susceptibility across different regions and climatic conditions (Marotti et al. 2023).

The recurrence of landslide events, as indicated by the combined RP, highlights the variability in their frequency across different regions. The combined RP is a key metric, integrating both the cumulative rainfall (R_{cum}) and 1-day rainfall intensity (I_{D1}), to provide a comprehensive assessment of landslide likelihood under specific rainfall conditions. Landslide events associated with longer combined RP are typically associated with rare extreme weather events. However, events with shorter combined RP, often driven by more common rainfall patterns, can still pose substantial risks to the affected areas.

For Sete Cidades rainfall station (Table 4.2), 21 landslide events were recorded, with nearly half (48%) exhibiting a combined RP of less than 2 years, indicating a high recurrence of events in this area. These frequent events suggest a strong susceptibility of the region to landslides under relatively common rainfall conditions. Notably, the events on 23 December 1983 and 15 December 2006 stood out for their rarity, with combined RP values of 32.3 years and 36.3 years, respectively. These events were likely associated with exceptional rainfall conditions.

Within the Ponta Delgada rainfall station influence area (Table 4.3), 12 landslide events were documented, making it the station with the fewest events among the four analysed. Of these, 4 events (approximately 33%) had a combined RP of less than 2 years, indicating a moderate recurrence of events. The event with the longest combined RP was triggered on 30 December 1996, with a value of 36.3 years, highlighting a rare instance of extreme rainfall conditions affecting this area.

For the Santana rainfall station (Table 4.4), a total of 22 landslide events were recorded, with 10 of these events (approximately 42%) exhibiting a combined RP of less than 2 years. This indicates a relatively high frequency of landslide occurrence in this region, comparable to Sete Cidades. The event with the longest combined RP occurred on 21 October 1996, with a value of 13.3 years, significantly lower than the rarest events recorded in other stations. This suggests that while landslides are frequent in Santana, they are generally less extreme compared to other areas.

The Furnas rainfall station influence area recorded the highest number of landslide events, with 41 occurrences documented (Table 4.5). Despite the abundance of events, only 11 of these (approximately 27%) had a combined RP of less than 2 years, indicating a slightly lower recurrence compared to Sete Cidades and Santana. This lower frequency may reflect a combination of unique geomorphological, geological, and hydrological conditions that require more specific rainfall patterns for landslide triggering. The event on 30 November 2000 is particularly noteworthy, as it represents the rarest landslide event in the entire dataset, with a combined RP of 42.2 years. This exceptional event likely reflects extreme weather conditions and underscores the vulnerability of the region to rare but impactful landslide occurrences.

Figure 4.9 and Table 4.7 present the preparatory and trigger thresholds for landslide occurrence at the four rainfall station influence areas.

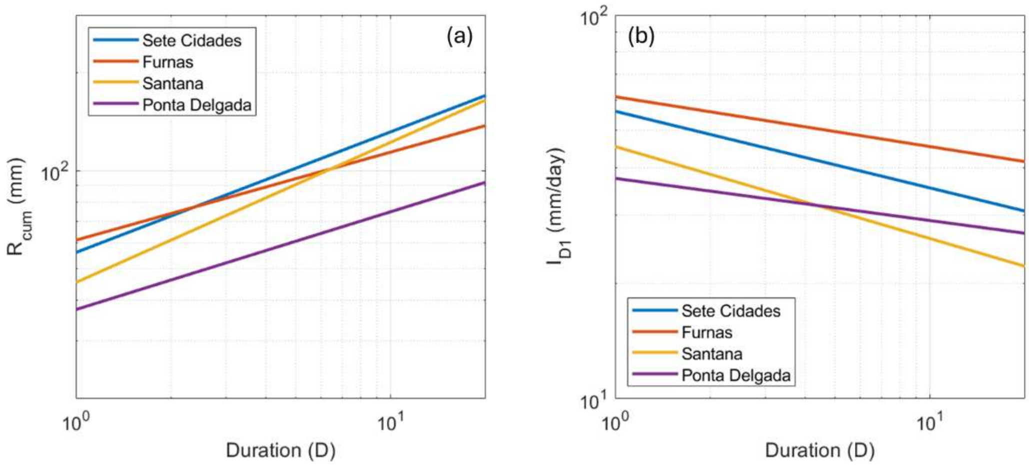

Figure 4.9 | (a) Preparatory thresholds and (b) trigger thresholds for the four rainfall stations.

Table 4.7 | Preparatory and trigger thresholds equations for the four rainfall stations.

Rainfall station	Preparatory Threshold	Trigger Threshold
Sete Cidades	$R_{cum} = 56.1D^{0.37}$	$I_{D1} = 56.1D^{-0.20}$
Santana	$R_{cum} = 45.4D^{0.43}$	$I_{D1} = 45.4D^{-0.24}$
Ponta Delgada	$R_{cum} = 37.5D^{0.30}$	$I_{D1} = 37.5D^{-0.11}$
Furnas	$R_{cum} = 61.2D^{0.27}$	$I_{D1} = 61.2D^{-0.13}$

The preparatory threshold ($R_{cum} = aD^b$) indicates the cumulative rainfall required over a certain duration to prepare the terrain for a potential landslide. In the equation, a and b are constants specific to each station.

At Sete Cidades, the preparatory threshold was notably higher than those associated with the other stations. This suggests that the region requires more accumulated rainfall to reach the threshold. In contrast, Santana exhibited a lower preparatory threshold for shorter rainfall durations compared to Sete Cidades. However, as the duration extended, Santana's threshold became slightly more demanding. Ponta Delgada showed the lowest preparatory threshold among all stations. The preparatory threshold for Furnas was slightly higher than Sete Cidades for shorter durations; yet, for longer durations, the threshold rose more gradually.

The trigger threshold ($I_{D1} = aD^b$) refers to the rainfall intensity on the event day required to trigger a landslide, considering the duration of the preparatory period. In this equation, a and b are constants specific to each station.

For all stations, the trigger threshold indicates that high rainfall intensity is required to trigger landslides when the duration of the preparatory period is shorter. However, as the rainfall duration increases, the intensity required to trigger a landslide event decreases, implying that prolonged rainfall events, even with lower intensity on the event day, can still trigger landslides. Furnas consistently recorded the highest rainfall intensity values on the day of the event for the entire range of durations of the preparatory period. Sete Cidades also showed high intensity values, but with a steeper slope, indicating that for longer durations of the preparatory period, the intensity required on the event day to trigger landslides decreases notably. Santana and Ponta Delgada displayed similar patterns. Santana had higher thresholds for durations up to 3 days, but for longer durations, Ponta Delgada's threshold surpassed Santana's, suggesting a change in the relative strength of these areas based on event rainfall duration.

4.4.2 | Rainfall Thresholds Validation

The ROC metrics associated with the preparatory and combined rainfall thresholds for the four rainfall stations are shown in Tables 4.8 and 4.9, respectively.

Table 4.8 |ROC metrics associated with the preparatory threshold for each rainfall station.

Rainfall Station	**FP**	**TN**	**TP**	**FN**	**TP_{rate}**	**FP_{rate}**	**FA_{rate}**	**TS**
Sete Cidades	943	1364	21	0	1	0.41	0.98	0.02
Ponta Delgada	650	603	12	0	1	0.52	0.98	0.02
Santana	356	970	22	0	1	0.27	0.94	0.06
Furnas	1451	953	41	0	1	0.60	0.97	0.03

Table 4.9 | ROC metrics associated with combined rainfall thresholds for each rainfall station.

Rainfall Station	**FP**	**TN**	**TP**	**FN**	**TP_{rate}**	**FP_{rate}**	**FA_{rate}**	**TS**
Sete Cidades	344	1963	21	0	1	0.15	0.94	0.06
Ponta Delgada	194	1059	12	0	1	0.15	0.94	0.06
Santana	198	1128	22	0	1	0.15	0.90	0.10
Furnas	326	2078	41	0	1	0.14	0.89	0.11

For both thresholds (preparatory and combined), the TP_{rate} was 1 across all stations, indicating that both thresholds correctly detected all the rainfall events that generated landslide activity (FN = 0 in both cases). This result was due to the criteria used to define the thresholds, ensuring accurate landslide event identification.

The combined threshold showed a significant reduction in FP values across all stations compared to the preparatory threshold, indicating greater effectiveness in reducing false positives. This improvement suggests that the combined threshold is more reliable in detecting landslide events and minimising false alarms. The FP_{rate} dropped considerably across all stations when using the combined threshold, reaching values between 0.14 and 0.15, whereas with the preparatory threshold, it ranged from 0.27 to 0.60. For example, at the Furnas station, the FP_{rate} decreased from 0.60 to 0.14, representing a substantial improvement.

Additionally, the FA_{rate} also decreased with the use of the combined threshold, although it remained relatively high due to the low number of catalogued landslide events in each station's influence area. This reduction indicates that the combined threshold is more effective at filtering out false alarms, especially in Furnas, where the FA_{rate} dropped from 0.97 to 0.89. This improvement suggests that the model is becoming more proficient at distinguishing rainfall patterns associated with landslide activity from those that are not.

The TS remained low across all stations when using only the preparatory threshold, ranging from 0.02 at Sete Cidades and Ponta Delgada to 0.06 at Santana and 0.03 at Furnas. However, the TS improved significantly with the combined threshold, reaching 0.06 for Sete Cidades and Ponta Delgada, and 0.10 and 0.11 for Santana and Furnas, respectively. This increase indicates that the combined threshold improves the proportion of correct predictions (true positives) relative to total predictions (including false positives), resulting in more robust overall performance.

The combined threshold demonstrates clear advantages over the preparatory threshold alone, particularly in reducing false positives and increasing accuracy in detecting landslide events, providing more efficient performance across all stations. While the TS remained modest, the reduction in false positives and the improvement in FP_{rate} and FA_{rate} signify that the combined threshold is a more reliable and efficient tool for landslide prediction, making it a promising approach for early warning systems.

4.4.3 | Rainfall Thresholds Normalised by the MAP

One widely accepted approach for linking the threshold to the total rainfall received in the area is normalising the amount and intensity of rainfall by the MAP. This normalisation makes the thresholds more comparable and applicable across different geomorphologic and geologic settings, highlighting the importance of accounting for local precipitation patterns (Guzzetti et al. 2007; Alam et al. 2023). The thresholds normalised by the MAP are presented in Figure 4.10 and Table 4.10, revealing that the thresholds were generally similar, with only minor differences across stations.

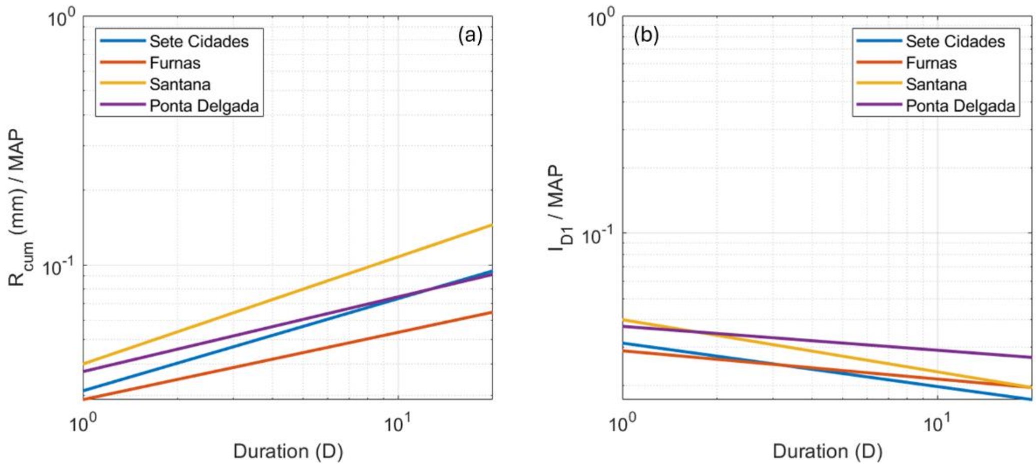

Figure 4.10 | (a) Preparatory thresholds and (b) trigger thresholds, both normalised by the MAP for the four rainfall stations.

Table 4.10 | Equations for preparatory and trigger thresholds normalised by the MAP for the four rainfall stations.

Rainfall station	Preparatory Threshold	Trigger Threshold
Sete Cidades	$R_{cum} = 0.03D^{0.37}$	$I_{D1} = 0.03D^{-0.20}$
Santana	$R_{cum} = 0.04D^{0.43}$	$I_{D1} = 0.04D^{-0.24}$
Ponta Delgada	$R_{cum} = 0.04D^{0.30}$	$I_{D1} = 0.04D^{-0.11}$
Furnas	$R_{cum} = 0.03D^{0.27}$	$I_{D1} = 0.03D^{-0.13}$

The normalised preparatory and trigger thresholds reflect the specific rainfall pattern in each area, but also the influence of other preparatory factors, such as geomorphology and geology.

Stations with higher MAP, such as Sete Cidades and Furnas, showed lower normalised thresholds. This reflects their high annual rainfall, where smaller percentages of MAP are sufficient to trigger landslides. Ponta Delgada and Santana, with lower MAP, exhibited higher thresholds. This indicates that they require relatively greater rainfall amounts or intensities (as a percentage of MAP) to reach critical landslide conditions.

In general, the rainfall amount and intensity required to trigger landslides were approximately 3–4% of the MAP for rainfall durations equal to 1 day (Table 4.9). For both normalised thresholds, Sete Cidades and Furnas shared the lowest *a* coefficient (0.03), reflecting a lower rainfall requirement relative to their MAP for slope preparation and landslide triggering. In contrast, Santana and Ponta Delgada had a slightly higher *a* coefficient (0.04), indicating more demanding rainfall conditions relative to MAP in these areas.

The *b* coefficient for the preparatory thresholds, which reflects the sensitivity of cumulative rainfall to duration, varied across stations. Sete Cidades (0.37) and Furnas (0.27) had lower coefficients, with Furnas exhibiting a steeper decline in threshold demand over longer durations. Santana, with the highest *b* coefficient (0.43), indicates that more demanding conditions of rainfall accumulated values are required for longer rainfall durations to prepare slopes for landslide occurrence compared to the other stations.

For the trigger thresholds, the negative *b* coefficient values highlight how threshold intensity decreases with increasing rainfall duration. Sete Cidades (−0.20) and Furnas (−0.13) exhibited slower declines in intensity requirements for landslide triggering, with Sete Cidades being less demanding for longer durations. Santana's exponent (−0.24) indicated the steepest decline, where short-duration rainfall events had higher intensity requirements. Ponta Delgada (−0.11) showed the slowest decrease in intensity requirements with increasing rainfall durations, reflecting a lower influence of the cumulative rainfall over time in reducing the necessary rainfall intensity for trigger landslides.

The geomorphology of the Sete Cidades and Furnas areas, characterised by relatively "young" landscapes with steep slopes that are still adjusting to their rainfall regime, plays a significant role in their lower threshold requirements. These areas contain friable materials such as pumice and loose volcanic deposits, which are less resistant to weathering and erosion. This geological composition, coupled with their steep topography, makes these regions more susceptible to landslides, requiring smaller rainfall amounts and intensities to reach critical thresholds.

In contrast, the influence areas of Ponta Delgada and Santana stations are located on the Picos Fissural Volcanic System. This region is dominated by basaltic lava flows and scoria, which are more resistant to weathering processes. The terrain in these areas is characterised by moderate slopes and a limited drainage network, contributing to relatively higher normalised threshold values. These regions require higher rainfall amounts and intensities, as a percentage of MAP, to trigger landslides, reflecting their drier climate and more stable geological setting.

Furthermore, the alignment between threshold variability and local climatic and geomorphologic characteristics highlights the necessity of site-specific calibration of rainfall thresholds. Understanding the geomorphological and geological context of each region is essential for accurately predicting and mitigating landslide risk, as these factors directly influence the terrain response to rainfall. This study demonstrates the effectiveness of a combined threshold approach that integrates antecedent and event-day rainfall into a single predictive model. By reducing false positives and improving overall prediction accuracy on landslide prediction across all rainfall stations, this approach offers a suitable tool for early-warning systems.

4.4.4 | Monthly Probability of Exceedance and Return Period of the Combined Thresholds

This section provides a detailed analysis of the monthly patterns of landslide occurrences and the respective probability of exceedance the combined rainfall thresholds. The primary objective was to explore the relationship between seasonality, rainfall event duration, and intensity in relation to the established thresholds while emphasising the specific return periods (RPs). A total of 240 GEV distributions were fitted using the MLE method. The monthly probability of exceedance the combined rainfall threshold for landslide occurrence along with the corresponding RP and monthly frequencies of catalogued landslide events are shown in Figure 4.11.

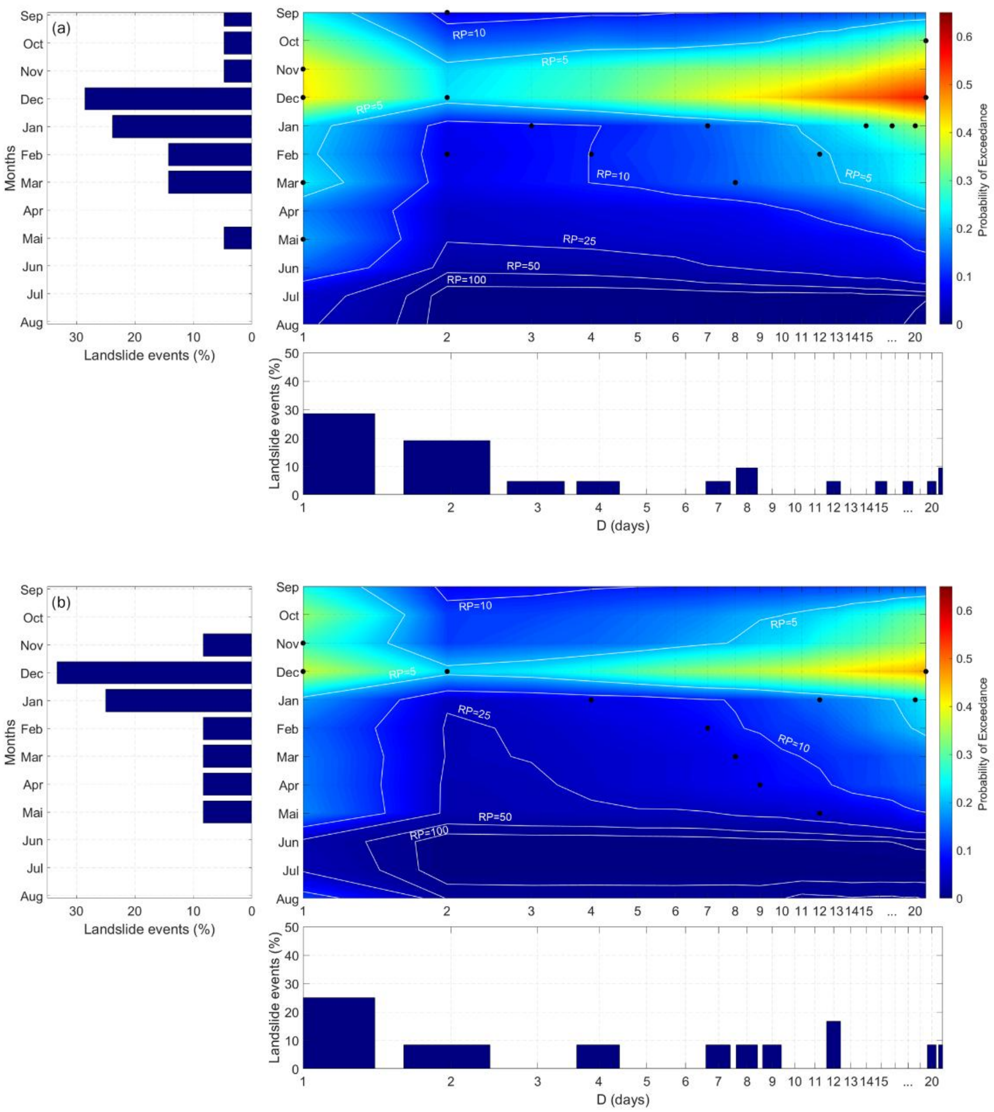

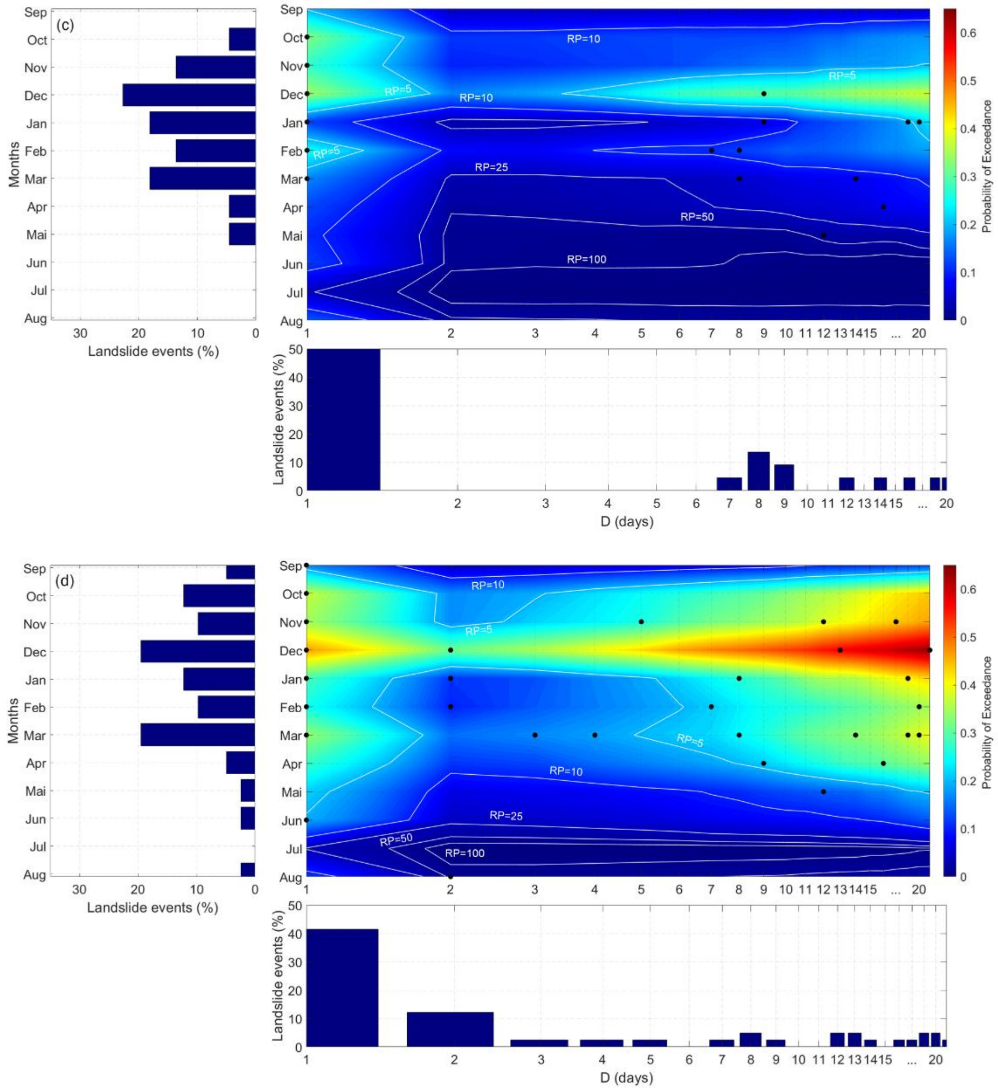

Figure 4.11| Monthly Probability of Exceedance the combined rainfall threshold for landslide occurrence, along with the corresponding return periods (RPs) for: (a) Sete Cidades, (b) Ponta Delgada, (c) Santana, and (d) Furnas. The figure also includes the monthly percentages of catalogued landslide events. The black dots represent landslide events.

All stations demonstrated a clear seasonal pattern, with the highest concentration of landslide events occurring during the winter months, particularly in December and January. This trend reflects the influence of increased rainfall during this period. Sete Cidades and Ponta Delgada exhibited pronounced peaks in December, with over 30% of the events occurring in this month. Santana and Furnas showed a broader distribution, with notable contributions in November, December and January.

Across all stations, most landslide events were associated with short-duration rainfall events lasting 1–3 days, highlighting the critical role of intense, short-lived storms as primary triggers. However, notable differences emerged between stations. Furnas stood out with a relatively higher proportion of landslide events associated with longer rainfall durations (>10 days). This indicates that prolonged periods of moderate to heavy rainfall significantly contribute to landslide triggering in this area, possibly due to cumulative soil saturation effects. In contrast, Sete Cidades, Santana, and Ponta Delgada showed a more pronounced reliance on shorter-duration events, with limited contributions from rainfall lasting longer than 5–6 days. This suggests that these regions are more sensitive to the intensity of rainfall rather than to its cumulative duration.

A strong correlation was observed between the landslide events and periods of higher probabilities of rainfall threshold exceedance. For short rainfall durations (1 day) characterised by high rainfall intensities, the probability of triggering landslides was particularly high between October and December for all stations. Sete Cidades and Furnas rainfall stations showed an additional peak in March, likely driven by early spring rainfall. At Santana station, an additional increase occurred in February, reflecting regional variations in seasonal rainfall distribution.

For cumulated rainfall periods exceeding 6 days, rainfall stations showed distinct seasonal trends. Sete Cidades showed a higher probability of exceedance between October and April, with the most critical period being October to January. At Ponta Delgada station, the highest probabilities of exceedance were concentrated between October and January, while at Santana station, it occurred between November and January. At Furnas station, the highest probabilities of exceedance were recorded between October and April, particularly from October to January.

At all stations, exceeding the combined rainfall threshold with an RP < 5 years was highly probable, underscoring the frequent nature of rainfall events capable of triggering slope failures. However, the temporal distribution varied by station and rainfall duration. At Sete Cidades station, for short-duration events, high probabilities occurred between September and January, with an additional peak in March. For longer-duration events, the high-probability period extended from September to May, reflecting the dual contribution of both intense storms and cumulative rainfall. At Ponta Delgada station, regardless of rainfall duration, the probability of landslides with a RP < 5 years was highest between September and January. At Santana station, for short-duration rainfall, the probability was higher between September and December, with an additional peak in February. For long-duration rainfall, the critical period spanned November to January, reflecting the role of prolonged rainfall events in landslide occurrence. At Furnas station, a high probability of landslides with an RP < 5 years was observed between September and May, regardless of the rainfall duration. This highlights the station's broad vulnerability to both intense and prolonged precipitation events.

The results align with observed patterns of MAP. Stations with lower MAP values, such as Ponta Delgada and Santana, showed lower probabilities of exceedance due to more demanding thresholds in relative terms. This suggests that these regions require higher-intensity or longer-duration rainfall to trigger landslides. In contrast, at stations with higher MAP values, such as Furnas and Sete Cidades, the thresholds were less demanding, resulting in higher probabilities of exceedance.

4.4.5 | Study Limitations and Future Perspectives

Despite the promising results, this study has some limitations that should be acknowledged. The landslide database was compiled through a review of local newspapers, which may lead to underreporting, particularly for events with limited impacts or those occurring in remote or sparsely populated areas. The absence of a report does not necessarily imply the absence of an event, potentially reducing the dataset's representativeness and, consequently, the reliability of the defined rainfall thresholds. In addition, the temporal distribution of the documented landslide events was not homogeneous, with identifiable gaps in certain periods. These gaps likely reflect temporal variations in reporting practices, media coverage, and institutional monitoring capacity rather than a true absence of landslide activity. Specifically, missing or undocumented landslide events may lead to an overestimation of FNs and an underestimation of TPs, leading to conservative performance metrics. Nonetheless, the inventory was considered sufficiently representative to capture the dominant rainfall-triggering conditions and seasonal patterns of rainfall-induced landslides in the study area.

Another limitation concerns the scarcity of long-term hourly rainfall records and the absence of precise timing for most landslide events, which prevented the integration of high-resolution precipitation data into the definition of rainfall thresholds. The spatial resolution of the rainfall stations also constitutes a constraint, potentially affecting the precision of localised rainfall estimates. With only four stations, the rainfall data may not have accurately captured the local conditions at specific landslide sites, particularly in regions characterised by complex geomorphology and rainfall variability.

Although the thresholds have not yet been validated in real-time, retrospective performance (back-analysis) showed good predictive performance of the combined thresholds, with a high success rate in detecting events and a significant reduction in false positives. These results support the robustness of the adopted methodology and its potential for operational application. Future research should focus on expanding the rainfall and landslide datasets and testing real-time implementation within an operational early warning system for São Miguel Island.

4.5 | Conclusions

This study demonstrates that the use of a combined rainfall threshold, integrating antecedent rainfall with event-day rainfall, significantly improved the landslide prediction on São Miguel Island. Compared to traditional single-threshold approaches, the combined model reduced false positives, increased predictive accuracy, and showed consistent performance across all rainfall stations.

Two main rainfall patterns were identified as responsible for triggering landslides: (i) long-duration events, characterised by significant rainfall accumulation over several consecutive days, and (ii) short-duration events, driven by extreme rainfall intensity within a single day. For short preparatory periods, high daily rainfall is required to trigger landslides, whereas longer preparatory rainfall reduces the intensity needed on the event day. Normalising thresholds by Mean Annual Precipitation (MAP) provided a more consistent basis for regional comparisons. Results indicate that in wetter areas, such as Sete Cidades and Furnas, the required rainfall amounts to trigger landslides are less demanding, whereas in drier regions, such as Ponta Delgada and Santana, higher rainfall values are required. This emphasises the combined influence of climatic and geological settings on slope response to rainfall and reinforces the importance of the site-specific calibration of thresholds.

Overall, the combined threshold approach proved to be a robust and operationally relevant tool for landslide early warning systems. By reducing false alarms and improving predictive reliability, it contributes to more effective risk mitigation and provides a methodological framework that can be adapted to other regions affected by rainfall-induced landslides.

References

Afungang, R. N., & Bateira, C. V. (2016). Temporal probability analysis of landslides triggered by intense rainfall in the Bamenda Mountain Region, Cameroon. *Environmental Earth Sciences, 75*. https://doi.org/10.1007/s12665-016-5835-7

Alam, A., Ahmed, B., Sammonds, P., & Kamal, A. M. (2023). Applying rainfall threshold estimates and frequency ratio model for landslide hazard assessment in the coastal mountain setting of South Asia. *Natural Hazards Research, 3*, 531–545. https://doi.org/10.1016/j.nhres.2023.08.002

Amaral, P. (2010). *Caracterização geotécnica e hidrológica de depósitos vulcânicos: Modelação da estabilidade de taludes no concelho da Povoação (Ilha de S. Miguel – Açores)* (PhD thesis). University of the Azores.

Amaral, P., Marques, R., Zêzere, J. L., Queiroz, G., & Marques, F. (2009). Distributed transient response modeling of rainfall-triggered shallow landslide for susceptibility assessment in Ribeira Quente valley (S. Miguel Island, Azores). In T. A. Bogaard et al. (Eds.), *Landslide processes: From geomorphologic mapping to dynamic modeling* (pp. 89–94). Centre d'Études de Risques Géologiques.

Azevedo, E. B. (2001). Condicionantes dinâmicas do clima no arquipélago dos Açores: Elementos para o seu estudo. *Açoreana, 9*, 309–317.

Beguería, S. (2006). Validation and evaluation of predictive models in hazard assessment and risk management. *Natural Hazards, 37*, 315–329. https://doi.org/10.1007/s11069-005-5182-6

Bogaard, T., & Greco, R. (2018). Invited perspectives: Hydrological perspectives on precipitation intensity–duration thresholds for landslide initiation: Proposing hydro-meteorological thresholds. *Natural Hazards and Earth System Sciences, 18*, 31–39. https://doi.org/10.5194/nhess-18-31-2018

Brunetti, M. T., Peruccacci, S., Rossi, M., Luciani, S., Valigi, D., & Guzzetti, F. (2010). Rainfall thresholds for the possible occurrence of landslides in Italy. *Natural Hazards and Earth System Sciences, 10*, 447–458. https://doi.org/10.5194/nhess-10-447-2010

Bui, D. T., Pradhan, B., Lofman, O., Revhaug, I., & Dick, Ø. (2013). Regional prediction of landslide hazard using probability analysis of intense rainfall in Hoa Binh Province, Vietnam. *Natural Hazards, 66*, 707–730. https://doi.org/10.1007/s11069-012-0510-0

Caine, N. (1980). The rainfall intensity–duration control of shallow landslides and debris flows. *Geografiska Annaler: Series A, Physical Geography, 62*, 23–27.

Carvalho, F. S., Meirelles, M. G., Henriques, D., Porteiro, J., Navarro, P., & Vasconcelos, H. C. (2023). Climate change and extreme events in Northeast Atlantic and Azores Islands Region. *Climate, 11*, 238. https://doi.org/10.3390/cli11120238

Chow, V. T., Maidment, D. R., & Mays, L. W. (1988). *Applied hydrology*. McGraw-Hill.

Clarke, R. T. (2013). How should trends in hydrological extremes be estimated? *Water Resources Research, 49*, 6756–6764. https://doi.org/10.1002/wrcr.20485

Coles, S. (2001). *An introduction to statistical modeling of extreme values*. Springer. https://doi.org/10.1007/978-1-4471-3675-0

Dahal, R. K., & Hasegawa, S. (2008). Representative rainfall thresholds for landslides in the Nepal Himalaya. *Geomorphology, 100*, 429–443. https://doi.org/10.1016/j.geomorph.2008.01.014

Duncan, A. M., Guest, J. E., Wallenstein, N., & Chester, D. K. (2015). The older volcanic complexes of São Miguel, Azores: Nordeste and Povoação. In J. L. Gaspar et al. (Eds.), *Volcanic geology of São Miguel Island* (Geological Society, London, Memoirs 44, pp. 147–153). https://doi.org/10.1144/M44.11

Ebrahim, K. M. P., Gomaa, S. M. M. H., Zayed, T. M., & Alfalah, G. (2025). Rainfall-induced landslide prediction models, part I: Empirical–statistical and physically based causative thresholds. *Water, 17*, 3273. https://doi.org/10.3390/w17223273

El Adlouni, S., Ouarda, T. B. M. J., Zhang, X., Roy, R., & Bobée, B. (2007). Generalized maximum likelihood estimators for the nonstationary generalized extreme value model. *Water Resources Research, 43*, W03410. https://doi.org/10.1029/2005WR004545

Ferreira, T., Gomes, A., Gaspar, J. L., & Guest, J. (2015). Distribution and significance of basaltic eruptive centres: São Miguel, Azores. In J. L. Gaspar et al. (Eds.), *Volcanic geology of São Miguel Island* (Geological Society, London, Memoirs 44, pp. 135–146). https://doi.org/10.1144/M44.10

Frattini, P., Sosio, R., & Crosta, G. (2009). Approaches for defining thresholds and return periods for rainfall-triggered shallow landslides. *Hydrological Processes, 23*, 1444–1460. https://doi.org/10.1002/hyp.7269

Gaspar, J. L., Queiroz, G., Ferreira, T., Medeiros, A. R., Goulart, C., & Medeiros, J. (2015). Earthquakes and volcanic eruptions in the Azores region. *Geological Society, London, Memoirs, 44*, 33–49. https://doi.org/10.1144/M44.4

Gonzalez, F. C. G., Cavacanti, M. D. C. R., Ribeiro, W. N., de Mendonça, M. B., & Haddad, A. N. (2024). A systematic review on rainfall thresholds for landslides occurrence. *Heliyon, 10*, e23247. https://doi.org/10.1016/j.heliyon.2023.e23247

Guest, J. E., Gaspar, J. L., Cole, P. D., Queiroz, G., Duncan, A. M., Wallenstein, N., Ferreira, T., & Pacheco, J. M. (1999). Volcanic geology of Furnas Volcano, São Miguel, Azores. *Journal of Volcanology and Geothermal Research, 92*, 1–29. https://doi.org/10.1016/S0377-0273(99)00064-5

Guest, J. E., Pacheco, J. M., Cole, P. D., Duncan, A. M., Wallenstein, N., Queiroz, G., Gaspar, J. L., & Ferreira, T. (2015). The volcanic history of Furnas volcano. In J. L. Gaspar et al. (Eds.), *Volcanic geology of São Miguel Island* (Geological Society, London, Memoirs 44, pp. 125–134). https://doi.org/10.1144/M44.9

Guzzetti, F., Peruccacci, S., Rossi, M., & Stark, C. P. (2007). Rainfall thresholds for the initiation of landslides in central and southern Europe. *Meteorology and Atmospheric Physics, 98*, 239–267. https://doi.org/10.1007/s00703-007-0262-7

Guzzetti, F., Peruccacci, S., Rossi, M., & Stark, C. P. (2008). The rainfall intensity–duration control of shallow landslides and debris flows: An update. *Landslides, 5*, 3–17. https://doi.org/10.1007/s10346-007-0112-1

Hernández, A., Kutiel, H., Trigo, R. M., Valente, M. A., Sigró, J., Cropper, T., & Santo, F. E. (2016). New Azores archipelago daily rainfall dataset and its links with climate variability. *International Journal of Climatology, 36*, 4439–4454. https://doi.org/10.1002/joc.4642

Jaiswal, P., van Westen, C. J., & Jetten, V. (2010). Quantitative landslide hazard assessment along a transportation corridor in southern India. *Engineering Geology, 116*, 236–250. https://doi.org/10.1016/j.enggeo.2010.09.005

Kotz, S., & Nadarajah, S. (2000). *Extreme value distributions: Theory and applications*. Imperial College Press.

Ma, T., Li, C., Lu, Z., & Bao, Q. (2015). Rainfall intensity–duration thresholds for landslide initiation in Zhejiang Province, China. *Geomorphology, 245*, 193–206. https://doi.org/10.1016/j.geomorph.2015.04.020

Marin, R. J. (2020). Physically based and distributed rainfall intensity and duration thresholds for shallow landslides. *Landslides, 17*, 2907–2917. https://doi.org/10.1007/s10346-020-01481-9

Marotti, J. C., Gomes, G. J. C., Velloso, R. Q., Vargas Júnior, E. A., Nunes, R. S., & Fernandes, N. F. (2023). Exploring extreme rainfall-triggered landslides using 3D unsaturated flow and spatially distributed soil depth. *Catena, 229*, 107241. https://doi.org/10.1016/j.catena.2023.107241

Marques, R. (2013). *Estudo de movimentos de vertente no concelho da Povoação (Ilha de São Miguel, Açores)* (PhD thesis). University of the Azores.

Marques, R., Amaral, P., Araújo, I., Gaspar, J. L., & Zêzere, J. L. (2015). Landslides on São Miguel Island (Azores): Susceptibility analysis and validation. In J. L. Gaspar et al. (Eds.), *Volcanic geology of São Miguel Island* (Geological Society, London, Memoirs 44, pp. 167–184). https://doi.org/10.1144/M44.1

Marques, R., Silva, R. F., Montalvo, A., & Oliveira, S. (2021b). *Desenvolvimento e implementação de um sistema de monitorização, aviso e alerta para a mitigação do risco de movimentos de vertente na obra do semitúnel da E.R. N.º 2-2ª para a Ribeira Quente (concelho da Povoação) - Memória descritiva.* DTC 025/IVAR/CIVISA/2021.

Marques, R., Silva, R. F., Montalvo, A., Oliveira, S., Amaral, P., Malheiro, A., & Marques, F. (2021a). *Parecer sobre intervenções a realizar e medidas de monitorização a implementar à segurança da obra do semitúnel na estrada de acesso à Ribeira Quente.* DTC 021/IVAR/CIVISA/2021.

Marques, R., Zêzere, J. L., Amaral, P., Gaspar, J., & Queiroz, G. (2010). Desenvolvimento de um sistema empírico de alerta para movimentos de vertente (ELEWS-Pov). In *V Congresso Nacional de Geomorfologia* (pp. 327–332).

Marques, R., Zêzere, J. L., Trigo, R., Gaspar, J., & Trigo, I. (2008). Rainfall patterns and critical values associated with landslides in Povoação County. *Hydrological Processes, 22*, 478–494. https://doi.org/10.1002/hyp.6879

Mathew, J., Babu, D. G., Kundu, S., Kumar, K. V., & Pant, C. C. (2014). Integrating intensity–duration rainfall threshold and antecedent conditions for landslide early warning. *Landslides, 11*, 575–588. https://doi.org/10.1007/s10346-013-0408-2

Nocentini, N., Medici, C., Barbadori, F., Gatto, A., Franceschini, R., Soldato, M. D., Rosi, A., & Segoni, S. (2023). Optimization of rainfall thresholds for landslide early warning through false alarm reduction and a multi-source validation. *Landslides*. https://doi.org/10.1007/s10346-023-02176-7

Palau, R. M., Berenguer, M., Hürlimann, M., & Sempere-Torres, D. (2023). Implementation of hydrometeorological thresholds for regional landslide warning in Catalonia (NE Spain). *Landslides*. https://doi.org/10.1007/s10346-023-02094-8

Palazzolo, N., Cancelliere, A., Zofei, R. D., & Peres, D. J. (2025). Use of delayed ERA5-Land soil moisture products for improving landslide early warning. *Natural Hazards and Earth System Sciences, 25*, 4907–4924. https://doi.org/10.5194/nhess-25-4907-2025

Petley, D. (2012). Global patterns of loss of life from landslides. *Geology, 40*, 927–930.

Piciullo, L., Tiranti, D., Pecoraro, G., et al. (2020). Standards for the performance assessment of territorial landslide early warning systems. *Landslides, 17*, 2533–2546. https://doi.org/10.1007/s10346-020-01486-4

Queiroz, G., Gaspar, J. L., Guest, J. E., Gomes, A., & Almeida, M. H. (2015). Eruptive history and evolution of Sete Cidades volcano. *Geological Society, London, Memoirs, 44*, 87–104. https://doi.org/10.1144/M44.7

Segoni, S., Piciullo, L., & Gariano, S. L. (2018). A review of recent literature on rainfall thresholds for landslide occurrence. *Landslides, 15*, 1483–1501. https://doi.org/10.1007/s10346-018-0966-4

Silva, R. F., Marques, R., & Zêzere, J. L. (2024). Spatial distribution, temporal trends and impact of landslides on São Miguel Island (1900–2020). *Natural Hazards, 120*, 2617–2638. https://doi.org/10.1007/s11069-023-06296-0

Silva, R. F., Marques, R., Zêzere, J. L., & Fragoso, M. (2025). Rainfall patterns and trends on São Miguel Island (Azores, Portugal): A hierarchical clustering and trend analysis approach. *Climate, 13*, 238. https://doi.org/10.3390/cli13110238

Staley, D. M., Kean, J. W., Cannon, S. H., Schmidt, K. M., & Laber, J. L. (2013). Objective definition of rainfall thresholds for post-fire debris flows. *Landslides, 10*, 547–562. https://doi.org/10.1007/s10346-012-0341-9

Vaz, T., Zêzere, J. L., Pereira, S., Oliveira, S. C., Garcia, R. A. C., & Quaresma, I. (2018). Regional rainfall thresholds for landslide occurrence using a centenary database. *Natural Hazards and Earth System Sciences, 18*, 1037–1054. https://doi.org/10.5194/nhess-18-1037-2018

Zêzere, J. L. (2023). Geohazards in Portugal: A state of the art. *Finisterra, 58*, 7–27.

Zêzere, J. L., Trigo, R., & Trigo, I. (2005). Shallow and deep landslides induced by rainfall in Lisbon. *Natural Hazards and Earth System Sciences, 5*, 331–344. https://doi.org/10.5194/nhess-5-331-2005

Zêzere, J. L., Vaz, T., Pereira, S., Oliveira, S. C., Marques, R., & Garcia, R. A. C. (2015). Rainfall thresholds for landslide activity in Portugal: A state of the art. *Environmental Earth Sciences, 73*, 2917–2936. https://doi.org/10.1007/s12665-014-3672-0

Zhang, L. M., Lü, Q., Deng, Z. H., & Zhang, J. (2025). Probabilistic approach to determine rainfall thresholds for rainstorm-induced shallow landslides using long-term local precipitation records. *Engineering Geology, 353*, 108139. https://doi.org/10.1016/j.enggeo.2025.108139

Supplementary Material

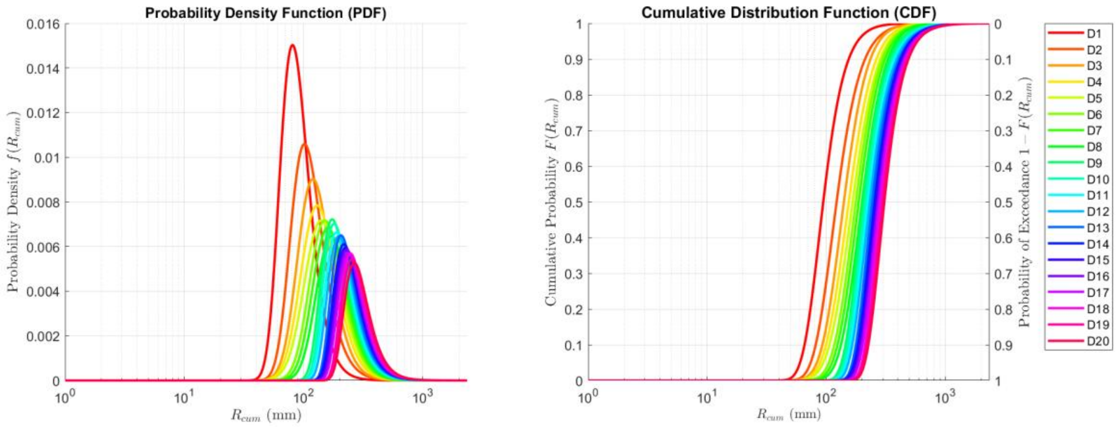

Figure S1 | GEV probabilistic models for Sete Cidades station for all considered rainfall durations ($D \in \mathbb{Z}$, D = [1, 20]). Left panel: Probability Density Function (PDF) of the random variable R_{cum}. Right panel: Cumulative Distribution Function (CDF) and Exceedance Probability (1-F).

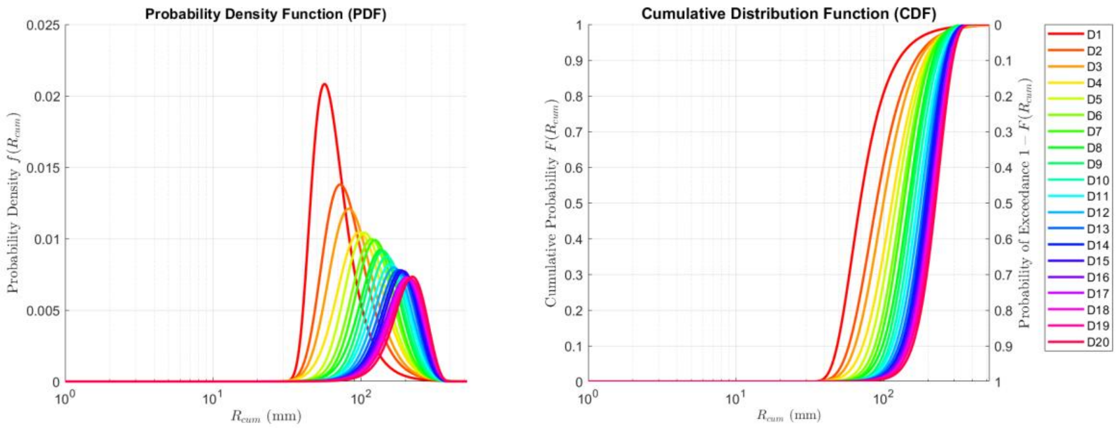

Figure S2 | GEV probabilistic models for Santana station for all considered rainfall durations ($D \in \mathbb{Z}$, D = [1, 20]). Left panel: Probability Density Function (PDF) of the random variable R_{cum}. Right panel: Cumulative Distribution Function (CDF) and Exceedance Probability (1-F).

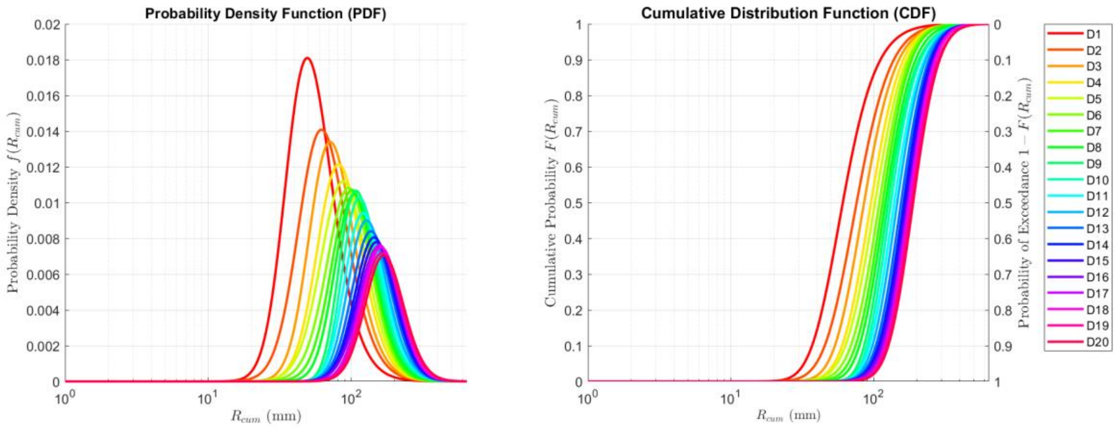

Figure S3 | GEV probabilistic models for Ponta Delgada station for all considered rainfall durations (*D* ∈ ℤ, *D* = [1, 20]). Left panel: Probability Density Function (PDF) of the random variable R_{cum}. Right panel: Cumulative Distribution Function (CDF) and Exceedance Probability (1-*F*).

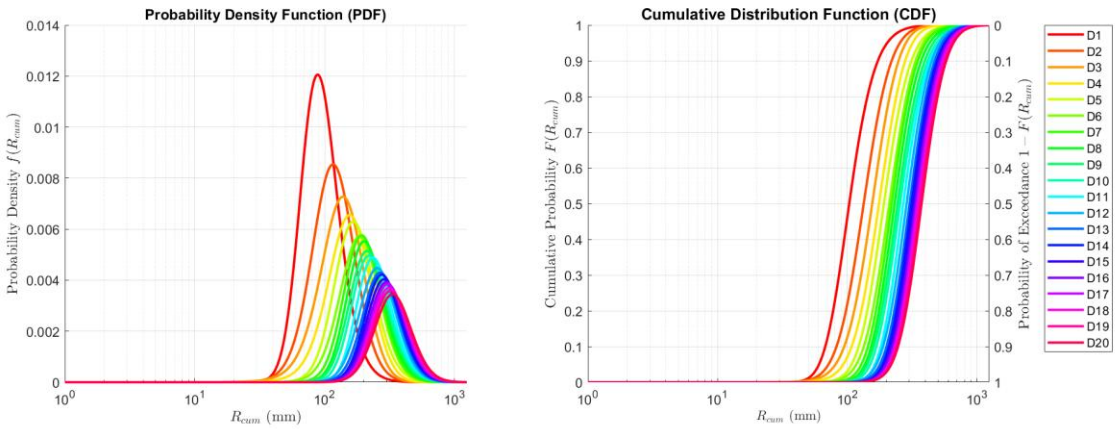

Figure S4 | GEV probabilistic models for Furnas station for all considered rainfall durations (*D* ∈ ℤ, *D* = [1, 20]). Left panel: Probability Density Function (PDF) of the random variable R_{cum}. Right panel: Cumulative Distribution Function (CDF) and Exceedance Probability (1-*F*).

CHAPTER 5

5 | FINAL DISCUSSION AND CONCLUSIONS

São Miguel Island is frequently affected by landslides, which represent one of the most prevalent and impactful natural hazards in the Azores archipelago. These events are driven by a complex interaction of natural and anthropogenic factors, including the island's volcanic geology, steep terrain, intense seismic activity, and climatic conditions, particularly rainfall patterns. The combination of steep slopes and poorly consolidated volcanic soils makes the island is highly susceptible to landslides, especially during periods of heavy rainfall.

The study of the spatiotemporal distribution and impacts of landslides on São Miguel Island between 1900 and 2020, supported by the updated NATHA database, allowed for the cataloguing of 236 landslide events. A critical finding of this research is the significant increase in event frequency since 1996, with 58% of the total events occurring in the last 21% of the study period. This trend is directly linked to changes in rainfall patterns, specifically an increase in the number of days with extreme precipitation, constituting the first scientific evidence of climate change influence on the occurrence of landslides in the Azores. This increase may reflect the broader impacts of global climate change, which has intensified extreme weather events, such as storms and torrential rains, worldwide.

Landslides have caused significant socio-economic impacts on São Miguel Island, resulting in fatalities, injuries, displacement, and property damage. Between 1900 and 2020, there were 82 fatalities, 41 injuries, 305 people made homeless, and 66 buildings were destroyed or damaged. The municipality of Povoação stands out as the most affected, accounting for 59% of the total recorded deaths (48 fatalities). The study demonstrated that, although landslides occur throughout the island, areas with more rugged morphologies and non-cohesive volcanic materials showed the highest susceptibility. Spatial analysis confirmed the existence of recurrence patterns that should be considered in land-use planning and risk management. Interestingly, events causing fatalities do not always coincide with months of highest accumulated rainfall, suggesting that rainfall intensity and short duration are key determinants of catastrophic events.

Trend analyses for the climatological years 1978/79–2019/20, using the Mann–Kendall test and Sen's slope estimator, indicated predominantly decreasing trends in annual and seasonal rainfall. However, statistically significant declines were detected only at a subset of stations. While some stations displayed marked reductions, the overall trend suggests a possible deviation from projections of global climate change models and from trends identified in previous long-term rainfall studies. It is important to note, however, that these changes are not uniformly statistically significant across the island.

The most pronounced reductions were observed in autumn, which exhibited the sharpest declines across several locations. This seasonal decrease can be partially explained by regional atmospheric changes, notably the strengthening of the Azores High. Previous studies projected increases in winter rainfall and decreases in summer rainfall as a result of climate change; however, this study suggest a different reality, with notable declines in both autumn and winter, which could negatively affect water availability on the island.

Analyses also reveal that the North Atlantic Oscillation (NAO) is the dominant large-scale driver of interannual rainfall variability in the Azores, consistently showing a negative correlation (i.e., years with higher NAO values correspond to lower annual rainfall totals). The predominantly positive NAO phase observed in recent years has likely contributed, at least partially, to the decrease in rainfall. However, the pronounced drying observed in the latest sub-dataset (post-2010) occurred even during neutral or negative NAO phases, suggesting that additional regional climate drivers may also be influencing the island's recent rainfall patterns.

The comparison between the sub-periods 1978/79–2009/10 and 2010/11–2019/20 revealed significant reductions in average rainfall values, ranging from 20% to 30% depending on the season and cluster analysed. This widespread decline points to a structural shift in rainfall regimes on the island, with potential consequences for essential sectors such as agriculture, water resource management, and environmental stability, particularly in areas vulnerable to landslides. This decline in rainfall is not necessarily incompatible with an increase in the number of days with high rainfall amounts. Instead, the results suggest that, although there may be more days of intense rainfall, this increase is insufficient to offset the overall reduction in annual rainfall totals, indicating a tendency toward more irregular and concentrated rainfall patterns.

Correlation analysis between altitude and rainfall was confirmed through linear regression analysis, indicating an average increase of 144 mm to 196 mm in rainfall for every 100 metres of elevation. This pattern reinforces the importance of topography in determining local rainfall regimes. However, some discrepancies, such as the inclusion of the Lagoa das Furnas station in a cluster characterised by higher altitudes, demonstrate the influence of volcanic calderas on local microclimates, producing rainfall patterns not strictly proportional to altitude.

The study of empirical rainfall thresholds for landslide prediction highlighted the importance of rainfall variability on the island and led to significant advances in the calibration of predictive models. It demonstrated that the use of a combined threshold, which considers both antecedent rainfall (preparation) and rainfall on the day of the event (trigger), is substantially more effective than using isolated preparatory thresholds. This combined approach resulted in a significant reduction in false positives and an increase in the accuracy of landslide prediction, making it a valuable tool for the development of early warning systems.

Two main rainfall patterns were identified as triggers for landslides: long-duration events, characterised by substantial accumulations of rainfall over several consecutive days, and short-duration events, in which extreme rainfall intensity occurs within a single day. Across all the stations analysed, it was found that the rainfall intensity required to trigger a landslide is higher when the preparatory period is shorter. As antecedent rainfall duration increased, the intensity required for triggering decreased, demonstrating that prolonged rainfall, even of lower intensity on the event day, can still initiate landslides.

Normalisation of rainfall thresholds by the MAP enabled a more consistent comparison between different regions of the island, adjusting rainfall values to local patterns. The results showed that in areas with high MAP the thresholds required to trigger landslides are less demanding, reflecting their wetter climates and potentially less consolidated soils. On the other hand, regions with lower MAP require higher rainfall volumes to reach equivalent thresholds, demonstrating more stable geological conditions.

Seasonal variability influence on landslide occurrence was also highlighted in the study. Sete Cidades and Furnas stations showed a higher monthly probability of exceeding thresholds, particularly between October and January, with some events extending into May. Ponta Delgada and Santana, with their more stringent thresholds, exhibited lower probabilities, aligning with their drier conditions. Despite these differences, both short- and long-duration intense rainfall events at all stations are associated with landslide return periods of less than five years, especially during the rainy season from September to January.

In conclusion, the study highlights the importance of historical databases, such as NATHA, for understanding and mitigating natural disasters. Such information assists authorities in identifying vulnerable areas and planning preventive measures. The influence of climate change on landslides on São Miguel Island reinforces the urgent need for adaptation and resilience strategies for the local population and infrastructure. The observed decline in rainfall on the island presents challenges in water management, requiring adaptation policies to ensure water security and mitigate environmental and agricultural impacts. The increased frequency of dry periods and the decline in rainfall during autumn and winter exacerbate the region's vulnerability to extreme events, such as prolonged droughts, as well as to enhanced erosion and landslide activity associated with high-intensity, short-duration rainfall events.

Addressing these challenges requires tailored regional prevention and mitigation strategies. Early warning systems, based on refined empirical models, provide crucial information for a rapid and effective response to critical events. Integrating meteorological radar data and spatialized rainfall thresholds allows comprehensive assessment of rainfall distribution beyond isolated stations, enhancing early warning capabilities. Continued research on rainfall–landslide relationships, combined with new remote sensing technologies and computational modelling, will further improve capabilities and preparedness, ultimately reducing the impacts of landslides on the region.

UNIVERSIDADE DOS AÇORES
Faculdade de Ciências e Tecnologia

Rua da Mãe de Deus
9500-321 Ponta Delgada
Açores, Portugal

Analysis of rainfall and its effect for landslide triggering in São Miguel Island

Rui Filipe Fagundes Silva

TD

SICUT AURORA SCIENTIA LUCET
UNIVERSIDADE DOS AÇORES

2026